NUREG/CR-2345, Vol. 4
HEDL-TME 81-36

LWR PRESSURE-VESSEL IRRADIATION SURVEILLANCE DOSIMETRY

QUARTERLY PROGRESS REPORT
OCTOBER 1981 - DECEMBER 1981

Handford Engineering Development Laboratory

Preparation coordinated by
G.L. Guthrie
W.N. McElroy

Prepared for the U.S. Nuclear Regulatory Commission

GPO Printed copy price: $6.00

NUREG/CR-2345, Vol. 4
HEDL-TME 81-36
R5

NUREG/CR--2345-Vol.4

DE83 002286

LWR PRESSURE-VESSEL IRRADIATION SURVEILLANCE DOSIMETRY

QUARTERLY PROGRESS REPORT OCTOBER 1981 - DECEMBER 1981

Handford Engineering Development Laboratory

Operated by Westinghouse Hanford Company
P.O. Box 1970 Richland, WA 99352
A Subsidiary of Westinghouse Electric Corporation

Preparation coordinated by
G.L. Guthrie
W.N. McElroy

Manuscript completed: July 1982
Date published: October 1982

Prepared for Division of Engineering Technology
Office of Nuclear Regulatory Research
U.S. Nuclear Regulatory Commission
Washington, DC 20555
NRC FIN No. B5988-7

i - ii

FOREWORD

The Light Water Reactor Pressure Vessel Surveillance Dosimetry Improvement Program (LWR-PV-SDIP) was established by NRC to improve, maintain, and standardize neutron dosimetry, damage correlation, and the associated reactor analysis data and procedures that are used to predict the integrated effect of neutron exposure to LWR-PV. A vigorous research effort attacking the same measurment and analysis problems exists worldwide, with strong cooperative links among NRC-supported activities at HEDL, ORNL, NBS, MEA, ENSA and those supported by CEN/SCK (Mol, Belgium), EPRI (Palo Alto, USA), KFA (Jülich, Germany), and several UK laboratories. These cooperative links are strengthened by the active membership of the scientific staff from many participating countries and laboratories in the ASTM E10 Committee on Nuclear Technology and Applications. Several subcommittees of ASTM E10 are responsible for the preparation of LWR-PV surveillance standards.

The primary objective of the multilaboratory program is to prepare an updated and improved set of physics-dosimetry-metallurgy, damage correlation, and associated reactor analysis ASTM Standards for LWR-PV irradiation surveillance programs. Supporting this objective are a series of analytical and experimental validation and calibration studies in "Standard, Reference, and Controlled Environment Benchmark Fields," reactor "Test Regions," and operating power reactor "Surveillance Positions."

These studies will establish and certify the precision and accuracy of the measurement and predictive methods recommended for use in the ASTM Standards. Consistent and accurate measurement and data analysis techniques and methods, therefore, will be developed and validated along with guidelines for required neutron field calculations used to correlate changes in material properties with the characteristics of the neutron radiation field. It is expected that the application of the established ASTM Standards will permit the reporting of measured materials property changes and neutron exposures to an accuracy and precision within bounds of 10 to 30%, depending on the measured metallurgical variable and neutron environment.

The assessment of the radiation-induced degradation of material properties in a power reactor pressure vessel requires accurate definition of the neutron field from the outer region of the reactor core to the outer boundaries of the pressure vessel. Problems with measuring neutron flux and spectrum are associated with two distinct components of LWR-PV irradiation surveillance procedures: 1) proper application of calculational estimates of the neutron fluence delivered to in-vessel surveillance positions, various locations in the vessel wall, and ex-vessel support structures and surveillance positions, and 2) understanding the relationship between material property changes in reactor vessels, in-vessel support structures, and in metallurgical test specimens in test reactors and at accelerated neutron flux positions in operating power reactors.

The first component requires validation and calibration experiments in a variety of neutron irradiation test facilities including LWR-PV mockups, power reactor surveillance positions, and related benchmark neutron fields. The benchmarks serve as a permanent reference measurement for neutron flux and fluence detection techniques, which are continually under development and widely applied by laboratories with different levels of capability. The second component requires a serious extrapolation of an observed neutron-induced mechanical property change from test reactor "Test Regions" and operating power reactor "Surveillance Positions" to locations inside the body of the pressure vessel wall and to ex-vessel support structures. The neutron flux at the vessel inner wall is up to one order of magnitude lower than at surveillance specimen positions and up to two orders of magnitude lower than for test reactor positions. At the vessel outer wall, the neutron flux is one order of magnitude or more lower than at the vessel inner wall. Further, the neutron spectrum at, within, and leaving the vessel is substantially different.

In order to meet the reactor pressure vessel radiation monitoring requirements, a variety of neutron flux and fluence detectors are employed, most of which are passive. Each detector must be validated for application to the higher flux and harder neutron spectrum of the test reactor "Test Region"

and to the lower flux and degraded neutron spectrum at "Surveillance Positions." Required detectors must respond to neutrons of various energies so that multigroup spectra can be determined with accuracy sufficient for adequate damage response estimates. Proposed detectors for the program include radiometric detectors, helium accumulation fluence monitors, solid state track recorders, and damage monitors.

The necessity for pressure vessel mockup facilities for dosimetry investigations and for irradiation of metallurgical specimens was recognized early in the formation of the NRC program. Experimental studies associated with high and low flux versions of a PWR pressure vessel mockup are in progress. The low flux version is known as the Poolside Critical Assembly (PCA) and the high flux version is known as the Poolside Facility (PSF). Both are located at ORNL. As specialized benchmarks, these facilities will provide well-characterized neutron environments where active and passive neutron dosimetry, various types of LWR-PV neutron field calculations, and temperature-controlled metallurgical specimen exposures are brought together.

The results of the measurement and calculational strategies outlined here will be made available for use by the nuclear industry as ASTM Standards. Federal Regulation 10CFR50 already requires adherence to several ASTM Standards that establish a surveillance program for each power reactor and incorporate flux monitors and neutron field evaluation. Revised and new standards in preparation will be carefully up-dated, flexible, and, above all, consistent.

CONTENTS

		Page
	Foreword	iii
	Figures	ix
	Tables	xi
	Acronyms	xii
	Acknowledgments	xiii
	Summary	S-1
HANFORD ENGINEERING DEVELOPMENT LABORATORY		HEDL-1
A.	Investigation and Verification of the Physics-Dosimetry-Metallurgy for Reactor Pressure Vessels and Support Structures Surveillance	HEDL-3
B.	Buffon Needle Method of Track Counting	HEDL-13
C.	Neutron Response Characteristics of CR-39 Polymer for Reactor and Dosimetry Applications	HEDL-25
D.	Optical Efficiency and Observer Objectivity for Fission Track Counting in Muscovite Solid State Track Recorders	HEDL-31
E.	Investigations of Effects of Reactor Core Loadings on PV Neutron Exposure	HEDL-35
APPENDIX	A Preliminary Study of the Use of Fuel Management Techniques for Slowing Pressure Vessel Embrittlement	HEDL-A1
OAK RIDGE NATIONAL LABORATORY		ORNL-1
A.	Light Water Reactor Pressure Vessel (LWR-PV) Benchmark Facilities (PCA, ORR-PSF, ORR-SDMF) at ORNL	ORNL-3
A-1	Pressure Vessel Benchmark Facility for Improvement and Validation of LWR Physics Calculations and Dosimetry (PCA)	ORNL-4
A-2	Pressure Vessel Benchmark Facility for LWR Metallurgical Testing of Reactor Pressure Vessel Steels (ORR-PSF)	ORNL-5

CONTENTS (Cont'd)

		Page
A-3	Surveillance Dosimetry Measurement Benchmark Facility (SDMF) for Validation and Certification of Neutron Exposures from Power Reactor Surveillance	ORNL-9
B.	ASTM Standards for Surveillance of Nuclear Reactor Pressure Vessels	ORNL-10
APPENDIX	Standard Guide for Application of Neutron Transport Methods for Reactor Vessel Surveillance [E706(II-D)]	ORNL-A1

FIGURES

Figure		Page
S-1	ASTM Standards for Surveillance of LWR Nuclear Reactor Pressure Vessels and Support Structures	S-2
S-2	ASTM LWR Standards Preparation Schedule	S-3
HEDL-1	Linear Least Squares Fit of the Visual Track Density Data ρv as a Function of -ln$p$ for "Rod" and "Point" Sampling	HEDL-21
HEDL-2	Track Diameter vs Total Energy for Normally Incident α-Particle Tracks on CR-39 Polymer	HEDL-28
HEDL-3	Diameter Distribution of Proton-Recoil Tracks Produced by 14-MeV Neutron Bombardment of CR-39 Polymer and a 2250-μm Polyethylene Proton Radiator	HEDL-30
HEDL-A1	Type A PWR with Two Types of Capsules	HEDL-A16
HEDL-A2	Mesh Line Description for (R,θ) Analysis of the Type A Reactor with Two Types of Surveillance Capsules	HEDL-A17
HEDL-A3	Dpa Exposure on the Vessel Inner Face for a Type A PWR	HEDL-A18
HEDL-A4	Dpa/Fluence vs Radial Position for a Type A PWR	HEDL-A19
HEDL-A5	Capsule Perturbation for a Type A PWR at the 3° Angular Position	HEDL-A20
HEDL-A6	Capsule Perturbation for a Type A PWR at the 35% Position	HEDL-A21
HEDL-A7	Type B, 2-Loop Reactor Geometry	HEDL-A22
HEDL-A8	(R,θ) DOT Mesh Detail Map for a Type B, 2-Loop Shield Reactor	HEDL-A23
HEDL-A9	Dpa Exposure on the Vessel Inner Face of a Type B, 2-Loop Shield Reactor	HEDL-A24
HEDL-A10	Capsule Flux Perturbation Effect for a 13° Capsule of a Type B, 2-Loop Shield Reactor with a Normal Fuel Loading	HEDL-A25
HEDL-A11	Capsule Perturbation for a Type B, 2-Loop Shield Reactor	HEDL-A26
HEDL-A12	Dpa/Fluence vs Radial Position for a Type B, 2-Loop Shield Reactor	HEDL-A27

FIGURES (Cont'd)

Figure		Page
HEDL-A13	Type C, 3-Loop Shield Reactor	HEDL-A28
HEDL-A14	(R,θ) DOT Mesh for a Modified Fuel, Type C, 3-Loop Shield Reactor	HEDL-A29
HEDL-A15	Dpa Exposure on the Vessel Inner Face of a Type C, 3-Loop Shield Reactor	HEDL-A30
HEDL-A16	Dpa/Fluence for a Type C, 3-Loop Shield Reactor	HEDL-A31
HEDL-A17	(x,y) Map for the Midplane of a Type D, 4-Loop Shield Reactor	HEDL-A32
HEDL-A18	(R,θ)DOT Map for the Midplane of a Modified Fuel, Type D, 4-Loop Shield Reactor	HEDL-A33
HEDL-A19	Dpa Exposure on the Vessel Inner Face of a Type D, 4-Loop Shield Reactor	HEDL-A34
HEDL-A20	Dpa/Fluence vs Radial Position for a Type D, 4-Loop Shield Reactor	HEDL-A35
HEDL-A21	Dpa at 1/4 T Position of a Type D, 4-Loop Shield Reactor	HEDL-A36
HEDL-A22	(x,y) Map for the Midplane of a Type E, 3-Loop Pad Reactor	HEDL-A37
HEDL-A23	(R,θ) DOT Map for a Type E, 3-Loop Pad Reactor	HEDL-A38
HEDL-A24	Dpa Exposure on the Vessel Inner Face of a Type E, 3-Loop Pad Reactor	HEDL-A39
HEDL-A25	Dpa Exposure at the 1/4 T Position in the Pressure Vessel of a Type E, 3-Loop Pad Reactor	HEDL-A40
HEDL-A26	Dpa/Fluence vs Radial for a Type E, 3-Loop Pad Reactor	HEDL-A41
HEDL-A27	Midplane Geometry for a Type F, 4-Loop Pad Reactor	HEDL-A42
HEDL-A28	(R,θ) DOT Map for a Type F, 4-Loop Pad Reactor	HEDL-A43
HEDL-A29	Dpa Exposure on the Vessel Inner Face of a Type F, 4-Loop Pad Reactor	HEDL-A44
HEDL-A30	Dpa/Fluence vs Radial Position for a Type F, 4-Loop Pad Reactor	HEDL-A45

TABLES

Table		Page
HEDL-1	Buffon Needle Track Densities from SEM Observations of Mica SSTR	HEDL-19
HEDL-2	CR-39 Sensitivity Obtained with Various Radiator Foils	HEDL-29
HEDL-3	Exposure and Track Counting Data	HEDL-33
HEDL-A1	Energy Group Structure and Fission Spectrum for DOT Calculations	HEDL-A4
HEDL-A2	Summary of Fuel Management Results	HEDL-A46
ORNL-1	Cumulative Irradiation and Temperature Distribution Data Through December 31, 1981	ORNL-6
ORNL-2	Cumulative Irradiation and Temperature Distribution Data from 1148, June 1, 1981, through 0200, September 25, 1981	ORNL-8

ACRONYMS

ASTM	American Society for Testing and Materials
BSR	Bulk Shielding Reactor
BWR	Boiling Water Reactor
CEN/SCK	Centre d'Études Nucleaires de Saclay (France)
ENSA	Engineering Services Associates
EPRI	Electric Power Research Institute
FBR	Fast Breeder Reactor
FSAR	Final Safety Analysis Review
HEDL	Hanford Engineering Development Laboratory
KFA	Kernforschungsanlage (Jülich, Germany)
LWR	Light Water Reactor
MEA	Materials Engineering Associates
MFR	Magnetic Fusion Reactor
NBS	National Bureau of Standards
NRC	Nuclear Regulatory Commission
ORNL	Oak Ridge National Laboratory
ORR	Oak Ridge Research Reactor (ORNL)
PCA	Poolside Critical Assembly
PSF	Poolside Facility (ORNL)
PV	Pressure Vessel
PWR	Pressurized Water Reactor
QA	Quality Assurance
RI	Rockwell International
SDIP	Surveillance Dosimetry Improvement Program
SDMF	Simulated Dosimetry Measurement Facility
SEM	Scanning Electron Microscope
SRM	Standard Reference Material
SSC	Simulated Surveillance Capsule
SSTR	Solid State Track Recorder
TLD	Thermoluminescent Dosimeter
UK	United Kingdom
WRSR	Water Reactor Safety Research

ACKNOWLEDGMENTS

The following organizations are presently participating in the Light Water Reactor Pressure Vessel Surveillance Dosimetry Improvement Program and will periodically contribute written reports, experimental data, or calculations.

Atomic Energy Research Establishment (AERE-H), Harwell, UK

Babcock & Wilcox Company (B&W), USA

Battelle Memorial Institute (BMI), Columbus Laboratory, USA

Brookhaven National Laboratory (BNL), USA

Centre d'Etude de l'Energie Nucleaire - Studiecentrum Voor Kernenergie (CEN/SCK), Mol, Belgium

Centre d'Etudes Nucleaires de Saclay (CEA, Saclay), Gif-sur-Yvette, France

Combustion Engineering, Inc. (CE), USA

EG&G ORTEC, USA

Electric Power Research Institute (EPRI), USA

Engineering Services Associates (ENSA), USA

Fracture Control Corporation (FCC), USA

General Electric Vallecitos Nuclear Center (GE-VNC), USA

Hanford Engineering Development Laboratory (HEDL), USA

Institüt für Kernenergetik und Energiesysteme der Universitat Stuttgart (IKE), Stuttgart, Germany

IRT Corporation (IRT), USA

Italian Atomic Power Authority (ENEL), Italy

Japan Atomic Energy Research Institute (JAERI), Japan

Kernforschungsanlage Jülich Gmbh (KFA), Germany

Kraftwerk Union, Germany

Materials Engineering Associates (MEA), USA

National Bureau of Standards (NBS), USA

Oak Ridge National Laboratory (ORNL), USA

Radiation Research Associates (RRA), USA

Rockwell International Energy Systems Group (RI-ESG), USA

Rolls-Royce and Associates Limited (RRAL), Derby, UK

Science Applications Incorporated (SAI), USA

Ship Research Institute (SRI), Japan

Southwest Research Institute (SWRI), USA

University of Arkansas (UA), USA

University of California, Santa Barbara (UCSB), USA

University of Tennessee (UT), USA

University of Tokyo, Japan

Westinghouse Electric Corporation - Nuclear Technology Division

Westinghouse Electric Corporation - Research and Development Division (WR&D)

SUMMARY

HANFORD ENGINEERING DEVELOPMENT LABORATORY (HEDL)

A brief program status report is presented with a list of planned NUREG reports that addresses individual and combined PWR and BWR physics-dosimetry-metallurgy issues. They will provide a reference base of information to support the preparation of the new set of LWR ASTM Standards (Figures S-1 and S-2).

A technique involving shifting of core fuel loadings was investigated as a method for reducing the neutron flux at points of high damage accumulation in the pressure vessel wall of a light water reactor. Calculations were run for six types of commercial generic PWR. In general, the fuel modification appears capable of reducing the existing exposure rate at the position of the existing maximum by factors of 5.8 to 17.9. The position of the maximum exposure point is shifted, however, and the ratio of the old maximum to the new maximum ranges between 1.58/1.0 and 3.44/1.0. Reference benchmark physics-dosimetry data will be obtained in FY 83-84 to help provide experimental verification of the accuracy of these and other calculations. The Mol, Belgium's VENUS and Winfrith, UK's NESDIP mockup tests of PWR core, pressure vessel, and cavity regions will be used for the benchmarking.

To support the experimental verification of the predicted effects from different fuel management schemes on neutron exposures to pressure vessels and support structures for operating LWR power plants, information is provided on the progress being made to develop and apply the Solid State Track Recorder (SSTR) method for in-situ in- and ex-vessel measurements of neutron exposure parameter values, such as fluence (E >1.0 MeV) and dpa in iron.

A new technique of quantitative track counting, the Buffon needle method, is advanced. It is based on random sampling of the SSTR surface. This new method extends quantitative track scanning to track densities well up into the track pile-up regime. The counting of high densities of tracks for

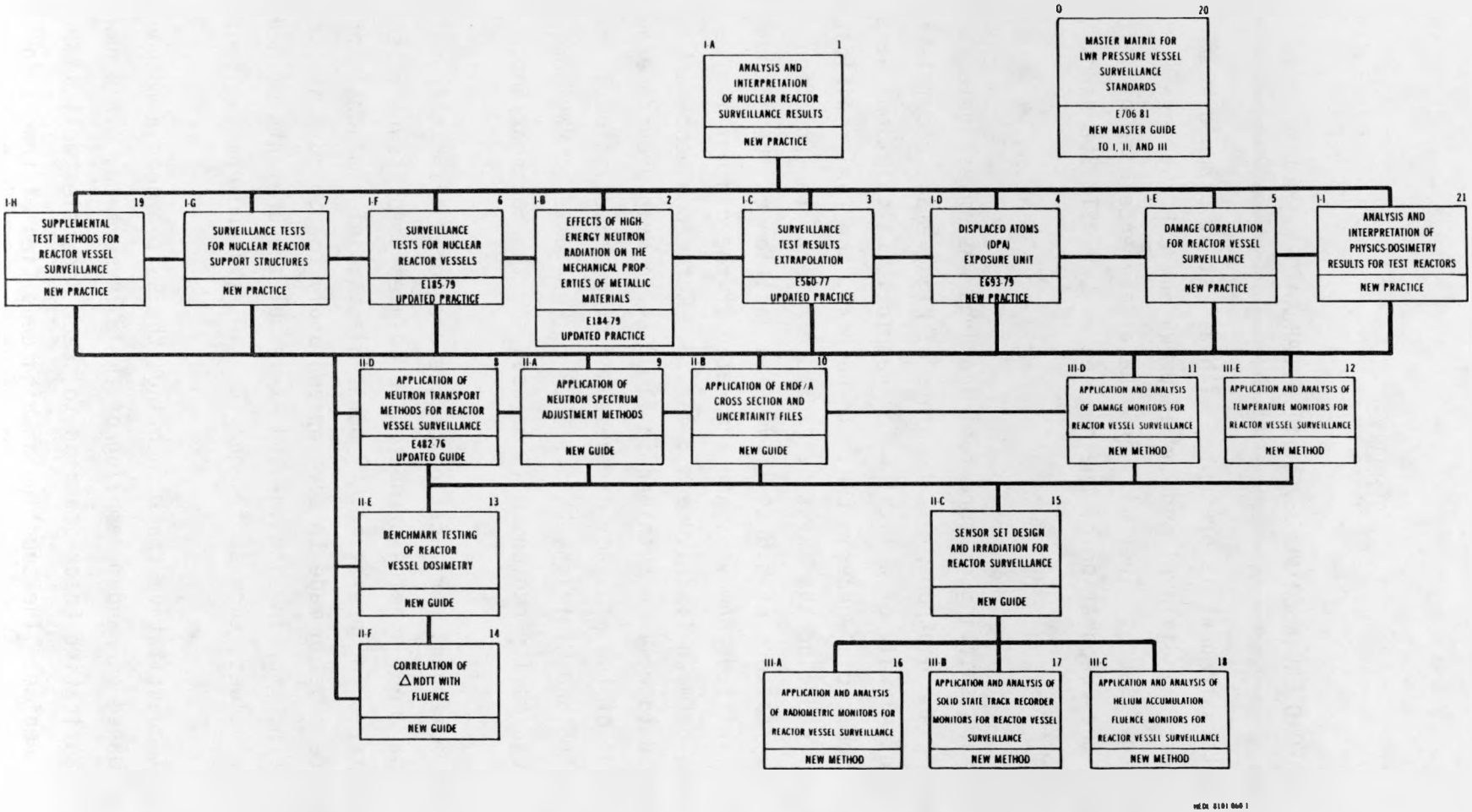

FIGURE S-1. ASTM Standards for Surveillance of LWR Nuclear Reactor Pressure Vessels and Support Structures.

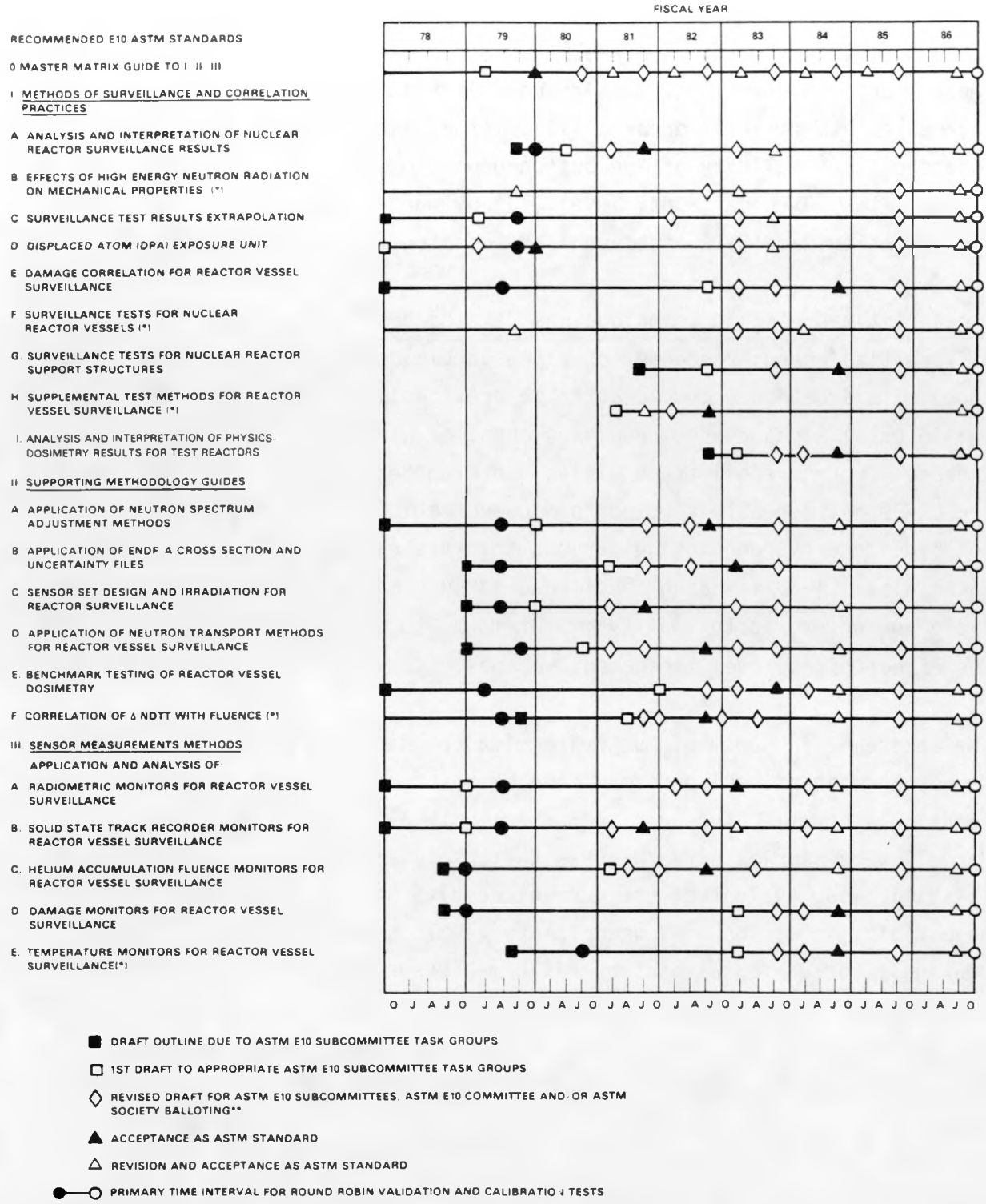

FIGURE S-2. ASTM LWR Standards Preparation Schedule.

HEDL 8202-144

^{235}U, ^{238}U, and ^{237}Np SSTR is required for high fluence in-vessel surveillance capsule applications of SSTR. The Buffon needle method shows a reduced dependence upon both track density nonuniformity and track size distribution. Sources of experimental error arising in the Buffon needle method are assessed. The validity of the Buffon needle method is demonstrated down to at least the 10% uncertainty level (1σ) by manual sampling of high fission track density mica SSTR observed with scanning electron microscopy.

A desensitized etching technique was developed that resulted in an excellent differential energy response for alpha particles in the 3- to 14-MeV energy range. This response complements the previously reported differential proton and integral alpha energy responses obtained with different etching techniques. Proton recoil track yields and diameter distributions were measured for CR-39 polymer SSTR exposed to monoenergetic neutron sources in the 0.57- to 15-MeV energy range using various thicknesses and types of proton radiator materials. CR-39 is being considered for use in low fluence LWR benchmark field and power reactor cavity measurements to support the verification of the effect of new fuel management schemes.

The optical efficiency of Muscovite mica for manual fission track counting is being redetermined to form a data base for comparison with automatic counting systems. Exposures in contact with a ^{252}Cf source prepared at Harwell were carried out. Whereas the absolute fission rate of the source is still being evaluated, the current results indicate that observer objectivity is at the 0.4% uncertainty level. Mica is now being used rather routinely for ex-vessel neutron field measurements of ^{235}U, ^{238}U, and ^{237}Np fission rates in a number of operating PWR. [Absolute measurement accuracies in the range of 3 to 10% (1σ) are required to obtain exposure parameter values (fluence $E > 1.0$ MeV, dpa, etc.) with accuracies in the 5 to 15% (1σ) range.]

OAK RIDGE NATIONAL LABORATORY (ORNL)

A coupled neutron-gamma cross section set is being generated to analyze photofission effects for the PCA and ORR LWR experiments.

Final cumulative irradiation and temperature data for the SSC-2 are reported.

Cumulative irradiation and temperature data for the Simulated Pressure Vessel Capsule through December 31, 1981 are reported.

"The ASTM Standard Guide for Application of Neutron Transport Methods for Reactor Vessel Surveillance" was balloted and approved by the E10 Committee and the E10.05 Subcommittee. The final version (Appendix 1) was sent to ASTM for final Society ballot.

HANFORD ENGINEERING DEVELOPMENT LABORATORY
(HEDL)

A. INVESTIGATION AND VERIFICATION OF THE PHYSICS-DOSIMETRY-METALLURGY FOR REACTOR PRESSURE VESSELS AND SUPPORT STRUCTURES SURVEILLANCE

W. N. McElroy - HEDL

Objective

The first objective of the present work is to ascertain the effects of reactor design and shifts in nuclear fuel core loading on the neutron field exposure parameter values of fluence (E > 1.0 MeV) and dpa at pressure vessel and support structure locations. Shifts in core loading to reduce the embrittlement rate at the points of highest accumulated damage on the pressure vessel, and the use of dpa as well as fluence (E > 1.0 MeV) are currently under consideration by the nuclear industry and licensing and regulatory bodies in the U.S. and other countries.

A second objective is to incorporate applicable information on the above in existing and/or new standards identified in the ASTM E706-81a, "Master Matrix for LWR-PV Surveillance Standards."

A third objective for LWR surveillance programs is to adapt, test, standardize and then routinely apply advanced but state-of-art, passive, active, and/or calculational dosimetry measurement and analysis methods now being used by the LWR-PV Program participants and the nuclear industry. These methods will be needed to verify the vendor/utility FSAR predictions of exposure parameter values and the effects of present reactor designs and future fuel management schemes on these values.

A fourth objective is to perform verification measurements (and analysis) that support the above and PWR and BWR plant safety, operations, licensing, and regulatory issues in a selected number of benchmark neutron and gamma fields:

1) Pool Critical Assembly (PCA) Physics-Dosimetry Pressure Vessel mockups (ORNL Chapter and References 1, 2, and 3)

2) Simulated Dosimetry Measurement Facility (SDMF) surveillance capsule mockups in the ORR-PSF (ORNL Chapter and Reference 1)

3) VENUS* PWR core source and azimuthal lead factor mockups (Reference 1)

4) NESDIP** PWR cavity and azimuthal lead factor mockups (Reference 1)

5) NBS and Mol cavity neutron and gamma standard neutron fields (References 2 and 3)

6) A number of operating LWR power plants; e.g., the H.B. Robinson low-leakage core physics-dosimetry surveillance capsule and cavity experiments (References 1, 2, and 3)

The last objective is to document the needed information in appropriate NUREG reports that address the individual and combined physics-dosimetry-metallurgy issues related to the above and that are of current concern to the utilities, vendors, service laboratories, licensing, and regulatory bodies.

In Section A of the HEDL contributions to this report, some information on the program and on planned documentation is provided that is of general interest and is relevant to the stated objectives in the HEDL, ORNL, and NBS Chapters of this, past, and future progress reports.

In Sections B, C and D, information has been gathered on work related to the adaption, testing, and documentation of measurements and analytical analyses that support the preparation and application of the ASTM Standard E706 (IIIB), "Application and Analysis of Solid State Track Recorder (SSTR)

*Critical facility at Mol, Belgium.
**NESTOR Reactor Surveillance Dosimetry Improvement Program (NESDIP) Ex-Vessel Cavity Mockup at Winrith, UK.

Monitors for Reactor Vessel Surveillance." Extensive use of the SSTR method is anticipated for surveillance capsule and reactor cavity measurements to provide experimental verification of FSAR predictions of key neutron exposure parameter values [fluence (E > 1.0 MeV), and dpa in iron] and the effects of reactor design and fuel management schemes on these values.

In Section E, some reactor physics work associated with the first objective related to ascertaining the effects of shifts in nuclear fuel core loading on the neutron field at the pressure vessel is considered.

Accomplishments and Status

PROGRAM REVIEW, DEFINITION, AND HIGHLIGHTS

The objective of the overall LWR Pressure Vessel Surveillance Dosimetry Improvement Program (LWR-PV-SDIP) is to make measurements in neutron field ("Benchmark" and reactor "Test and Surveillance Regions") for the subsequent validation/calibration of available state-of-the-art dosimetry, damage correlation, and associated reactor analysis data and procedures.[1-3] The data and procedures are in turn used to predict the integrated effects of neutron exposure for LWR-PV and support structure steel test irradiation and surveillance programs. The program work includes selection of the neutron fields, validation/calibration of dosimetry and damage exposure and correlation procedures in these fields, and establishment of a set of 21 ASTM-recommended standard practices, guides, and methods (see Figures S-1 and S-2).

The minutes for the 7th and 8th LWR Program Review Meeting were completed and distributed to program participants in early November 1981. Of particular interest was the establishment of preliminary plans for: 1) the VENUS (Mol, Belgium) core source and azimuthal lead factor PWR mockup tests to start in FY83 and 2) the NESDIP (Winfrith, U.K.) cavity and azimuthal lead factor PWR mockup test to start in FY82-83.

Work was completed on the preparation of a special paper on "Surveillance Dosimetry of Operation Power Plants," and the paper was presented at the NRC 9th Water Reactor Safety Research (WRSR) information meeting in late October 1981.[1] This paper was revised for presentation at the 4th ASTM-EURATOM Symposium in March 1982. A number of other HEDL papers are in preparation for presentation at this symposium. Additional information will be provided in a subsequent progress report.

Program Task A - Neutron Fields

Poolside Critical Assembly - Poolside Facility (PCA-PSF) -- SSTR were exposed simultaneously in all seven locations of the PCA 12/13 configuration to determine radial reaction rate distributions for ^{235}U, ^{238}U and ^{237}Np. The ^{238}U and ^{237}Np reaction rate measurements were also made in the PV block and void box locations of the PCA 8/7 configuration. Emulsion exposures were made in the block and void box locations of the PCA 8/7 configuration and all seven locations of the PCA 12/13 configuration. Analysis of these SSTR and emulsions is in progress.

Preliminary analysis of recent LWR-PV gamma-ray measurements in the 4/12 and 12/13 configurations reveals that acceptable data have been obtained. Preliminary Si(Li)-gamma-ray dose measurements in the 4/12 configuration agreed, within the experimental error, with Thermoluminescent Dosimeter (TLD) measurements performed by Mol in 1980.

Point Beach Capsule R Surveillance Dosimeter Quality Assurance -- Three each of the irradiated Co/Al alloy dosimeter samples were shipped to NBS along with samples of NBS standard reference material (SRM) 956, ~0.1% Co-Al. These samples will be irradiated in a certified thermal flux and returned to HEDL for radiometric analysis. The Co contents of the background-corrected samples will be determined by calculations from the certified sample using flux-fluence and thermal cross sections as well as direct ratios to the SRM material. Co/Al and Cu dosimeters were also shipped to Rockwell International (RI) for He analysis. Direct comparison of the measured total He

generated from the two Cu samples with the HEDL $^{63}Cu(n,\alpha)$ radiometric measurements reported by L. Kellogg et al. showed excellent relative agreement with the He analysis being ~8% higher. This difference is very close to that expected from the additional He production from the ^{65}Cu isotope. While some correlation work is to be done, this indicates that the Co impurity content of the Cu dosimeters is minimal and the measurement of He may indeed be a good method for post-irradiation QA confirmation of the Cu material. It was also reported by B. Oliver and H. Farrar of RI that, while four of the sample masses measured by RI agreed quite closely with those reported by HEDL, the value obtained by RI for sample 1648 (top-base Co/Al) was 12.5% higher than the HEDL-reported value. Previously, HEDL had only spot checked two of the fourteen reported wire mass values (including three Co/Al samples) and the 1648 sample was not included in the rechecks. Subsequent discussions with RI personnel and additional calculations by RI to determine the initial weight from the remaining etched specimens has confirmed this discrepancy.

Program Task B - Recommended ASTM Standards and Program Documentation

Figures S-1 and S-2 provide information on the interrelationships and schedule for the preparation and acceptance of the set of 21 ASTM standards. Results of ASTM balloting for the IA, IIA, IID, IIIB, and IIIC standards are to be discussed at the January 1982 Houston ASTM E10 Meeting. Figures S-1 and S-2 will be updated at the Houston meeting and will be reviewed by the E10.05 Nuclear Radiation Metrology and E10.02 Metallurgy Subcommittee members to better coordinate the preparation of the entire set of standards.

The following list of planned NRC NUREG reports is provided for reference purposes. These documents are expected to be completed during the period September 1982 to September 1985, with subsequent annual updating of the loose leaf documents, as required.

NUREG REPORT #1 (ISSUE DATE: SEPTEMBER 1982)
LWR-PV SURVEILLANCE DOSIMETRY IMPROVEMENT PROGRAM:
PCA DOSIMETRY IN SUPPORT OF THE PSF PHYSICS-DOSIMETRY-METALLURGY EXPERIMENTS
(4/12, 4/12 & SSC Configurations and Update of 8/7 and 12/13 Configurations)
W. N. McElroy, Editor

This document will provide reference physics-dosimetry information needed to support the analysis of the PSF metallurgical experiment. It will also provide updated and supplemental data in support of the previous publication: "PCA Experiments and Blind Test," NUREG/CR-1861, HEDL-TME 80-87, July 1981.

NUREG REPORT #2: (ISSUE DATE: SEPTEMBER 1983)
LWR-PV SURVEILLANCE DOSIMETRY IMPROVEMENT PROGRAM:
PSF PHYSICS-DOSIMETRY-METALLURGY EXPERIMENTS

Part I - PSF Physics-Dosimetry Characterization Program
W. N. McElroy, Editor

This document will provide reference startup physics-dosimetry information in support of the PSF metallurgical experiment.

NUREG REPORT #3 (ISSUE DATE: SEPTEMBER 1983)
LWR-PV SURVEILLANCE DOSIMETRY IMPROVEMENT PROGRAM:
PSF PHYSICS-DOSIMETRY-METALLURGY EXPERIMENTS

Part II - SSC-1 and SSC-2 Metallurgical Program
W. N. McElroy, Editor

This document will provide reference matallurgical information on measured property changes in a number of different pressure vessel and reference steels for simulated surveillance capsule (SSC) tests for two different neutron exposures of $\sim 2 \times 10^{19}$ and $\sim 4 \times 10^{19}$ n/cm^2 (E > 1.0 MeV).

NUREG REPORT #4 (ISSUE DATE: SEPTEMBER 1982)
LWR-PV SURVEILLANCE DOSIMETRY IMPROVEMENT PROGRAM:
LWR POWER REACTOR SURVEILLANCE PHYSICS-DOSIMETRY COMPENDIUM
W. N. McElroy and G. L. Guthrie, Editors

This loose-leaf document will provide new and/or reevaluated exposure parameter values (fluence >1.0 MeV, dpa, etc.) for individual surveillance capsules removed from operating PWR and BWR power plants--all in support of the development of the NRC-MPC-EPRI-ASTM metallurgical data bases. The document will be revised annually as information in new and old surveillance reports is reevaluated with the FERRET-SAND and other developed methodologies.

NUREG REPORT #5 (ISSUE DATE: SEPTEMBER 1984)
LWR-PV SURVEILLANCE DOSIMETRY IMPROVEMENT PROGRAM:
PSF PHYSICS-DOSIMETRY-METALLURGY EXPERIMENTS

Part III - PVS and Void Box Physics-Dosimetry Program
W. N. McElroy, Editor

This document will provide reference in-situ physics-dosimetry information in support of the PSF metallurgical experiment.

NUREG REPORT #6: (ISSUE DATE: SEPTEMBER 1984)
LWR-PV SURVEILLANCE DOSIMETRY IMPROVEMENT PROGRAM:
PSF PHYSICS-DOSIMETRY-METALLURGY EXPERIMENTS

PART IV - PVS and Void Box Metallurgy Program
W. N. McElroy, Editor

This document will provide reference metallurgical information on measured property changes in a number of different pressure vessel and reference steels for simulated PV locations at the inner surface, 1/4 T and 1/2 T positions of a PWR PV wall mockup. The corresponding neutron exposures are $\sim 4 \times 10^{19}$, $\sim 2 \times 10^{19}$, and $\sim 1 \times 10^{19}$ n/cm^2, respectively.

This document will also provide reference metallurgical information on measured property changes in a number of different pressure vessel support structure and reference steels for a simulated ex-vessel cavity neutron exposure of ~5-6 x 10^{17} n/cm^2 (E > 1.0 MeV)*.

NUREG REPORT #7 (ISSUE DATE: SEPTEMBER 1983)
LWR-PV SURVEILLANCE DOSIMETRY IMPROVEMENT PROGRAM:
PSF SURVEILLANCE DOSIMETRY MEASUREMENT FACILITY (SDMF)
W. N. McElroy, F. B. K. Kam, E. D. McGarry, Editors

This will be a loose-leaf volume of results to certify the accuracy of exposure paramter/perturbation effects for surveillance capsules removed from PWR and BWR power plants. It will be updated periodically, as required.

NUREG REPORT #8: (ISSUE DATE: SEPTEMBER 1985)
LWR-PV SURVEILLANCE DOSIMETRY IMPROVEMENT PROGRAM:
LWR TEST REACTOR PHYSICS-DOSIMETRY COMPENDIUM
W. N. McElroy, F. B. K. Kam, E. D. McGarry, Editors

This will be a loose-leaf volume of results from FERRET-SAND, LSL, and other least square type code analyses of physics-dosimetry for US (BSR, PSF, Buffalo, Virginia,), UK (DIDO, HERALD, etc.), Belgium (BR-2, etc.), Germany (FRJ1, FRJh, etc), and other participating countries. It will provide needed exposure parameter values (fluence E> 1.0 MeV, dpa, etc.) and uncertainties for correlating test reactor property change data with that obtained from PWR and BWR power plants (surveillance capsules).

*This estimate is based on preliminary ORNL calculations, as yet unsubstantiated by measurements.

NUREG REPORT #9 (ISSUE DATE: SEPTEMBER 1983)
LWR-PV SURVEILLANCE DOSIMETRY IMPROVEMENT PROGRAM:
VENUS PWR CORE SOURCE AND AZIMUTHAL LEAD FACTOR EXPERIMENTS AND CALCULATIONAL TESTS
A. Fabry and W. N. McElroy, Editors

This document will provide reference physics-dosimetry information on active, passive, and calculational dosimetry studies involving CEN/SCK, HEDL, NBS, ORNL, and other LWR program participants.

NUREG REPORT #10 (ISSUE DATE: SEPTEMBER 1984)
LWR-PV SURVEILLANCE DOSIMETRY IMPORVEMENT PROGRAM:
NESDIP PWR CAVITY AND AZIMUTHAL LEAD FACTOR EXPERIMENTS AND CALCULATIONAL TESTS
J. Butler, M. Austin, A. Fudge, and W. N. McElroy, Editors

This document will provide reference physics-dosimetry information on active, passive, and calculational dosimetry studies involving Winfrith, CEN/SCK, HEDL, NBS, and other LWR program participants.

Program Task C - Damage Exposure and Correlation Procedures

Calculations have been made that indicate the use of $\phi(E > 1\ MeV)$ results in a nonconservative estimate of the neutron-produced embrittlement for deep penetration in the PV wall. Calculations made for a PWR power plant and in the adjusted spectrum from the PCA data indicate that a more accurate exposure indicator is dpa. The damage produced, as indicated by dpa, is about 50% higher at the 3/4 T position when compared to damage calculated using $\phi(E > 1\ MeV)$.

The major DOT-III transport calculations have been completed in the cooperative HEDL-WNTD (Westinghouse-Nuclear Technology Division) effort. The calculations were intended to indicate whether simple mid-life shifts in core loading could be used to cause a significant reduction in the rate of embrittlement at the points on the vessel wall that have accumulated the

highest level of neutron damage. The calculations were done for six generic reactor types for two different vendors. It appears that replacement of corner fuel subassemblies reduces the rate of damage accumulation by factors ranging from 5/1 to 18/1 at the points of highest damage accumulations. The long-term critical point on the PV wall then shifts to a less damaged region where the rate of accumulation has remained essentially unchanged and the resultant extension of life expectancy is the order of a factor of 1.6/1 to 3.5/1 (see Section E).

Expected Future Accomplishments

To provide updated program status reports and comments on program direction, results, and planned documentation.

References

1. W. N. McElroy et al., "Surveillance Dosimetry of Operating Power Plants," HEDL SA-2546, Proceedings of the NRC 9th Water Reactor Safety Research Information Meeting, October 1981 and the 4th ASTM-EURATOM Symposium on Reactor Dosimetry, March 1982. (This report also serves as the 1981 Annual Report for the LWR-PV-Surveillance Dosimetry Improvement Program).

2. W. N. McElroy et al., LWR-PV-Surveillance Dosimetry Improvement Program: 1980 Annual Report, NUREG/CR-1747, HEDL-TME 80-73, Nuclear Regulatory Commission, Washington, DC, March 1981.

3. W. N. McElroy et al., LWR-PV-Surveillance Dosimetry Improvement Program: 1979 Annual Report, NUREG/CR-1291, HEDL-SA-1949, Nuclear Regulatory Commission, Washington, DC, February 1980.

B. BUFFON NEEDLE METHOD OF TRACK COUNTING

R. Gold, J. H. Roberts and F. H. Ruddy - HEDL

Objective

Define the limitations of solid state track recorders (SSTRs) for in-vessel surveillance capsule and cavity dosimetry in light water reactor pressure vessel (LWR-PV) environments. To this end, Standard E706(IIIB) entitled: "Application and Analysis of Solid State Track Recorder (SSTR) Monitors for Reactor Vessel Surveillance" was prepared within the ASTM Master Matrix for LWR-PV Standards E706-81a. In high fluence LWR-PV irradiations, track pileup can become significant. Hence, techniques are required to determine precise correction factors for track pileup at high track density. Implementation of such techniques for automated SSTR scanning systems will significantly enhance the cost effectiveness of SSTR dosimetry for LWR-PV applications.

Summary

A new technique of quantitative track counting, the Buffon needle method, is advanced. It is based on random sampling of the SSTR surface. This new method extends quantitative track scanning to track densities well up into the track pile-up regime. The Buffon needle method possesses a reduced dependence upon both track density nonuniformity and track size distribution. Sources of experimental error arising in the Buffon needle method are assessed. The validity of the Buffon needle method is demonstrated down to at least the 10% uncertainty level (1σ) by manual sampling of high fission track density mica SSTR observed with scanning electron microscopy.

Accomplishments and Status

Due to the high sensitivity of the SSTR method, track pileup represents a significant limitation in quantitative applications. This is especially true for neutron-induced reaction rate measurements in high fluence in-situ reactor irradiations.[1-4]

Pile-up effects are negligible using optical microscopy and manual scanning techniques at track densities $<10^5$ tracks/cm^2. However, difficulties arise as track density ρ increases. In fact, for $\rho > 2 \cdot 10^6$ tracks/cm^2, track pileup can be extensive enough to preclude quantitative manual scanning using optical microscopy. Even at lower track densities where manual scanning is still possible, experimental error is increased because pileup decreases the objectivity of manual scanning observations.

Hence, methods or techniques capable of extending quantitative track scanning into the high density pile-up region would be quite useful. In particular, methods that can be applied independent of track size are highly desirable.

Effects of pileup were recognized in earlier quantitative work with a computer-controlled optical microscopy system developed for automated SSTR scanning.[5-7] In these efforts, a useful correspondence was introduced between track scanning and the pulse counting techniques of nuclear instrumentation. On the basis of this analogy, the simple paralyzable counter model was introduced to describe track pileup, and this model provided excellent agreement with experimental results.

The success demonstrated by accurately describing these automated SSTR data confirmed a very simple formula for the probability p of observing tracks without pileup, namely:

$$p = e^{-\alpha\rho}, \qquad (1)$$

where α is the characteristic area for track pileup. In the theory of stochastic processes,[8-9] this exponential holding formula is characteristic of the simplest continuous Markovian stochastic process, namely a Poisson process.

This simple Poisson holding formula forms the basis of a new track scanning method. Equation (1) provides a means to determine the (true) track density ρ in terms of probability p. Hence, rather than attempt to count individual

tracks directly, as is customary in manual scanning, one has the alternative of measuring probability p and then solving Eq. (1) for ρ. One has the simple relation

$$\rho = -\alpha^{-1} \ln p. \tag{2}$$

Since p is the probability of the available area (i.e., relative to the total area scanned) for observing tracks without pileup, it is possible to measure p using random sampling techniques. In this method, the SSTR surface is randomly sampled and one tallies whether the area element sampled is occupied by tracks or not. The area element sampled can be chosen to be the mean track area $\bar{X}$. In the limit of a sufficiently high number of trials, the ratio of unoccupied trials to total trials will approach p. This SSTR random sampling technique represents the simplest type of discrete stochastic chain process, namely a Markovian process, since each sample is obviously independent of the outcome of previous sampling results.

This concept was first tested manually by randomly striking onto the surface of scanning electron microscope (SEM) microphotographs of fission tracks in mica SSTR with the end of a rod. The area of the end of the rod was chosen to match the mean track area $\bar{X}$. In an attempt to maintain a random (unbiased) sampling technique, the microphotograph was not viewed during the striking process. Such a manual random sampling technique possesses an illustrious historical analogue, namely the famous "Buffon needle" problem considered in the 18th century by the Count de Buffon (1707-1788). Hence, Gold, Ruddy, and Roberts have called this track counting technique the Buffon needle method.[10] Correspondingly, the characteristic area parameter α is called the Buffon area.

An expression for the uncertainty in the track density deduced by the Buffon needle method is easily obtained from Eq. (2):

$$(\delta\rho/\rho)^2 = (\delta\alpha/\alpha)^2 + (\ln p)^{-2} \cdot (\delta p/p)^2, \tag{3}$$

where $(\delta\rho/\rho)^2$, $(\delta\alpha/\alpha)^2$, and $(\delta p/p)^2$ are the relative variances of ρ, α, and p, respectively. The binomial probability distribution provides a valid description of random sampling estimates of p. Hence, for the n random trials, the relative variance of p is given by

$$(\delta p/p)^2 = \frac{p^{-1} - 1}{n} \quad . \tag{4}$$

Thus, Eq. (3) becomes

$$(\delta\rho/\rho)^2 = (\delta\alpha/\alpha)^2 + (\ln p)^{-2} (p^{-1} - 1)/n. \tag{5}$$

The first term in Eq. (5) represents the error component arising from the uncertainty in the Buffon area α. The Buffon area can be determined in a number of different ways. The earlier work of Gold and Cohn[6] with the computer-controlled optical microscopy system illustrates a method that can, in principle, determine the Buffon area very accurately. Another method, which utilizes the Buffon needle method itself to measure α, is illustrated below.

The second term in Eq. (5) provides the error component introduced through random sampling. This expression can be compared with the error that arises in ordinary manual track scanning, where Poisson statistics are applicable.[11] Hence, the relative error in the observation of n tracks by manual scanning is simply $n^{-1/2}$. Assuming a one-to-one correspondence between the number of random trials and the number of observed tracks, one finds that the factor $|(\ln p)^{-1} \cdot (p^{-1}-1)^{1/2}|$ expresses the deviation of the relative error of random sampling from that of ordinary track counting statistics.

Outside the neighborhood of the two singularities at $p = 0$ and $p = 1$, the increase in relative error is modest. In fact, in the region $0.01 \leq p \leq 0.9$, the increase in relative error ranges from $\sim$1.25 up to 3.0. This overall interpretation requires some caution, however, since this comparison tacitly assumes that a single random trial of the Buffon needle method and the manual observation of a single track can be carried out with equal effort. However, this assumption is not generally valid. Indeed for automated systems, random sampling requires considerably less effort.

EFFECTS DUE TO NONUNIFORM TRACK DENSITY AND TRACK SIZE DISTRIBUTION

In SSTR work, variation of both track density and track size produce limitations in quantitative manual track scanning. Hence, it is important to examine the consequences of nonuniform track density and track size distribution for the Buffon needle method. On the basis of a more general analysis that accounts for both of these effects, it can be shown that

$$\rho_0 = \frac{\alpha_0}{\sigma_\alpha^2}\left\{1 - \left[1 - \frac{\sigma_\alpha^2}{\alpha_0^2}\left(\sigma_\rho^2\alpha_0^2 - 2[1-\sigma_\alpha^2\sigma_\rho^2]\right.\right.\right. \cdot \ln[(1-\sigma_\alpha^2\sigma_\rho^2)^{1/2}\bar{p}]\left.\left.\right)\right]^{1/2}\left.\right\} \tag{6}$$

where ρ_0 and σ_p are the mean and standard deviation of the track density distribution, respectively; and α_0 and σ_α are the mean and standard deviation of the Buffon area distribution, respectively. Equation (6) can be used to obtain a solution for ρ_0 in series expansion form. To first order in $(\sigma_\alpha\sigma_\rho)^2$, one finds

$$\rho_0 = \frac{-\ln\bar{p}}{\alpha_0} + \frac{\ln\bar{p}}{\alpha_0}\left[\frac{\eta_\alpha^2}{2}\ln\bar{p} - \frac{\eta_\alpha^4}{2}(\ln\bar{p})^2\right] + \frac{\alpha_0\sigma_\rho^2}{2}$$

$$+ \frac{(\sigma_\alpha\sigma_p)^2}{2\alpha_0}\left[1 + \ln\bar{p} - \eta_\alpha^2\ln\bar{p} - 2\eta_\alpha^2(\ln\bar{p})^2\right], \tag{7}$$

where $\eta_\alpha = \sigma_\alpha/\alpha_0$ and $\eta_\rho = \sigma_\rho/\rho_0$ are the relative standard deviations of α and ρ, respectively.

In this series representation, terms are grouped to correspond to different physical effects. The first term represents the simple Buffon needle result given in Eq. (2) in absence of both effects. The second term in Eq. (7)

represents the effect due to the track area distribution alone, whereas the third term represents the effect of the track density distribution alone. The last term in Eq. (7) represents the interaction between these two effects, since this term obviously vanishes if either $\sigma_\rho \to 0$ or $\sigma_\alpha \to 0$. In the special cases wherein either effect is negligible, proper expressions can be obtained by evaluation of Eqs. (6) or (7) in the limit $\sigma_\alpha \to 0$ or $\sigma_\rho \to 0$.

While the magnitude of the various terms in Eq. (7) will obviously depend on the values of $\bar{p}$, α_0, σ_α, and σ_ρ, it is apparent that effects due to nonuniform track density and track size distribution are only of second order. Hence, the Buffon needle method possesses the significant advantage of a reduced dependence upon both track density nonuniformity and track size distribution.

SEM APPLICATION OF THE BUFFON NEEDLE METHOD

Extensive SSTR neutron dosimetry was conducted in a critical assembly mockup of a LWR-PV.[12] Since results of the highest possible accuracy were desired, all of these SSTR were simultaneously etched using the standardized procedure developed for mica. While most of these SSTR possessed acceptable track density, six of mica SSTR used with asymptotically thick deposits had very high track density. It was decided to use SEM techniques so that these six high track density SSTR could be examined at higher magnification. However, even at ~2000X, pileup made it difficult to manually scan these SSTR accurately and objectively.

To apply the Buffon needle method to these SSTR, ten microphotographs were taken of each SSTR. With each SSTR, randomly selected surface areas were chosen for these ten SEM microphotographs. Approximately 100 random samples were carried out on each microphotograph, or a total of about 1000 random samples for each SSTR. Measured values of p obtained for these six mica SSTR are summarized in Table HEDL-1.

To deduce track densities from these measurements, the Buffon area α must be known. In this work, α was measured using the Buffon needle method itself. In this case, Eq. (1) is not solved for ρ, but rather for α. One has

$$\alpha = -\rho^{-1} \cdot \ln p. \qquad (8)$$

The uncertainty in this determination of α is given by

$$(\delta\alpha/\alpha)^2 = (\delta\rho/\rho)^2 + (\ln p)^{-2} \cdot \left(\frac{p^{-1} - 1}{n}\right). \qquad (9)$$

In order to measure α with the Buffon needle method, ten randomly selected SEM microphotographs were taken of a low fission track density mica SSTR. In these measurements, the track density ρ was obtained by directly counting tracks in each of the ten SEM microphotographs. The chosen SSTR possessed a track density low enough to avoid any pileup recognition problems at the chosen SEM magnification, ~2000X. Approximately 100 random samples were taken on each SEM microphotograph. The mean value for the Buffon area obtained from these ten SEM microphotographs was $\alpha = (4.58 \pm 0.36) \times 10^{-7}$ cm^2.

Track densities for the six high density SSTR were obtained using this Buffon needle measured value of α in Eq. (2) together with the observed p values. Resulting track densities, given in Table HEDL-1, range from 1.9 to 3.8 x 10^6 tracks/cm^2. The relative error in these track density measurements is about 10% and is dominated by the 9% relative error in α.

TABLE HEDL-1

BUFFON NEEDLE TRACK DENSITIES* FROM SEM OBSERVATIONS OF MICA SSTR

Dosimeter Label	p	ρ	ρ_o	ρ_v**	ρ_v/ρ_o
23-28-1′	0.405 ± 0.015	2.00 ± 0.20	2.02 ± 0.20	2.02	1.00
23-28-2′	0.339 ± 0.013	2.39 ± 0.23	2.44 ± 0.23	2.21	0.91
23-28-3′	0.306 ± 0.014	2.47 ± 0.24	2.53 ± 0.24	2.90	1.15
23-28-4′	0.288 ± 0.014	2.76 ± 0.27	2.84 ± 0.27	3.28	1.15
23-28-5′	0.422 ± 0.015	1.91 ± 0.19	1.93 ± 0.19	2.00	1.04
24-25-3′	0.178 ± 0.012	3.82 ± 0.37	4.01 ± 0.37	3.66	0.91
				Average:	1.03 ± 0.11

*Units of 10^6 tracks/cm^2.
**10% (1σ) uncertainty was estimated for visual SEM observations.

On the basis of the higher order treatment described by Eqs. (6) and (7), corrected Buffon needle results were obtained. The corrected Buffon area was $\alpha_0 = (4.63 \pm 0.37) \times 10^{-7}$ cm^2 and corrected ρ_0 track densities are included in Table HEDL-1. It can be seen that correction for higher order effects ranges from ∿1 to 5%.

An attempt to confirm these corrected Buffon needle results was carried out by visually scanning these SEM microphotographs. However, this task is obviously not straightforward. Due to pileup, the number of tracks observed is often ambiguous. Consequently, the objectivity of such observations cannot be guaranteed. Nevertheless, ∿300 tracks were counted for each of these mica SSTR dosimeters and the corresponding area scanned on the SEM microphotographs was determined. The visual track density so obtained, ρ_v, can also be found in Table HEDL-1.

The deviation between visual and corrected Buffon needle track densities is within experimental error for each of these six comparisons. In fact, the observed absolute deviations between visual and corrected Buffon needle track densities averaged over these six SSTR is only about 9%. Hence, this comparison provides confirmation of the validity of the Buffon needle method down to at least the 10% uncertainty level (1σ).

An alternative comparison can be obtained using the (ρ_v, p) data points. A linear least squares fit of the ρ_v data as a function of (-lnp) is presented in Fig. HEDL-1. This least squares fit verifies the simple Poisson holding formula and provides a Buffon area value of $\alpha = (4.55 \pm 0.78) \times 10^{-7}$ cm^2. This least squares value of α is in excellent agreement with the Buffon area obtained by random sampling. Consequently, this alternative comparison again confirms the validity of the Buffon needle method.

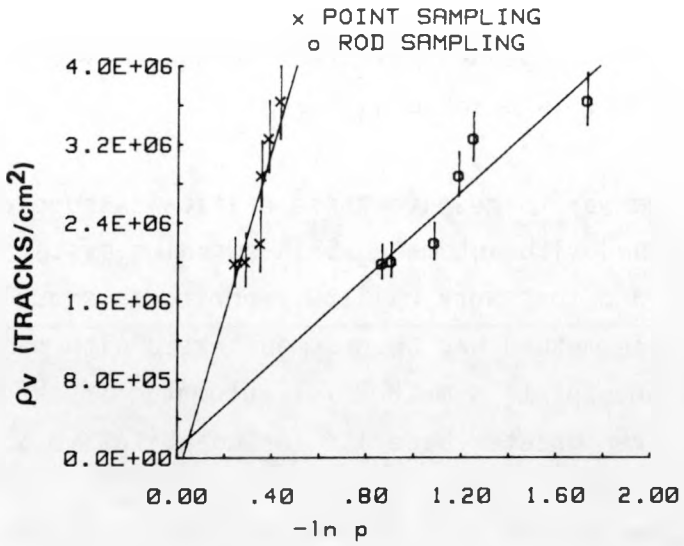

FIGURE HEDL-1. Linear Least Squares Fit of the Visual Track Density Data ρ_V as a Function of -lnp for "Rod" and "Point" Sampling. Neg 8106492-3

The same microphotographs of these six dosimeters were then sampled randomly with a point instead of the end of a rod. The least squares fit of these "point" sampling data, as shown in Fig. HEDL-1, also verifies the simple Poisson holding formula. However, for "point" sampling, the Buffon area should simply be the average track size. Direct SEM observations yielded an average track size of $(0.94 \pm 0.26) \times 10^{-7}$ cm^2. On the other hand, the Buffon area obtained from the least squares analysis of the "point" sampling data was $\alpha = (1.18 \pm 0.28) \times 10^{-7}$ cm^2. This excellent agreement provides an independent confirmation of the validity of the Buffon needle method.

Conclusions

The comparisons presented above confirm the validity of the Buffon needle method. This does not imply that the method is actually applicable without limitations. Of particular interest is the domain of track density over which the Buffon needle method is applicable. Efforts to date have confirmed that this method can be used to extend quantitative SSTR scanning by at least an

order of magnitude in track density. In spite of these efforts, the domain of validity of the simple Poisson holding formula, which underlies the Buffon needle method, has not been definitively established. Indeed, the concept of a Buffon area α that is independent of track density may possess only a limited range of validity in track density space.

Work is currently underway to resolve these critical issues. Application of the Buffon needle method with automated SSTR scanning systems is being used in these investigations and this work will be reported in sequel. In this regard, while the Buffon needle method has been demonstrated with manual techniques, the intrinsic advantages of this method for automated track scanning can be expected to produce even greater benefits for quantitative SSTR work.

Indeed, a major factor limiting the cost-effectiveness of the SSTR method is the necessity of visual or manual counting of tracks, a task that requires care, patience, and dedication. This drawback is clearly manifested in precision measurements, where inherent statistical limitations require the observation of large numbers of tracks for adequate precision and make this task time consuming as well as expensive. As a consequence, automation of this task has been aggressively pursued for some time now for LWR, FBR, and MFR development programs at HEDL and elsewhere.

As has occurred so often in scientific pursuits, help toward the solution of this automation problem has arisen in the most unexpected way. In this particular case, a completely new approach for automated track scanning has been engendered by the existence of track pileup at high track density. Efforts to treat this pile-up effect have opened up an entirely new direction for automated track scanning, namely the random sampling techniques of the Buffon needle method. The reduced dependence of the Buffon needle method upon both track density nonuniformity and track size distribution are very important advantages for automated track scanning. However, an even more significant advantage exists, namely elimination of the need for pattern recognition of tracks in the automation process. This rather complex procedure can now be replaced, in principle, with the simple random sampling techniques used in the Buffon needle method.

Expected Future Accomplishments

Establish the applicability and limitations of the Buffon needle method with automated SSTR scanning systems.

References

1. J. H. Roberts and R. Gold, "SSTR and Emulsion Techniques and Their Applications for FBR, LWR, and MFR Programs," Dosimetry Methods for Fuels, Cladding, and Structural Materials, Proc. 2nd ASTM-EURATOM Symposium on Reactor Dosimetry, October 3-7, 1977, NUREG/CP-0004, Vol. 2, pp. 739-774, 1978.

2. R. Gold, J. H. Roberts and F. H. Ruddy, "Solid State Track Recorder Materials for Use in Light Water Reactor Pressure Vessel Exposures," J. A. Sprague and D. Kramer, Eds., Effects of Radiation on Structral Materials, ASTM STP 683, Am. Soc. for Testing and Materials, Philadelphia, PA, pp. 402-423, 1978.

3. R. Gold, F. H. Ruddy and J. H. Roberts, "Application of Solid State Track Recorders in United States Nuclear Reactor Energy Programs," H. Francois et al., Eds., Solid State Nuclear Track Detectors, Proc. 10th Int. Conf. Lyon, July 2-6, 1979, Pergamon Press, Oxford, England, pp. 533-547, 1980.

4. R. Gold, F. H. Ruddy and J. H. Roberts, "Solid State Track Recorder Applications in U.S. Nuclear Reactor Energy Programs," Trans. Am. Nucl. Soc. 34, pp. 146-148, 1980.

5. R. Gold, and C. E. Cohn, "Analysis of Automatic Fission Track Scanning Data," Trans. Am. Nucl. Soc. 14, p. 500, 1971.

6. C. E. Cohn and R. Gold, "A Computer-Controlled Microscope for Automatic Scanning of Solid State Nuclear Track Records," Rev. Sci. Instrum. 43, pp. 12-17, 1972.

7. R. Gold, and C. E. Cohn, "Analysis of Automatic Fission Track Scanning in Solid State Nuclear Track Recorders," Rev. Sci. Instrum. 43, pp. 18-28, 1972.

8. A. T. Bharucha-Reid, Elements of the Theory of Markov Processes and Their Applications, McGraw Hill, NY, 1960.

9. W. Feller, An Introduction to Probability Theory and Its Applications, Vols. I and II, John Wiley and Sons, New York, NY, 1966.

10. R. Gold, R. H. Ruddy and J. H. Roberts, "Buffon Needle Method of Track Scanning at High Track Density," Bull. Am. Phys. Soc. 25, p. 484, 1980.

11. R. Gold, R. J. Armani and J. H. Roberts, "Absolute Fission Rate Measurements With Solid State Track Recorders," Nucl. Sci. & Eng. 34, pp. 13-32, 1968.

12. F. H. Ruddy, R. Gold and J. H. Roberts, "Solid State Track Recorder Measurements in the Poolside Critical Assembly," Dosimetry Methods for Fuels Cladding, and Structural Materials, Proc. 3rd ASTM-EURATOM Symposium on Reactor Dosimetry, October 1-5, 1979, EUR 6813, Vol. II, pp. 1069-1075, 1980.

C. NEUTRON RESPONSE CHARACTERISTICS OF CR-39 POLYMER FOR REACTOR AND DOSIMETRY APPLICATIONS

F. H. Ruddy*, R. Gold*, J. H. Roberts*, C. C. Preston*, E. V. Benton**, and H. Schraube***

Objective

Define the limitations of Solid State Track Recorders (SSTR) for surveillance dosimetry in light water reactor pressure vessel (LWR-PV) environment. To this end, Standard E706(IIIB) entitled: "Application and Analysis of Solid State Track Recorder (SSTR) Monitors for Reactor Vessel Surveillance" was prepared within the ASTM Master Matrix for LWR-PV Standards, E706-81a. In this context, the capabilities of CR-39, a new plastic SSTR of unprecedented sensitivity, were investigated for low fluence LWR applications (especially cavity measurements), which would support the on-going need for verification of the effects of fuel management schemes on pressure vessel and support structure neutron exposures.

Summary

A desensitized etching technique was developed that has resulted in an excellent differential energy response for alpha particles in the 3- to 14-MeV energy range. This response complements the previously reported differential proton and integral alpha energy responses obtained with different etching techniques.

Proton recoil track yields and diameter distributions were measured for CR-39 polymer SSTR exposed to monoenergetic neutron sources in the 0.57- to 15.1-MeV energy range using various thicknesses and types of proton radiator materials.

*Hanford Engineering Development Laboratory, Richland, WA.
**University of San Francisco, San Francisco, CA.
***Institut fur Strahlenschutz, Neuherberg, Federal Republic of Germany.

Accomplishments and Status

CR-39 polymer® is an extremely promising material for use as an SSTR in high energy neutron dosimetry. Its unprecedented wide energy response for protons, variable response characteristics and high optical quality make it ideal for this purpose. In addition, CR-39 polymer is highly resistant to radiation damage.[1] Samples of CR-39 polymer have been exposed to 10^7 rad of β,γ irradiation and still retained acceptable optical quality after etching. CR-39 polymer is also more resistant to track fading at elevated temperatures than other plastic SSTR having sufficiently low ionization thresholds to be useful in photon- and alpha-detection applications. Measurable annealing occurs only at temperatures in excess of about 70°C. Because of these unique characteristics, applications of CR-39 polymer in magnetic fusion energy, light water reactor, and fast breeder reactor environments are currently being developed. Results of collaborative Hanford Engineering Development Laboratory (HEDL) - University of San Francisco (USF) work with CR-39 polymer SSTRs have been reported in several publications.[2-4] More recent work has concentrated on an exploration of the following two areas:

1) Alpha spectrometry using a desensitized etch technique.
2) Optimization of the radiator type and thickness for in-situ neutron induced proton recoil spectrometry using CR-39 polymer.

ALPHA SPECTROMETRY

In previous publications,[2-4] results of track diameter vs energy calibrations for CR-39 polymer were reported, and the excellent potential of this material as a proton spectrometer in the 0.2- to 18-MeV energy range was shown. Under the same etch conditions, CR-39 polymer track diameters were relatively insensitive to changes in alpha particle energy in the 3.2- to 6.1-MeV energy range. This integral response to alpha particles can be an

®CR-39 is a registered trademark of PPG Industries, Pittsburgh, PA.

advantage for certain dosimetry applications.[4] However, when etched under less sensitive chemical conditions, proton tracks are not revealed in CR-39 polymer, and the alpha particle energy response becomes differential.[5] This type of response would be advantageous for applications based on the use of radiators that emit alpha particles under neutron irradiation, such as ^{6}Li and ^{10}B. Radiators composed of such isotopes could then also provide useful neutron spectral information. Alpha spectrometry with CR-39 polymer could be used to perform neutron spectrometry through (n,α) reactions on these and other isotopes.

Experiments were initiated* to determine the alpha particle response characteristics of CR-39 polymer under a variety of etching conditions designed to be less chemically sensitive than the conditions used for the previously reported integral response.[2] After extensive experimentation, a set of etching conditions was derived that resulted in the alpha track diameter vs energy response shown in Fig. HEDL-2. An excellent differential energy response was obtained for normally incident alpha particle track diameters in the 3- to 14-MeV energy range . The use of these desensitized etching conditions would presumably also result in a considerable decrease in the registration efficiency for protons, allowing (n,α) spectrometry to be carried out with a greatly reduced background of (n,p) tracks. The etch consisted of three steps at 70° C:1 hour in 7.5 N NaOH; 3 hours in PEW_{10} (15 g KOH, 10 g ethanol, 75 g water); 1 hour in 7.5 HaOH. Experiments are in progress to further refine etching conditions for alpha particle spectrometry.

(n,p) SPECTROMETRY

In order to use the calibration curves for proton or alpha particle track diameter vs energy directly for (n,p) or (n,α) spectrometry, one would have to design a measurement that employs carefully controlled experimental geometry to ensure that tracks from the protron or alpha particle radiator impinge on the CR-39 polymer SSTR at normal or near normal incidence. Neutron

---

*USF efforts were supported in part by Bureau of Mines Contract JO 18803.

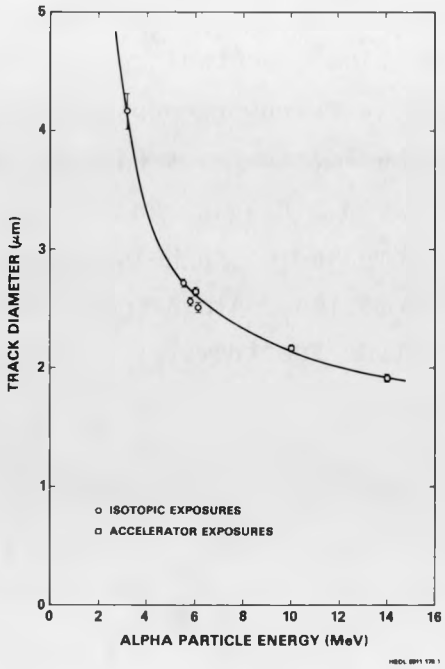

FIGURE HEDL-2. Track Diameter vs Total Energy for Normally Incident α-Particle Tracks on CR-39 Polymer. Isotopic exposures were performed with ^{148}Gd (3.18 MeV), ^{241}Am (5.49 MeV), ^{244}Cm (5.81 MeV), and ^{252}Cf (6.12 MeV). Accelerator exposures were carried out at Frankfurt using 6-, 10-, and 14-MeV α-particles. Neg 8014968-1

dosimetry is simplified considerably if one can interpret measurements where the SSTR and proton radiator are in direct contact. Analyses of track diameter distributions show valuable neutron spectral information might be obtained from such measurements.[4] Indeed, neutron irradiations of CR-39 polymer SSTR in surface contact with thick polyethylene radiators from monoenergetic neutron sources of 0.57, 2.1, 5.3, and 15.1 MeV resulted in track diameter distributions with peaks corresponding to proton energies close to the incident neutron energy. In order to quantitatively interpret these track diameter distributions, further neutron irradiations of CR-39 polymer were carried out using various thicknesses and types of proton radiator material. Au, Ni, Polyethylene, CR-39, and air were used as the radiator material resulting in the proton recoil track yields shown in Table HEDL-2. The relatively high yield of proton recoils in the case of the air radiator is somewhat surprising and apparently results from (n,p) reactions on

TABLE HEDL-2

CR-39 SENSITIVITY OBTAINED WITH VARIOUS RADIATOR FOILS

Radiator	Sensitivity (tracks/cm^2/mRem) Neutron Energy 0.57 MeV	2.1 MeV	5.3 MeV	14.1 MeV
750 μm Polyethylene	---	15.60	20.41	8.34
1500 μm Polyethylene	12.97	14.11	20.89	9.26
2250 μm Polyethylene	13.18	14.11	21.84	12.32
3000 μm Polyethylene	13.44	14.28	22.08	---
4500 μm Polyethylene	---	---	---	13.27
1060 μm CR-39	---	---	---	4.48
2120 μm CR-39	---	---	---	7.13
3180 μm CR-39	---	---	---	6.87
750 μm Nickel	12.50	4.77	2.17	2.04
500 μm Gold	---	---	---	1.48
Air	11.24	3.44	2.46	11.7

nitrogen. The high value at 14.1 MeV may be due to the interaction of room return neutrons with nitrogen. The relatively low yields for Au and Ni reflect the low (n,p) cross sections for Au and isotopes of Ni.

The track diameter distribution obtained for a thick polyethylene radiator at 14 MeV is shown in Fig. HEDL-3. Track diameter distributions for this and all of the radiator combinations listed above for 14-MeV neutrons resulted in a peak at a diameter of ~3.5 μm, corresponding to a proton energy approximately equal to the 14-MeV maximum proton recoil energy. The intensity of this peak reflects the track yields in Table HEDL-2. Further experiments are in progress to develop etching conditions for optimum interpretation of these diameter distributions and to investigate the diameter distributions for various radiators at other energies.

Expected Future Accomplishments

Develop and refine the capabilities of CR-39 for SSTR dosimetry at low fluence in LWR-PV environments. In particular, the temperature and fluence limits for CR-39 polymer SSTR in reactor cavity measurements will be investigated.

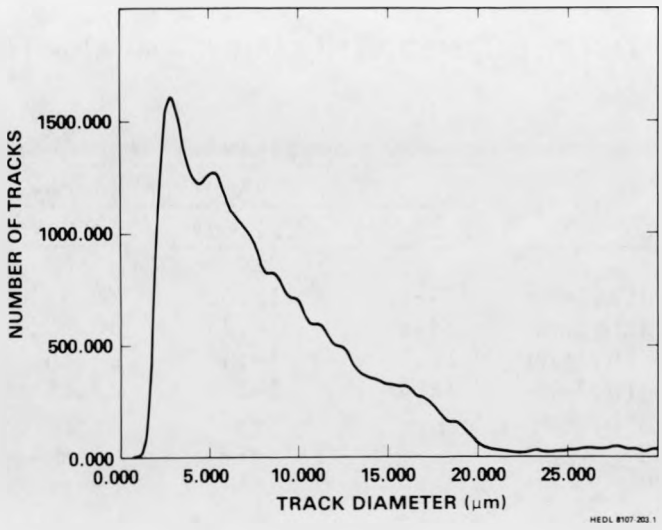

FIGURE HEDL-3. Diameter Distribution of Proton-Recoil Tracks Produced by 14-MeV Neutron Bombardment of CR-39 Polymer and a 2250-μm Polyethylene Proton Radiator. Neg 8107028-1

References

1. R. Gold, F. H. Ruddy, E. P. Lippincott, W. N. McElroy and J. H. Roberts, Spent Thermal Reactor Fuel Assembly Characterization with Solid State Track Recorders, HEDL-TME 78-89, Hanford Engineering Development Laboratory, Richland, WA, June 1979.

2. E. V. Benton, C. C. Preston, F. H. Ruddy, R. Gold and J. H. Roberts, "Proton and Alpha-Particle Response Characteristics of CR-39 Polymer for Reactor and Dosimetry Applications," Proc. 10th Int. Conf. Solid State Nuclear Track Detectors, Pergamon Press, Oxford, England, pp. 459-467, 1980.

3. R. Gold, F.H. Ruddy, C. C. Preston, J. H. Roberts and W. N. McElroy, "Neutron Camera for Fusion Diagnostics," Bull. Am. Phys. Soc. 25, p. 687, 1980.

4. F. H. Ruddy, C. C. Preston, R. Gold, E. V. Benton and J. H. Ropberts, "CR-39 Polymer: A Promising New Solid State Track Recorder for High Energy Neutron Applications," Symposium on Neutron Cross-Sections from 10-50 MeV, Vol. II, BNl-NCS-51245, pp. 599-616, Brookhaven National Laboratory, Upton, NY, 1980.

5. G. Symogi and I. Hunyadi, "Etching Properties of CR-39 Polymer Nuclear Track Detector," Proc. 10th Int. Conf. on Solid State Nuclear Track Detectors, Pergamon Press, Oxford, England, pp. 443-452, 1980.

D. OPTICAL EFFICIENCY AND OBSERVER OBJECTIVITY FOR FISSION TRACK COUNTING IN MUSCOVITE SOLID STATE TRACK RECORDERS

J. H. Roberts, R. Gold and F. H. Ruddy - HEDL

Objective

Define the accuracy limitations of Solid State Track Recorders (SSTR) for surveillance dosimetry in light water reactor pressure vessel (LWR-PV) environments. To this end, Standard E706(IIIB) entitled: "Application and Analysis of Solid State Track Recorder (SSTR) Monitors for Reactor Vessel Surveillance" has been prepared within the ASTM Master Matrix for LWR-PV Standards, E706-81a. Two significant contributors to the uncertainty of the manual SSTR scanning method have been identified as observer objectivity and optical efficiency, respectively. A quantitative re-evaluation of earlier work defining these two factors has been undertaken. Accuracy requirements for passive SSTR integral reaction rate measurements in in-vessel surveillance capsules and ex-vessel cavity locations are set in the 2 to 5% (1σ) range since subsequently derived exposure parameter (ϕt > 1.0 MeV, dpa, etc.) values need to be determined with uncertainties in the 5 to 20% (1σ) range.

Summary

The optical efficiency of Muscovite mica for manual fission track counting is being redetermined to form a data base for comparison with automatic counting systems. Exposures in contact with a ^{252}Cf source prepared at Harwell were carried out. Whereas, the absolute fission rate of the source is still being evaluated, the current results indicate that observer objectivity is at the 0.4% uncertainty level.

Accomplishments and Status

As the solid state track recorder (SSTR) laboratory at Westinghouse Hanford Company moves towards reliance upon automated systems for track counting and

characterization, it is important to have good data from manual scanning as a basis for comparison and evaluation. For this reason, it was decided to repeat earlier studies of observer objectivity and "optical efficiency" for fission track counting in Muscovite mica.[1] "Optical efficiency" is defined as the ratio of tracks counted to fission events occurring in a thin actinide deposit placed in direct contact with the mica.

A technique was also developed that standardizes the size distribution of tracks from one sample of mica to another, regardless of bulk etch rate variations.[2]

Several samples were counted by four observers to test observer objectivity. Two observers were experienced scanners, and the other two were students with no previous track counting experience.

A ^{252}Cf deposit on stainless steel backing, prepared at Harwell and calibrated for absolute fission rate, was used to determine the optical efficiency of the mica.

EXPERIMENTAL PROCEDURE

Mica obtained from two suppliers* was selected for its optical quality and low fossil fission track background. Samples were pre-etched for ~5 hours in 49% HF at room temperature. Disks with a diameter of 3/4 in. (1.91 cm) were exposed in direct contact with ^{252}Cf source having an area of 1.27 cm^2. Exposures were usually timed to give ~25,000 fission tracks. The backside of the mica was exposed in a vacuum to normally incident full energy fission fragments.

After exposure, the mica was etched in 49% HF at 23.2°C for 1 hour. A digitized filar micrometer was used to measure the length of the larger diagonal of the normally incident fission fragment tracks. Since the length of this

---

*Perfection Mica Co. and United Mineral Corp.

diagonal grows linearly with etching time,[2] the additional etching time required to bring this diagonal up to a standard length of 5.5 μm could be determined and accomplished.

The inexperienced scanners were taught how to use the microscopes and how to obtain good Kohler illumination. They were asked to examine the mica in the region containing fission tracks and in the unexposed region. Apart from this, they were not told what to count. Counting was done with transmitted light at a magnification of 250X.

Exposure and counting data are given in Table HEDL-3. The absolute fission rate of the ^{252}Cf source is still being evaluated. Measurements were made at Harwell, and the source is also being evaluated by various methods at HEDL. SSTR and surface barrier detectors are being used in a low geometry configuration to observe both alpha and fission fragment emission from the source. Proportional counters are being used to observe alpha and fission fragment emission in a 2π geometry. The results for the optical efficiency will be reported in a subsequent publication.

TABLE HEDL-3

EXPOSURE AND TRACK COUNTING DATA

Sample Number	Mica Source*	Exposure		Track Counts				
		Date	Time (h)	Obs. 1	Obs. 2	Obs. 3	Obs. 4	Average
1	P	1/2/81	7.750	---	26064	---	---	26064
2	P	1/9/81	7.750	26288	26232	26144	26185	26212
3	P	1/14/81	7.739	25948	25796	---	26091	25945
4	P	1/15/81	7.750	26026	---	26216	---	26121
5	P	1/21/81	8.133	27091	27259	27282	27209	27210
6	UM	2/13/81	7.750	---	25227	---	---	25227
7	UM	2/19/81	7.500	24663	24895	24679	24646	24721
8	UM	2/23/81	7.833	25269	25320	---	---	25295
9	UM	2/24/81	7.750	25303	25550	25448	---	25434

*P is from the Perfection Mica Co.
UM is from the United Mineral Corp.

Of significant interest is the observer objectivity. Take, for example, the measurements on mica samples 2, 5, and 7 (Table HEDL-3), where the tracks were counted by all four observers. The percentages of standard deviations for these measurements are 0.24, 0.31, and 0.47, respectively. For samples 3 and 9, counted by three observers, the results are 0.57 and 0.49%. The average value of these determinations is (0.42 ± 0.13)%. Thus, where high precision for fission rates is required, observer objectivity is at the 0.4% uncertainty level.

Expected Future Accomplishments

The optical efficiency of mica SSTR for manual fission track scanning will be re-evaluated. On the basis of this re-evaluation, SSTR observations in the standard ^{252}Cf neutron field (NBS) will be compared with absolute fission chamber results.

References

1. R. Gold, R. J. Armani and J. H. Roberts, "Absolute Fission Rate Measurements With Solid State Track Recorders," Nucl. Sci. Eng. 34, pp. 13-32, 1968.

2. R. Gold, J. H. Roberts and F. H. Ruddy, "Solid State Track Recorder Materials for Use in Light Water Reactor Pressure Vessel Surveillance Exposures," ASTM STP 683, pp. 402-423, Am. Soc. for Testing and Materials, Philadelphia, PA, 1979.

E. INVESTIGATIONS OF EFFECTS OF REACTOR CORE LOADINGS ON PV NEUTRON EXPOSURE

G. L. Guthrie and W. N. McElroy - HEDL
S. L. Anderson - Westinghouse Nuclear Technology Division

Objective

The objective of this work is to ascertain the effect of shifts in nuclear core loading on the neutron field at the pressure vessel. It may be possible to use a simple shift in core loading to reduce the embrittlement rate at the points of highest accumulated damage on the pressure vessel. Additional objectives are to determine the necessity for using dpa as an alternate exposure unit in quoting exposure at depths in the pressure vessel wall >1/4T.

Summary

The DOT-3 W neutron transport code was used to make transport calculations for six generic commercial reactor types. Prior to the calculations, particular fuel elements (e.g., in some cases the corner elements) were identified as contributing most heavily to the flux at the vessel wall surface position with the highest damage accumulation rate. For each reactor type, 2-D calculations were used to calculate the neutron field for two core configurations: 1) with a normal fuel loading, and 2) with the high damage contribution elements removed. In general, fuel modification appears capable of reducing the existing exposure rate at the position of the existing maximum by factors of 5.8 to 17.9. The position of the maximum exposure rate point is shifted, however, and the ratio of the old maximum to the new maximum ranges from 1.58/1.0 to 3.44/1.0. In the pressure vessel wall, the ratio of dpa/φt (E > 1.0 MeV) is a function of a radial position, and this ratio (dpa/φt) increases roughly by a factor of two going from the inner surface of the pressure vessel to the outer surface.

In general, it appears that fuel management techniques for reducing neutron exposure rates at points of high accumulated exposure show considerable promise.

Accomplishments and Status

The effects of replacing certain fuel elements by stainless steel dummies (with appropriate water fractions) in commercial PWR cores were studied. The item of interest was the flux (or dpa/s) in the pressure vessel wall. A report on the subject was sent to the NRC and is attached as an appendix.

Expected Future Accomplishments

One of the aspects of the problem, which has not yet been adequately addressed, is the effect of shifting core power distributions on surveillance capsule lead factors. This subject will ultimately be included as part of the ASTM standard on extrapolation E706(IE), but completion of the supporting analytical work is dependent on completion and documentation of the benchmark experiments mentioned as part of the fourth and fifth objective statements in the Summary. More detailed information on the planned documentation is given in Section A.

APPENDIX A PRELIMINARY STUDY OF THE USE OF FUEL MANAGEMENT TECHNIQUES FOR SLOWING PRESSURE VESSEL EMBRITTLEMENT*

G. L. Guthrie and W. N. McElroy - HEDL
S. L. Anderson - Westinghouse Nuclear Technology Division

Introduction

A technique involving the shifting of core fuel loadings is investigated as a method for reducing the neutron flux at points of high damage accumulation in the pressure vessel (PV) wall of a light water reactor.

Particular core fuel assemblies can be identified as contributing most heavily to the flux at the point on the PV wall with the highest damage accumulation rate. These assemblies can be replaced by spent fuel, zircaloy, stainless steel, or water to reduce the damage rate at the point of greatest accumulated exposure in the PV wall. Presumably, the rest of the core would then have to be refueled with a higher enrichment of fissionable fuel. Another scheme for damage reduction involves loading fresh fuel into the center of the core and moving it outward in later cycles. The present report does not specifically investigate this latter method of PV damage rate reduction.

As a preliminary guide in deciding whether any proposals of the types suggested above are practical, HEDL and Westinghouse Nuclear Technology Division cooperated in a study of the benefits to be derived from a very simple change in core power distribution. A 2-D transport calculation was used to determine the benefit gained by replacing a few fuel assemblies with stainless

*This work was supported by the Nuclear Regulatory Commission, Division of Engineering Technology, Materials Engineering Branch; C. Z. Serpan, Branch Chief.

steel dummies, with appropriate water fractions to account for the coolant. The core power distribution in the remaining fuel assemblies was assumed to be unchanged except for a renormalization factor, which maintained the same total power output. Calculations were run for six types of commercial generic pressurized water reactors (PWRs). The choice of reactor types was made primarily on the basis of the immediate availability of required information. Calculations merely indicate whether NRC could reasonably suggest to the utilities that further investigations in greater depth might be worthwhile.

The PWR types are:

1) Type A, both accelerated and wall capsules, (2600 MWt)
2) Type B, 2-loop shield reactor (1960 MWt), accelerated capsules only
3) Type C, 3-loop shield reactor (2900 MWt), accelerated capsules only
4) Type D, 4-loop shield reactor (3565 MWt), accelerated capsules only
5) Type E, 3-loop "pad" reactor (2900 MWt), accelerated capsules only
6) Type F, 4-loop "pad" reactor (3565 MWt), accelerated capsules only

In general, fuel modification appears capable of reducing the existing exposure rate at the position of the existing maximum by factors of 5.8 to 17.9. The position of the maximum exposure point is shifted, however, and the ratio of the old maximum to the new maximum ranges between 1.58/1.0 and 3.44/1.0.

It appears that fuel management techniques for reducing the neutron exposure at points of high accumulated exposure show considerable promise. However, there are other potential solutions to the overall embittlement problem and in-depth studies of all solutions and the associated economic implications are required before firm decisions are made.

TRANSPORT CODE FEATURES AND REACTOR TYPES

Calculations were done with the Westinghouse version of the DOT-3 neutron transport code using a P_1S_8 angular description* and a 21-group energy structure as shown in Table HEDL-A1.** An (R,θ) 2-D calculation was used in one octant of the reactor, with P_1 cross-section descriptions derived from the GAMB-1T cross section library. This combination was benchmarked in the Pool Critical Assembly (PCA) at Oak Ridge National Laboratory (ORNL) and gaveresults that compared well (±10%) to results from Monte Carlo calculations and dosimetry measurements. The iteration scheme used a fixed source in the core, emitting a Cranberg fission spectrum. For the six different reactor types, the core power distribution was based on core power calculations verified by experimental data. For the five reactor types with 17 x 17 in arrays in the fuel subassemblies, each subassembly was divided into a 17 x 17 (x,y) mesh detail for power distribution purposes, and this was remapped into the (R,θ) mesh. Transport calculations for all six generic types were run with sufficient surveillance capsules rotated into the octant under examination to allow interpretation of all surveillance results. DOT runs were made: a) with the capsules in place and a normal fuel distribution, b) with capsules in place and high damage contributing fuel subassemblies replaced by dummies, and c) with normal fuel and surveillance capsules removed. Case c (capsules out) was run for only two of the six generic reactors. For all six reactor types, the power level was renormalized for the modified-fuel cases to maintain the same total power level. However, in the modified-fuel cases, the shape of the power distribution was assumed unchanged in those fuel assemblies retained, while the power in the dummy assemblies was of course set to zero.

---

*An S_8 angular ordinate system and $P_1(+P_0)$ scattering laws.

**Calculations were done with a neutron energy group boundary at 1.05 MeV. Fluence and flux (E > 1.05 MeV) were, therefore, readily available from the calculations and were used to infer conclusions regarding use of fluence and/or flux (E > 1.0 MeV) as independent variables in damage studies. For convenience in the discussions, terminologies of (E > 1.05 MeV) and (E > 1.0 MeV) are used interchangeably in drawing qualitative conclusions from results of the current studies.

TABLE HEDL-A1

ENERGY GROUP STRUCTURE AND FISSION SPECTRUM
FOR DOT CALCULATIONS

Group No.	Lower Energy (MeV)	F(E)
1	7.79	5.9642×10^{-3}
2	6.07	1.7059×10^{-2}
3	4.72	3.9468×10^{-2}
4	3.68	6.8770×10^{-2}
5	2.87	9.6324×10^{-2}
6	2.23	1.1411×10^{-1}
7	1.74	1.1895×10^{-1}
8	1.35	1.1244×10^{-1}
9	1.05	9.8671×10^{-2}
10	0.821	8.1806×10^{-2}
11	0.388	1.5219×10^{-1}
12	0.111	7.8617×10^{-2}
13	0.0409	1.2486×10^{-2}
14	0.0150	2.8786×10^{-3}
15	5.53×10^{-3}	2.6119×10^{-4}
16	5.83×10^{-4}	
17	7.89×10^{-5}	
18	1.07×10^{-5}	
19	1.86×10^{-6}	
20	3.00×10^{-7}	
21	0.00	

Individual Reactor Calculations

1. TYPE A Reactor (both accelerated and wall capsules)

For the Type A reactor, calculations were done for all 3 conditions: a) full fuel, capsules in, b) modified fuel, capsules in, and c) full fuel, capsules out. The (R,θ) meshes were the same for all three cases. The core map in (x,y) geometry is shown in Figure HEDL-A1. Dimensions used in the calculation were as-built dimensions applicable to a particular reactor installation. Figure HEDL-A2 shows the Type A reactor in an (R,θ) map, which indicates the mesh detail in the DOT calculation. A comparison of Figures HEDL-A1 and HEDL-A2 shows two outer fuel assemblies in the general region near ($0° < \theta < 10°$) were replaced by stainless steel dummies (with appropriate water fractions) in the modified-fuel DOT calculation. For the capsules-out case (case c), all three capsules were removed and a normal fuel load was assumed.

Figure HEDL-A3 compares the dpa damage dose on the front face of the PV after 32 years of full-power operation for the two cases where: a) a full fuel load is assumed and b) two fuel subassemblies were replaced by stainless steel-water dummies and the power distribution renormalized to return to full power. Reduction in dpa damage exposure rate at the $\theta = 0°$ position is 13.6/1.0, but the peak damage accumulation is shifted to the 29° angular position. The ratio of the normal-fuel, maximum-damage rate to the modified-fuel, maximum-damage rate is 1.58/1.0.

Assuming dpa is a true indicator of accumulated microscopic damage, then the inadvisability of relying solely on fluence ($E > 1.0$ MeV) is indicated in Figure HEDL-A4. A radial sweep from the core out through a capsule at the $\theta = 35°$ angular position is shown in Figure HEDL-A4. $dpa/\phi t$ ($E > 1.05$ MeV) was calculated, normalized to unity at the center of the capsule. As Figure HEDL-A4 shows, the $dpa/\phi t$ ratio at the 1/4 T position is not too different from the similar ratio at the surveillance capsule position, but the $dpa/\phi t$ ratio varies by a factor of 2.23 going from the front to the rear of

the PV. Therefore, if ϕt (E > 1.0 MeV) information is used in conjunction with surveillance capsule mechanical properties data to develop in-vessel material property change trend curves, the conclusions drawn from such information will be nonconservative, and the exposures will be nonconservative by a factor of two if the trend curve is used in connection with ϕt (E > 1.0 MeV) exposure information for positions near the rear of the PV wall.

For the Type A (accelerated and wall capsules) reactor, each capsule was modeled as a 15-region rectangle (3 theta regions x 5 radial regions). The center lines of the capsules are located at 3°, 35°, and 45°. The capsule perturbation effect can be seen in Figures HEDL-A5 and HEDL-A6 where radial traverse values of dpa are plotted at the 3° and 35° angular positions giving a comparison (capsule in and capsule out) for the 32 full-power year dpa exposure. The presence of the capsule causes an increase in the neutron exposure, measured either in dpa or in fluence (E > 1.0 MeV) units. At the capsule center, the presence of the capsule causes an increase of 24.1% in the dpa exposure value or an increase of 22.9% in the fluence (E > 1.05 MeV) for the wall capsule located at a 3° angular position. For the accelerated capsule located on the core side of the thermal shield, similar increases are 26.9% for the dpa exposure and 24.0% for fluence (E > 1.05 MeV). For this type of power plant and surveillance capsule configuration, transport code solutions obtained without explicit capsule modeling can be expected to require corrections of the magnitude indicated above, when the transport solution is used directly to provide a "lead factor."

2. Type B, 2-Loop Shield Reactor

The Type B, 2-loop shield reactor is representative of an older generic model capable of 1960-MWT power output. The thermal shield is 360° in extent, in contrast to the reduced angular sweep of the "pad" used in later, larger reactor designs. In the current study, three capsules were assumed to be in the octant under study. They are located at 13°, 23°, and 33° on the vessel side of the thermal shield. The 2-loop reactor was studied under all three

conditions: a) full fuel, b) modified fuel, and c) full fuel with all the capsules removed. The (x,y) map of the reactor midplane is shown in Figure HEDL-A7 and an (R,θ) map of the DOT mesh detail is shown in Figure HEDL-A8. The surveillance capsules were each modeled as a (5 x 5) mesh in (R,θ) with an outer layer of stainless steel and the inner (3 x 3) mesh of samples and dosimeters, modeled as low alloy steel. (The same steel as that found in the PV walls.) For the 2-loop reactor, the region of high exposure at the PV wall is near the 0° angle, where the wall is opposite a "flat" region of the core. Therefore, in the modified fuel part of the study, 1-1/2 fuel subassemblies per octant were replaced by stainless steel in the 0° angular region in the approximate range (0 < x < 30 cm), (110 cm < y < 130 cm). This can be seen from examination of Figures HEDL-A7 and HEDL-A8.

Core modeling for all three cases followed the 17 x 17 mesh method described earlier. The modified fuel case (case a) was run by using stainless steel replacement dummies (with an appropriate water fraction) in the 1-1/2 assemblies on the "flat," while full-fuel power distribution was maintained in the remaining fuel subassemblies, which were renormalized to the original total power.

The dpa exposure on the front face of the PV is shown in Figure HEDL-A9, which gives a comparison of the full-fuel and modified-fuel cases plotted as a function of angular position. The exposure rate at the original point of maximum damage accumulation is decreased by a factor of 11.64/1.0 by the fuel modification. However, the point of most rapid damage accumulation shifts to θ = 32.1°, and the ratio of full-fuel, maximum-damage rate to modified-fuel, maximim-damage rate is 2.33/1.0.

The capsule perturbation effect can be seen in Figure HEDL-A10, where neutron flux is plotted as a function of radial position in a radial traverse at the 13° angular position, which goes through the center of a surveillance capsule. The plot compares the flux for the two cases: a) full fuel, capsule in place and b) full fuel, capsule removed. The capsule perturbation effect for this capsule is 26.5%. That is, the fluence (n/cm^2, E > 1.05 MeV) calculated at the center of the capsule is 26.5% higher when the capsule is

present, compared to the case where the capsule is removed. When a transport calculation is performed without explicit capsule modeling, a 26.5% correction is needed in the calculation of the "lead factor," based on fluence ($E > 1.05$ MeV).

A similar plot for the 13° capsule, using dpa as the exposure unit, is shown in Figure HEDL-A11. For dpa, the perturbation correction factor is 34.9% at the capsule center. This difference in lead factor corrections (34.9% vs 26.5%) illustrates the importance of using an exposure index that correlates well with property degradation.

The disadvantages of using a poorly chosen exposure index are also shown in Figure HEDL-A12, where the ratio of dpa/ϕt ($E > 1.05$ MeV) is plotted as a function of radial position in a radial traverse through the center of the 13° capsule for the full-fuel case. The ratio is normalized to the value at the center of the surveillance capsule. The ratio increases by 62.3% going from the front of the PV to the rear surface of the vessel. The discussion of this phenomenon, as given in the Type A reactor section, also applies here.

3. Type C, 3-Loop Shield Reactor

The Type C, 3-loop shield reactor is an older model 2900-MWT reactor with a thermal shield that extends for 360°. The surveillance capsules are on the vessel side of the thermal shield. For this reactor type, two DOT cases were run, namely a normal fuel configuration and a modified fuel configuration. No DOT capsule perturbation study was performed for this reactor type. Fuel modeling and replacement modeling by stainless steel dummies followed the arrangements described under "Transport Code Features and Reactor Types." For the modified fuel case, 1-1/2 fuel subassemblies were replaced by stainless steel dummies (with appropriate water fractions) in the outer fuel layer in the region between 0° and 30°. Three and one-half surveillance capsules were modeled in the octant under study. The (x,y) plot of the reactor midplane is given in Figure HEDL-A13 and the (R,θ) DOT mesh model for the

modified-fuel case is given in Figure HEDL-A14. The capsules are centered at 15°, 25°, 35°, and 45°. A plot of dpa for 32 full-power years on the front face of the PV is given in Figure HEDL-A15. This plot (Figure HEDL-A15) shows exposure vs angular position and compares the normal-fuel case to the modified-fuel case. For normal-fuel loading, the most rapid exposure accumulation in the wall occurs at an angular position of 0°, and at this location the modified loading reduces the dpa exposure rate by a factor of 17.9/1.0. However, with modified-fuel loading, after the power level is readjusted, there is a new location for the maximum dpa exposure rate on the PV front surface, and this is at ∿23°. The ratio of the maximum exposure rate with normal fuel loading to the maximum exposure rate with the modified loading (and power level readjusted) is 3.44/1.0.

A plot of dpa/ϕt (E > 1.05 MeV) vs radial position is given in Figure HEDL-A16 for a radial traverse through the 14.7° angular position. The ratio dpa/ϕt (E > 1.05 MeV) is normalized to unity at the surveillance capsule position. The dpa/ϕt ratio changes by a factor of ∿1.95/1.0 going from the front to the rear of the PV wall, once again exhibiting the possible short-comings of ϕt (E > 1.0 MeV) as a reliable indicator of mechanical property degradation.

4. Type D, 4-Loop Shield Reactor

The Type D, 4-loop shield reactor is representative of an older model 3565-MWT reactor with a thermal shield that extends for 360°. The surveillance capsules are on the vessel side of the thermal shield. The DOT calculations for this reactor type included the normal-fuel and modified-fuel cases but did not include a surveillance capsule perturbation study. Two surveillance capsules were modeled in the octant under observation, at 4° and 40°. For the modified-fuel case, two corner fuel subassemblies were replaced by stainless steel dummies (with appropriate water fractions). The two corner subassemblies replaced were the outer elements in the angular regions near θ = 25° and θ = 40°. The (x,y) map of the reactor midplane is shown in Figure HEDL-A17, and an (R,θ) map of the DOT mesh for the modified fuel case is shown in Figure HEDL-A18.

Treatment of the power distribution was similar to that described for the Type B, 2-loop case and similar to the description found in the section "Transport Code Features and Reactor Types."

The effect of the fuel modification on PV neutron exposure is shown in Figure HEDL-A19, which is a plot of dpa accumulated at the vessel inner radius after 32 full-power years of operation. The exposure, in dpa, is plotted as a function of angular position for both the normal fuel and modified fuel cases. With the regular fuel loading, the angular position with the highest exposure rate on the PV inner radius is at $\theta = 45°$. At this location, the change in fuel loading reduces the rate of exposure accumulation by a factor of 5.81. The position of the maximum rate of damage accumulation on the PV inner radius with the modified-fuel loading is at $\theta = 8°$. The ratio of the maximum damage rate (PV inner radius) with normal fuel to the maximum damage rate (PV inner radius) with modified fuel is 2.74/1.0.

A plot of dpa/ϕt (E > 1.05 MeV) vs radial position is shown in Figure HEDL-A20 for a radial traverse in the $\theta = 39.7°$ direction. In the plot, dpa/ϕt (E > 1.05 MeV) is normalized to unity at the center of the surveillance capsule (located at $\theta = 40°$, near the vessel side of the thermal shield). The ratio of dpa/ϕt (E > 1.05 MeV) changes by a factor of $\sim$2.12/1.0 going from the inner to the outer surface of the PV. Assuming dpa is a well-chosen independent variable (exposure index) for use in describing damage relations (trend curves), then ϕt (E > 1.0 MeV) is not very useful if the analyst intends to apply the trend curves at both the inner and outer surfaces of the PV wall. The error in transferring damage information using ϕt (E > 1.0 MeV) does not appear to be serious in using data accumulated in surveillance capsules to make predictions at the 1/4 T position in the PV wall, since the dpa/ϕt ratios in these two positions are nearly equal.

Figure HEDL-A21 shows a comparison of dpa at the 1/4 T position for the normal- and modified-fuel load cases. The reduction in exposure rate at the 45° location is 5.80/1.0, while the ratio of the two maxima (at the 45° angular position in the normal case and at the 8° angular position in the modified case) is 2.79/1.0. These factors are almost the same as those found at the PV inner radius, mentioned in the comments regarding Figure HEDL-A19 (5.81 vs 5.80 and 2.74 vs 2.79).

5. Type E, 3-Loop Pad Reactor

One of the functions of the thermal shield is to provide inelastic scattering of neutrons out of the 6- to 7-MeV region of neutron energy space. For neutrons in this region, iron is a better moderator than an equal thickness of water. Of course, at lower energies, water is a more effective neutron moderator than iron. For small thicknesses of iron, the combination of iron transport barriers early in the neutron path and water transport barriers late in the path (further from the core) is a more effective moderating system than an equal total thickness of water. However, expense of construction argues in favor of deleting the iron wherever possible, especially in cases where the extra moderation is not needed.

In later designs for many commercial reactors, the design of the thermal shield was changed to remove the shield in those regions where the PV wall was more distant from the edge of the core, and the shield was only retained in regions (θ = 25° for the 3-loop pad reactor) where the distance from the core edge to the PV was short (i.e., where the neutrons would be most damaging to the PV mechanical properties). This abbreviated shield is called a neutron pad. The Type E, 3-loop pad reactor modeled in this report is typical of a generic reactor having a 2900-MWT power output.

For the 3-loop pad reactor in the present study, DOT calculations were performed for a normal-fuel loading and for a modified-fuel loading with 1-1/2

fuel subassemblies replaced by stainless steel dummies* in the octant under investigation. The 1-1/2 fuel subassemblies replaced were in the outer row in the θ region from zero to ~12 degrees. Two surveillance capsules were modeled in the calculation at θ positions of 17° and 19.67° on the vessel side of the pad. The (x,y) plot of the reactor midplane is shown in Figure HEDL-A22, and the map showing the (R,θ) mesh for the modified-fuel case is shown in Figure HEDL-A23.

Treatment of the power distribution was similar to that described for the Type B, 2-loop shield reactor and also as described under "Transport Code Features and Reactor Types." No capsule perturbation calculations were performed for the 3-loop pad reactor.

Figure HEDL-A24 shows the effect of the fuel modification on the accumulation rate of dpa neutron exposure at the inner surface of the pressure vessel. The dpa exposure for 32 full-power years is plotted as a function of angular position at the vessel front face for both the normal-fuel loading and for the modified-fuel loading, with equal power outputs as described under "Transport Code Features and Reactor Types."

For the normal-fuel case in the 3-loop pad reactor, the angular position of the maximum rate of dpa exposure accumulation occurs at θ = 0°. The fuel modification (with equal power levels) reduces the 32 full-power year dpa exposure at this position from 7.69×10^{-2} dpa to 4.68×10^{-3} dpa. This is a ratio of 16.43/1.0. With the modification, the angular location of the maximum shifts to the location θ = 28.75°, and the exposure rate at the new maximum is 3.51×10^{-2} dpa for 32 full power years. The ratio of the maximum with normal loading to the maximum with a modified loading is 2.19/1.0. This latter ratio is slightly lower than the corresponding ratios (2.33, 3.44, 2.74) calculated for the 2-, 3-, and 4-loop shield reactors because the fuel modification for this case shifted the peak to a position

*With an appropriate water fraction.

slightly beyond the angular extent of the pad (28.75° vs 25°). Figure HEDL-A25 shows the dpa at the 1/4 T position in the PV wall for various angular positions after 32 years of full-power operation. The dpa exposure is plotted vs angular position for both the normal-fuel loading and the modified-fuel loading. The normal loading maximum exposure of 5.24×10^{-2} dpa at an angular position of $\theta = 0°$ is reduced to 3.36×10^{-3} dpa for a ratio of 15.60/1.0. The position of the maximum with the modified loading is at $\theta = 28.75$, and the maximum value is 2.33×10^{-2} dpa for 32 years. The ratio of the two maxima (normal loading/modified loading) is 2.25/1.0.

Figure HEDL-A26 is a plot of $dpa/\phi t$ ($E > 1.05$ MeV) vs radial position for a radial traverse in the direction $\theta = 19.875°$. This traverse cuts through the approximate center of a surveillance capsule (19.67°). The values of $dpa/\phi t$ are normalized to unity at the radius of the capsule center.

The ratio of $dpa/\phi t$ changes by a factor of 2.0 going from the inner to the outer radius of the PV. Again, assuming dpa is a suitable independent variable for use in developing trend curves, then fluence (n/cm^2, $E > 1.0$ MeV) is of doubtful value if the information developed is intended for use at depths beyond 1/2 T in the vessel wall. However, if information on mechanical properties is developed at the surveillance position and applied at the 1/4 T position, the mechanical property error caused by the effect just noted will only be on the order of 2% or less for reactors similar to the Type E, 3-loop pad reactor.

6. Type F, 4-Loop Pad Reactor

The Type F, 4-loop pad reactor is a 3565-MWT reactor with a neutron pad, rather than a 360° thermal shield, between the core barrel and PV. The (x,y) map of the midplane is shown in Figure HEDL-A27, and the (R,θ) plot of the modified fuel DOT mesh system is shown in Figure HEDL-A28. For this reactor type, two DOT calculations were performed. One calculation was done with a normal-fuel loading and one with a modified-fuel loading. The total

power levels were equal, and the power distribution treatment was similar to the ones already described. (See "Transport Code Features and Reactor Types" for details.)

One octant of the reactor was modeled and investigated using the DOT Code. Two surveillance capsules located on the vessel side of the neutron pad at $\theta = 29°$ and $\theta = 31.5°$ were included in the calculations. For the modified fuel case, two fuel subassemblies were replaced by stainless steel dummies with appropriate water fractions. These subassemblies are at 2 corner locations in the outer layer and are located near the angular positions $\theta = 25°$ and $\theta = 40°$.

Figure HEDL-A29 is a plot of dpa at the inner surface of the PV after 32 years of full power operation. The dpa on the inner surface of the vessel is plotted as a function of angular position for both the normal- and modified-fuel loadings. The modified loading reduces the height of the existing maximum by a ratio of 5.82/1.0. (2.99×10^{-2} dpa vs 5.14×10^{-3} dpa for 32 full-power years of operations.)

The introduction of the modification shifts the location of the maximum from $\theta = 45°$ to $\theta = 9.25°$ and reduces the magnitude from 2.99×10^{-2} dpa to 1.87×10^{-2} dpa for 32 full power years of operation, giving a reduction ratio of 1.60/1.0.

A plot of $dpa/\phi t$ as a function of radial position is given in Figure HEDL-A30 for a radial traverse at the $\theta = 31.7°$ angular position. This traverse cuts near the center of a surveillance capsule located at 31.5°. Values of $dpa/\phi t$ are normalized to the value unity at the radius of the surveillance capsule center. The $dpa/\phi t$ ratio is seen to change by a factor of 2.18 going from the inner to the outer surface of the PV wall. For comments on the implications regarding advisability of using ϕt ($E > 1.0$ MeV) rather than dpa as an exposure parameter, see the section on the Type E reactor.

Summary and Conclusions

The principal results of the present study are condensed in Table HEDL-A2. In general, fuel modification appears capable of reducing the existing exposure rate at the position of the existing maximum by factors of 5.8 to 17.9. The position of the maximum exposure point is shifted, however, and the ratio of the old maximum to the new maximum ranges between 1.58/1.0 and 3.44/1.0. In the PV wall, the ratio of dpa/ϕt (E > 1.0 MeV) is a function of radial position, and this ratio (dpa/ϕt) changes by roughly a factor of two going from the inner surface of the PV to the outer surface. The actual factors varied between 1.62 and 2.23. Capsule perturbation studies undertaken for the Type A and Type B reactors show that the presence of the surveillance capsule increases the neutron exposure at the center of the capsule by 25% to 35%.

In general, it appears that fuel management techniques for reducing the neutron exposure at points of high accumulated exposure show considerable promise. However, there are other potential solutions to the overall embrittlement problem, and in-depth studies of all solutions and the associated economic implications are required before firm decisions are made.

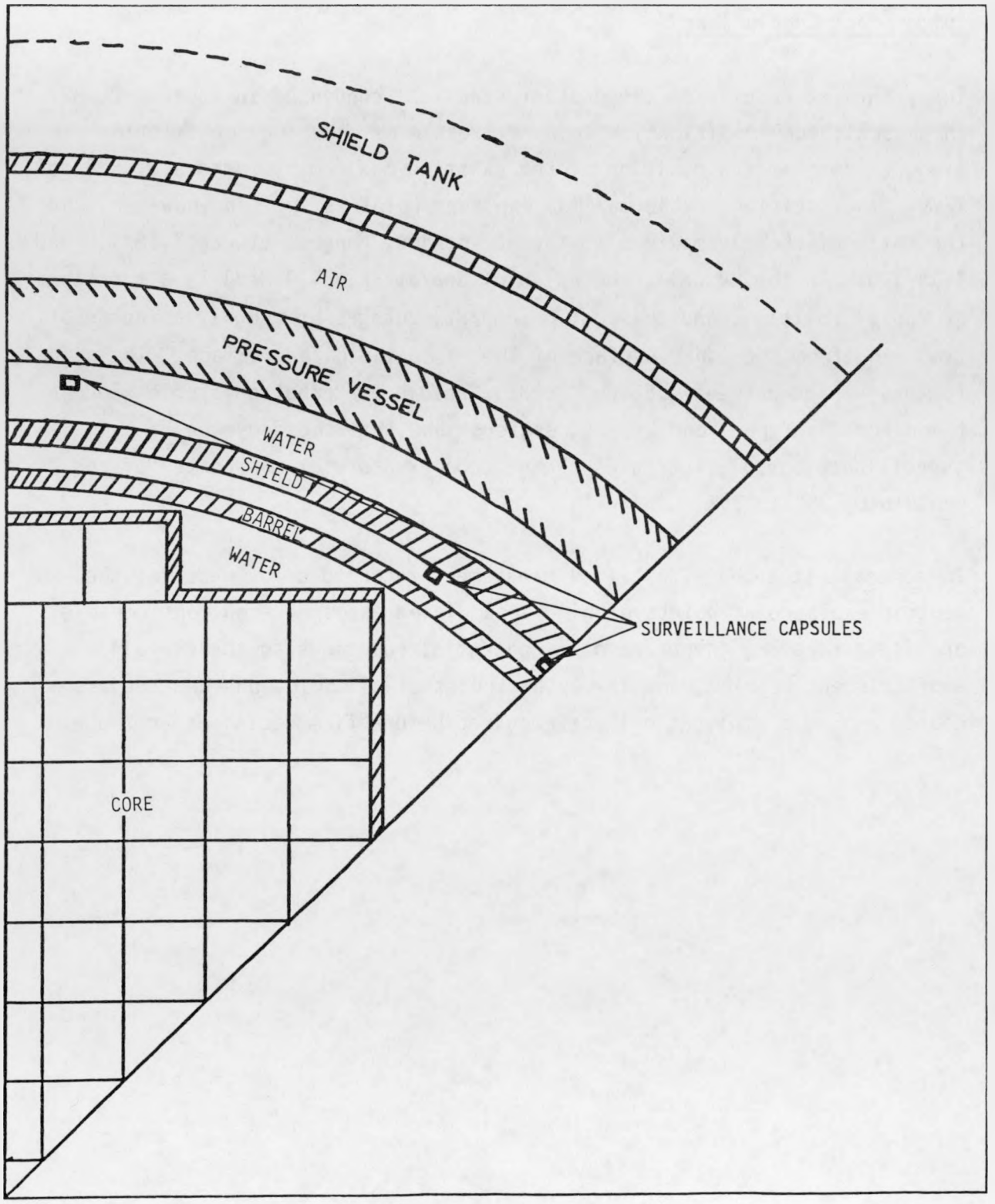

Fig. HEDL-A1. Type A PWR With Two Types of Capsules.

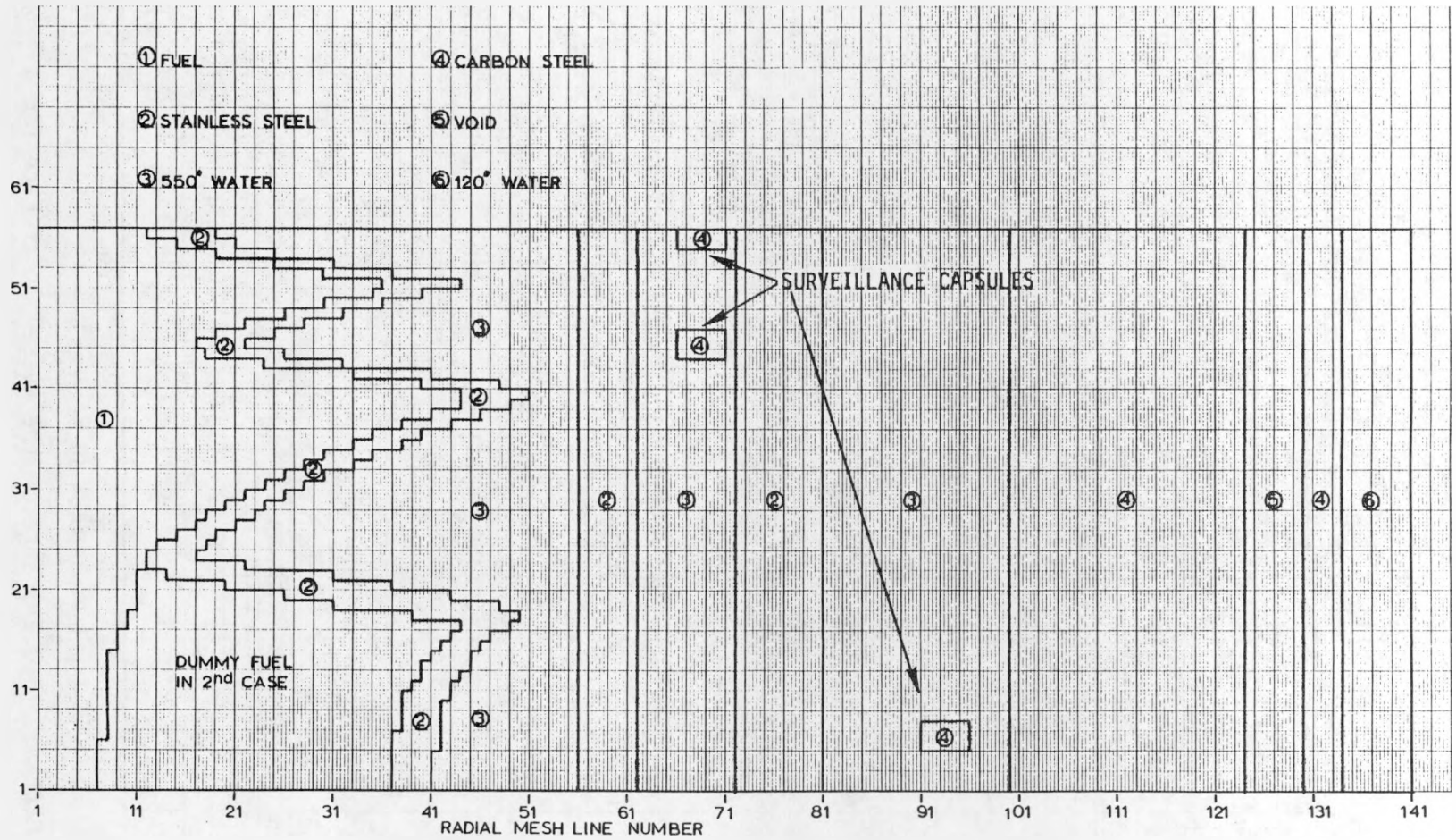

Fig. HEDL-A2. Mesh Line Description for (R,θ) Analysis of the Type A Reactor with Two Types of Surveillance Capsules.

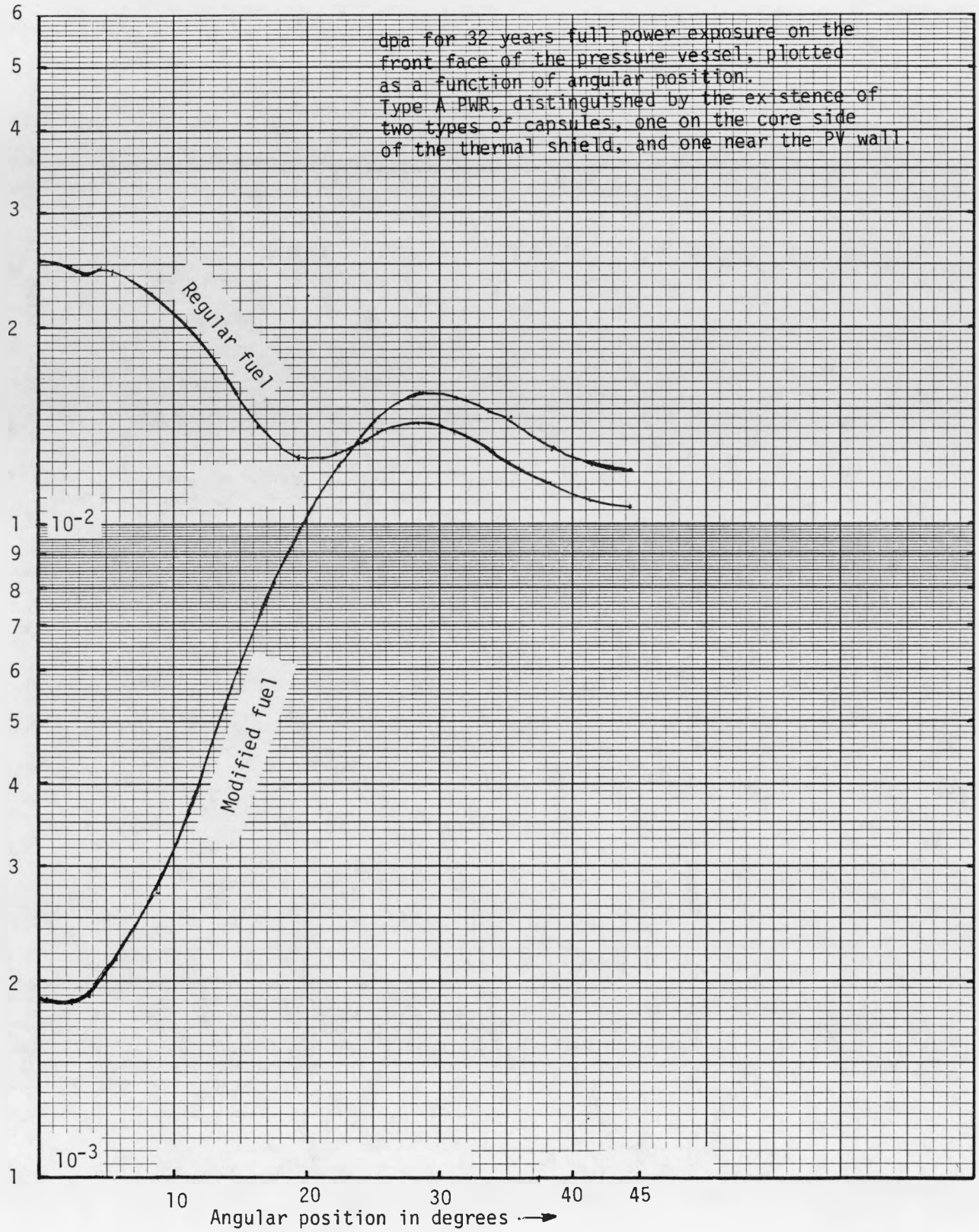

Fig. HEDL-A3. Dpa Exposure on the Vessel Inner Face for a Type A PWR.

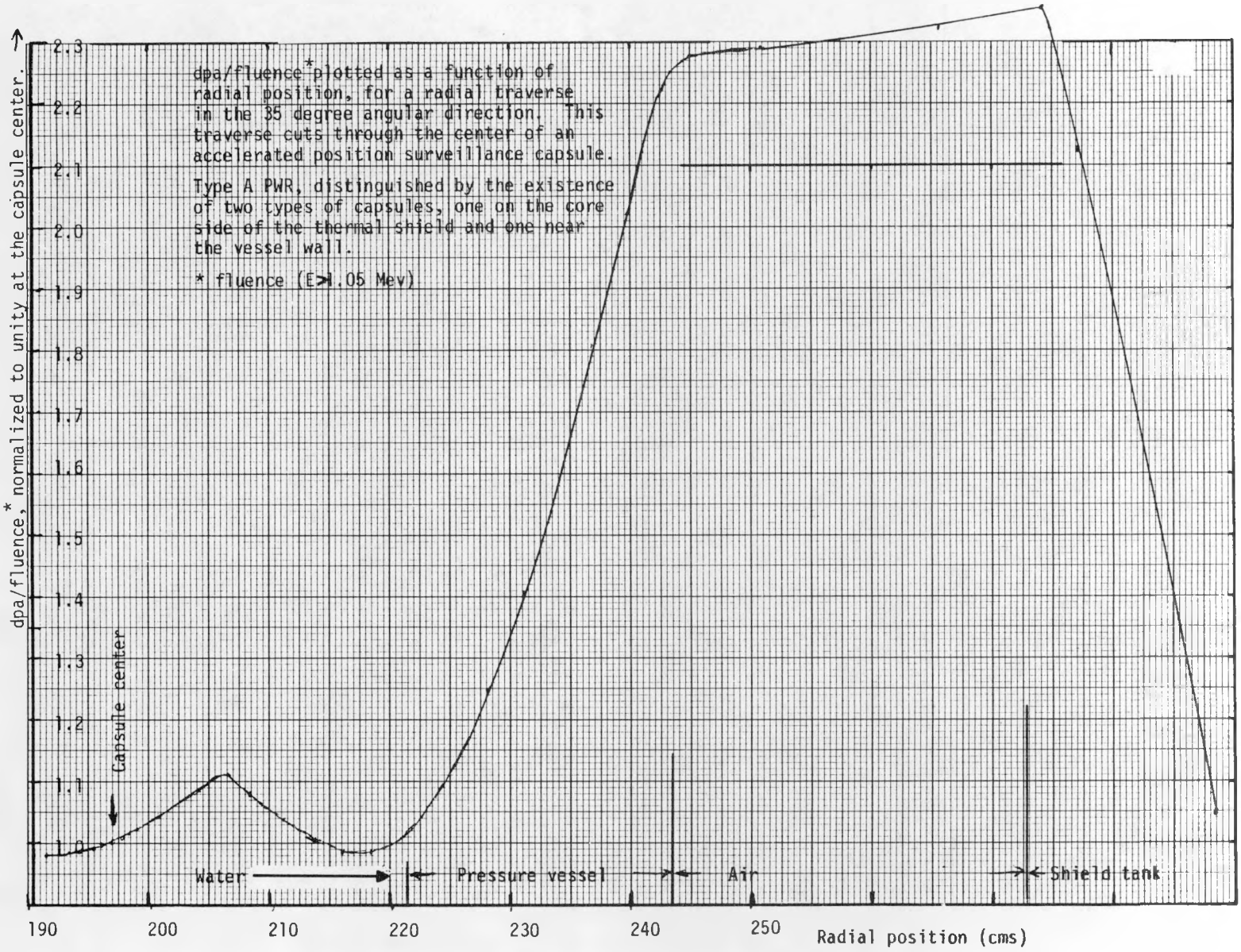

Fig. HEDL-A4. Dpa/Fluence vs Radial Position for a Type A PWR.

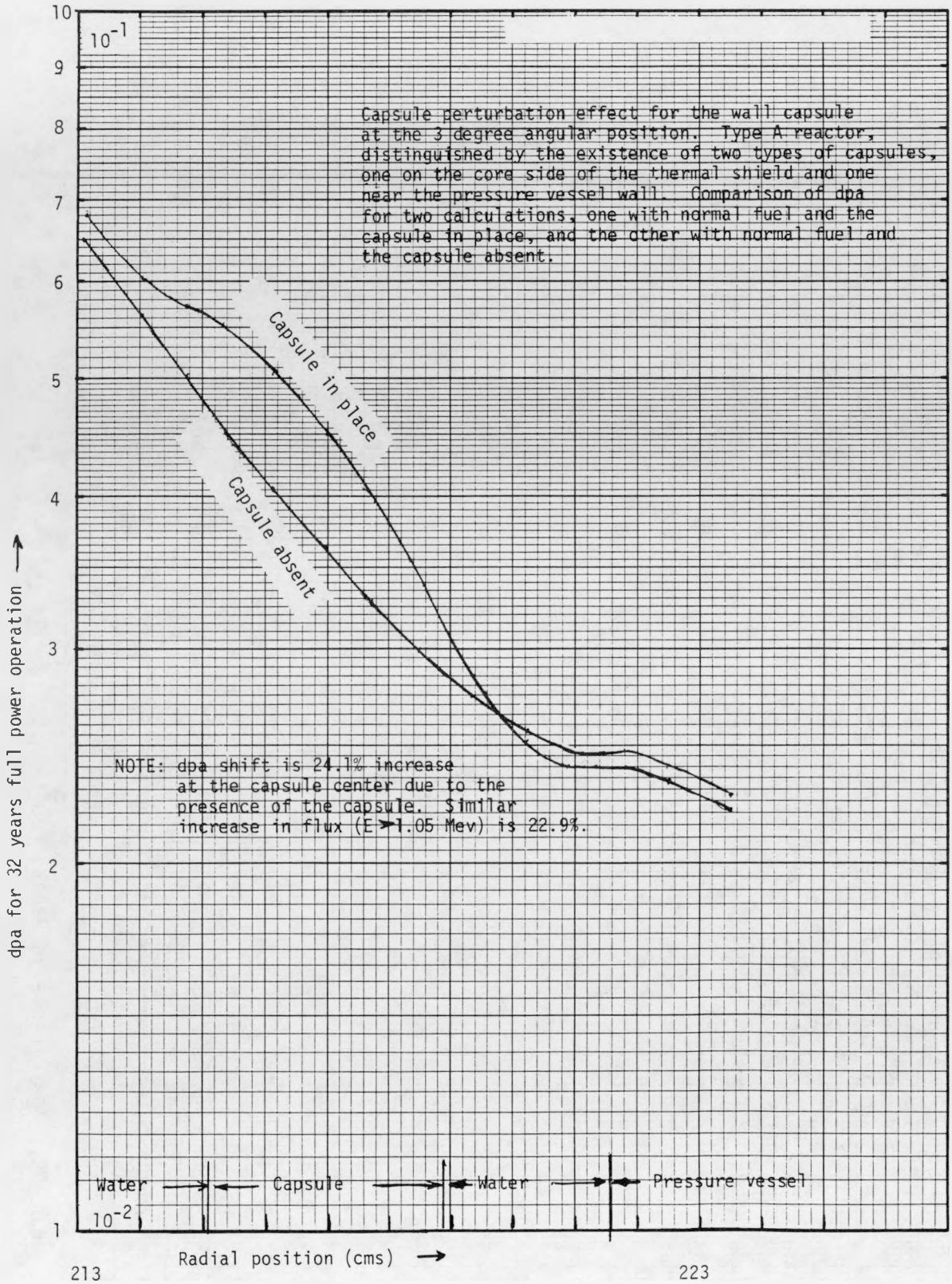

Fig. HEDL-A5. Capsule Perturbation for Type A PWR at the 3° Angular Position.

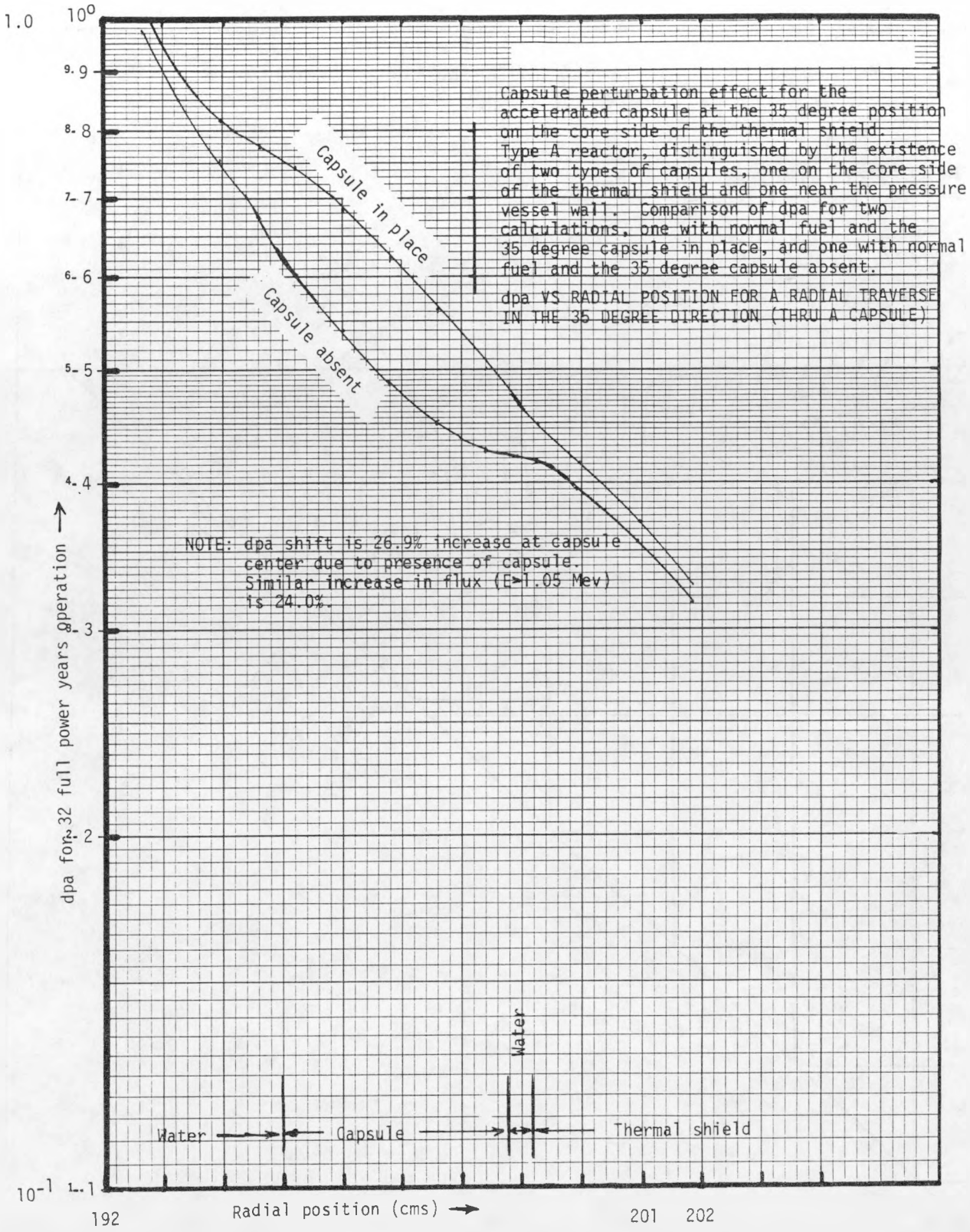

Fig. HEDL-A6. Capsule Perturbation for a Type A PWR at the 35° Angular Position.

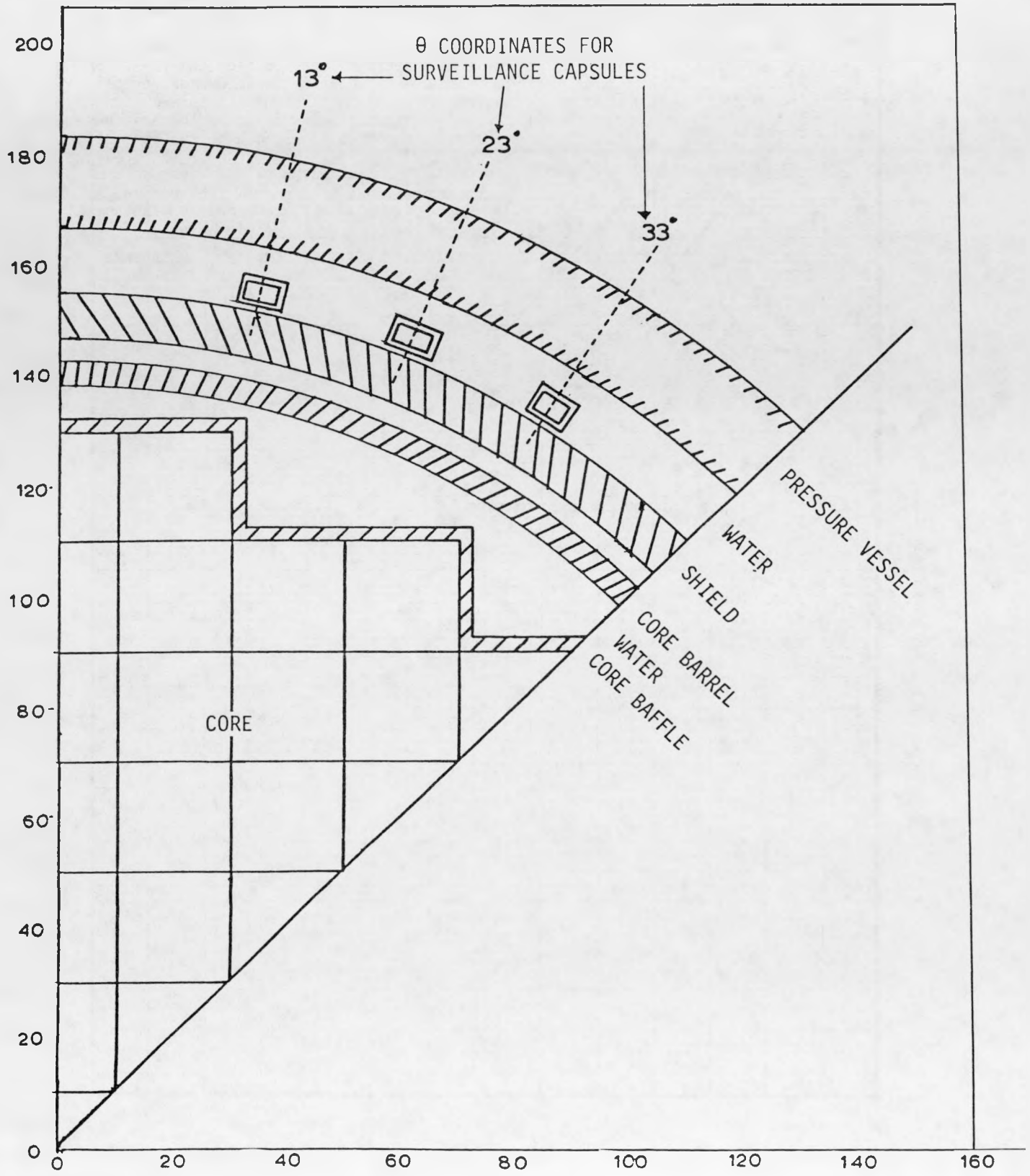

Fig. HEDL-A7. Type B, 2-Loop Reactor Geometry.

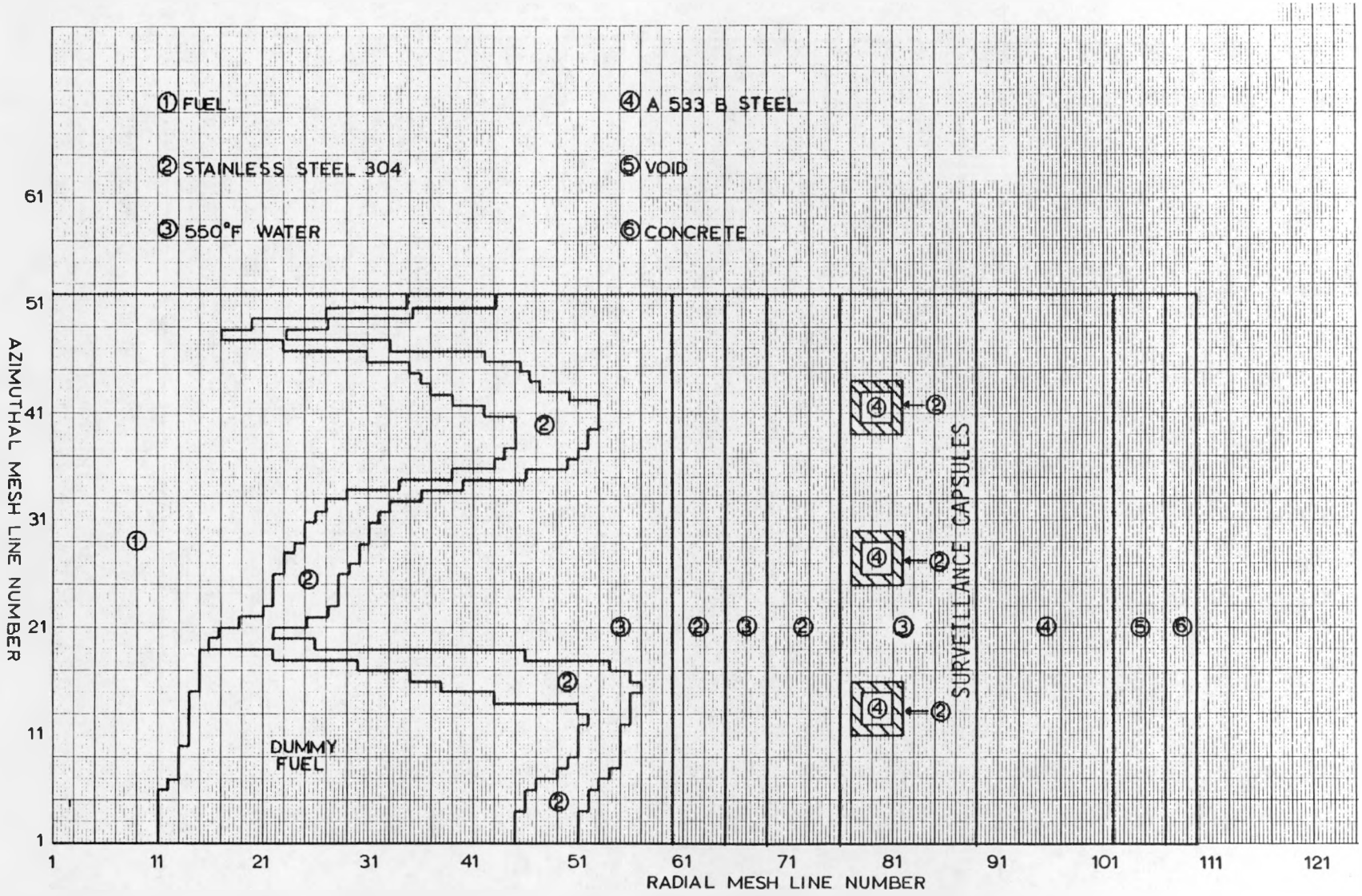

Fig. HEDL-A8. (R,θ) DOT Mesh Detail Map for a Type B, 2-Loop Shield Reactor.

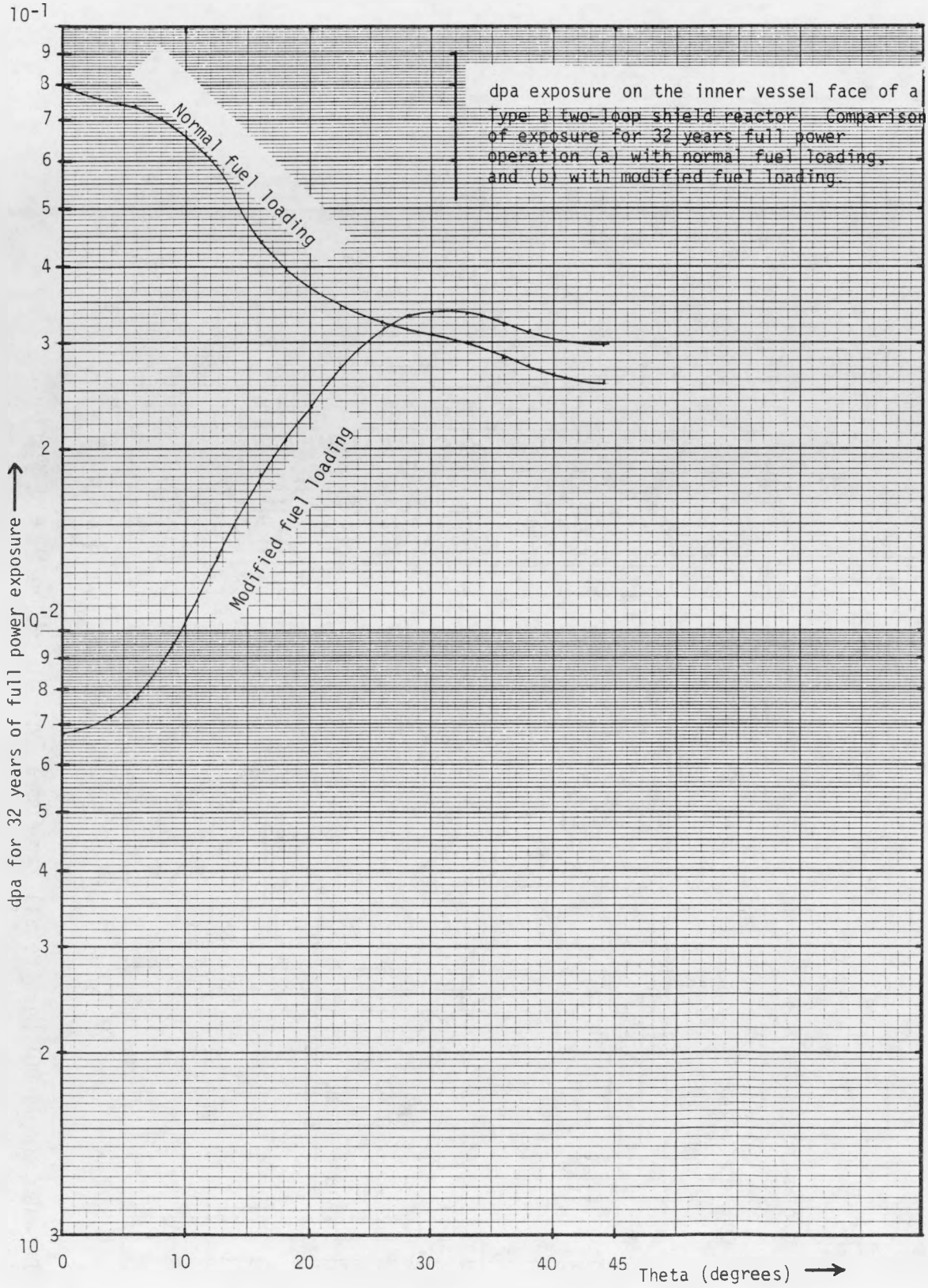

Fig. HEDL-A9. Dpa Exposure on the Vessel Inner Face of a Type B, 2-Loop Shield Reactor.

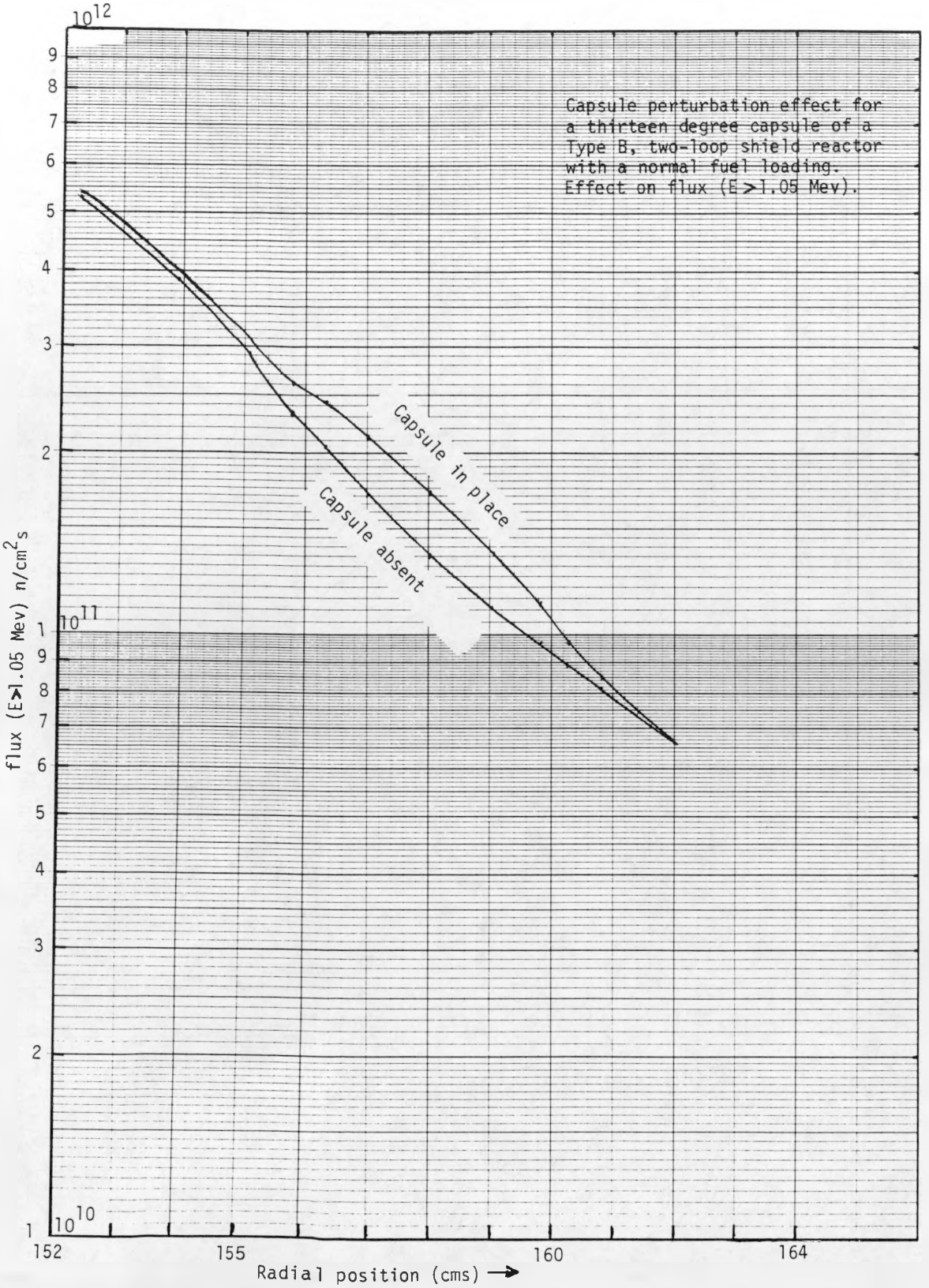

Fig. HEDL-A10. Capsule Flux Perturbation Effect for a 13° Capsule of a Type B, 2-Loop Shield Reactor with Normal Fuel Loading.

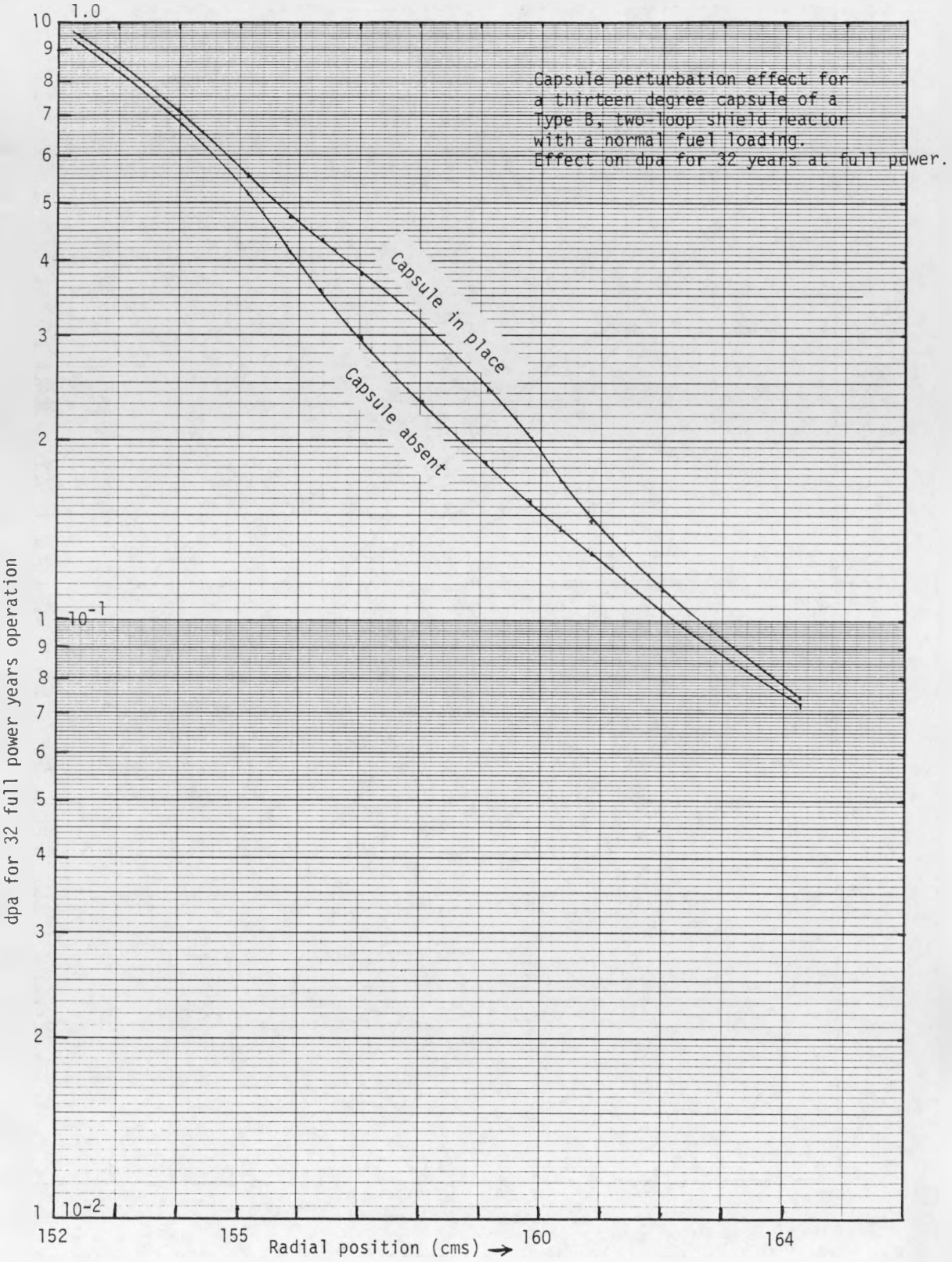

Fig. HEDL-A11. Capsule Perturbation for a Type B, 2-Loop Shield Reactor.

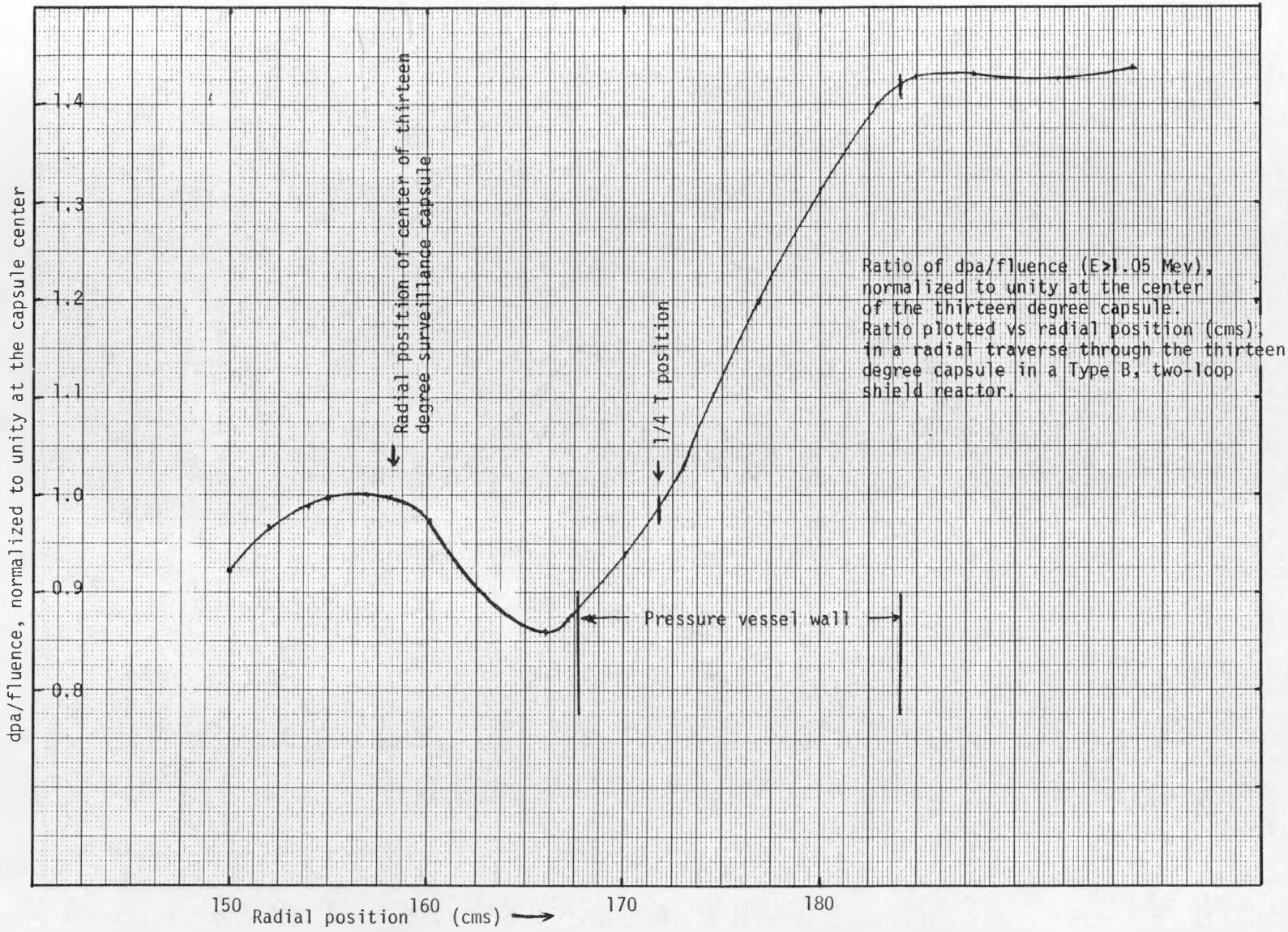

Fig. HEDL-A12. Dpa/Fluence vs Radial Position for a Type B, 2-Loop Shield Reactor.

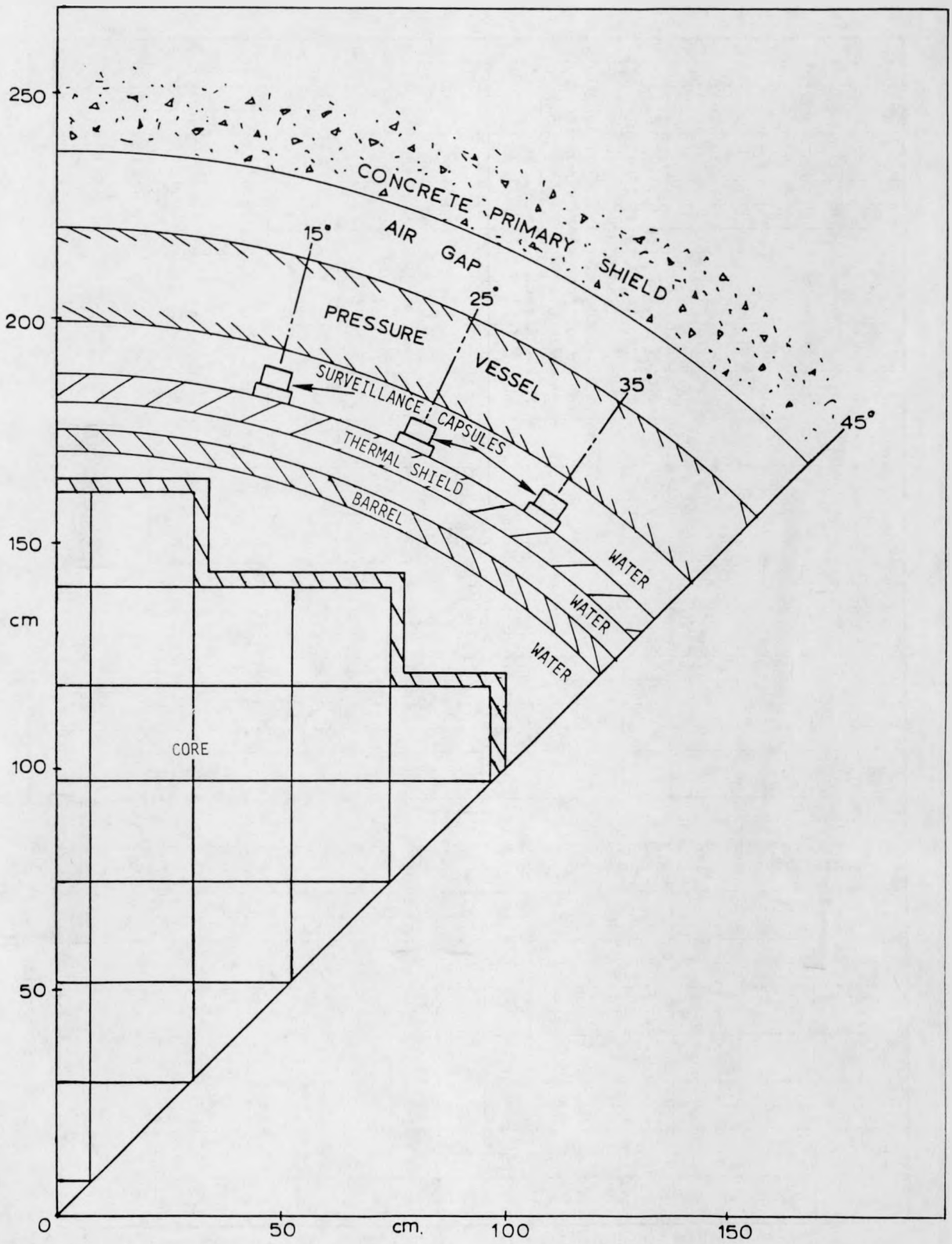

Fig. HEDL-A13. Type C, 3-Loop Shield Reactor.

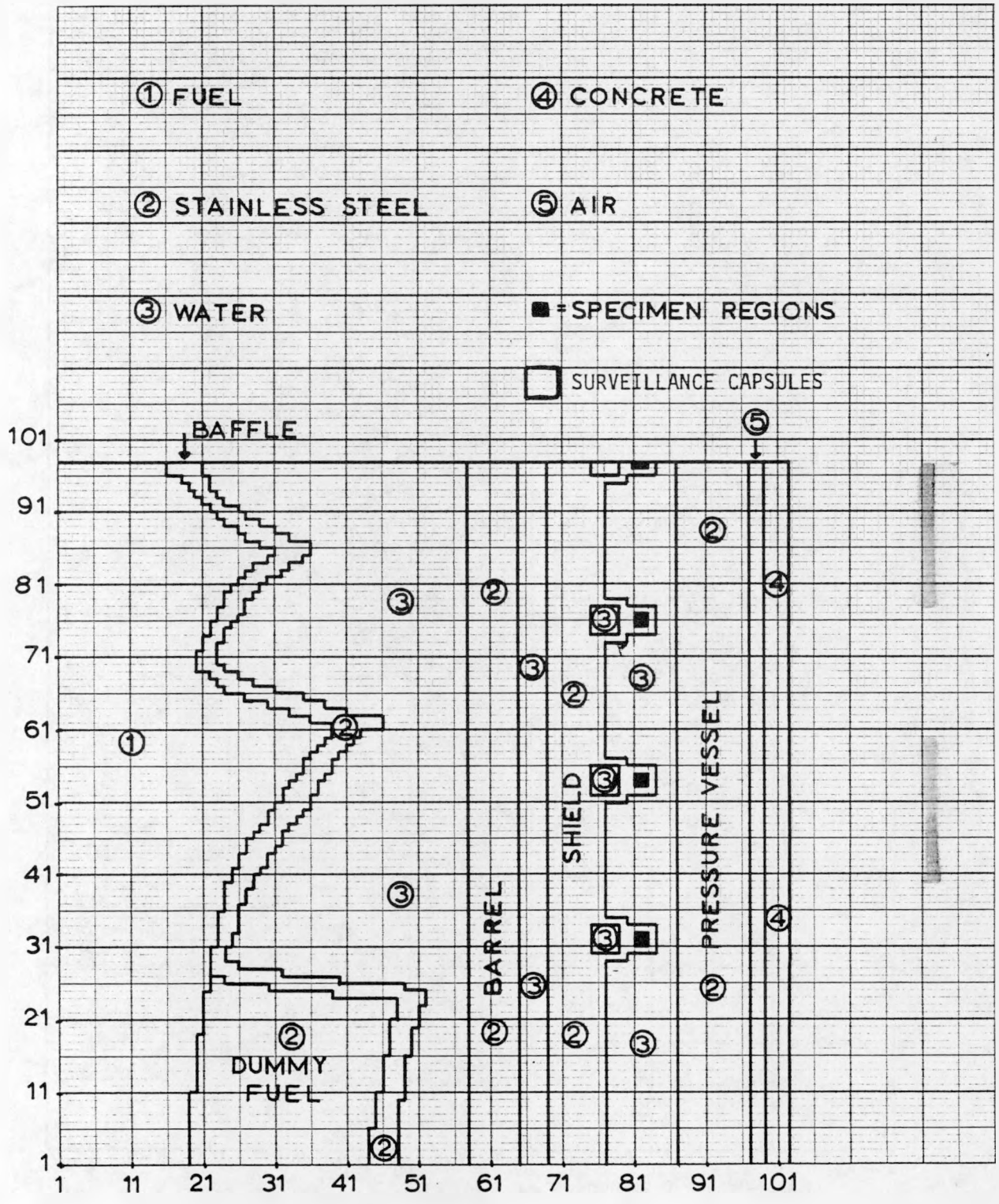

Fig. HEDL-A14. (R,θ) DOT Mesh for a Modified Fuel, Type C, 3-Loop Shield Reactor.

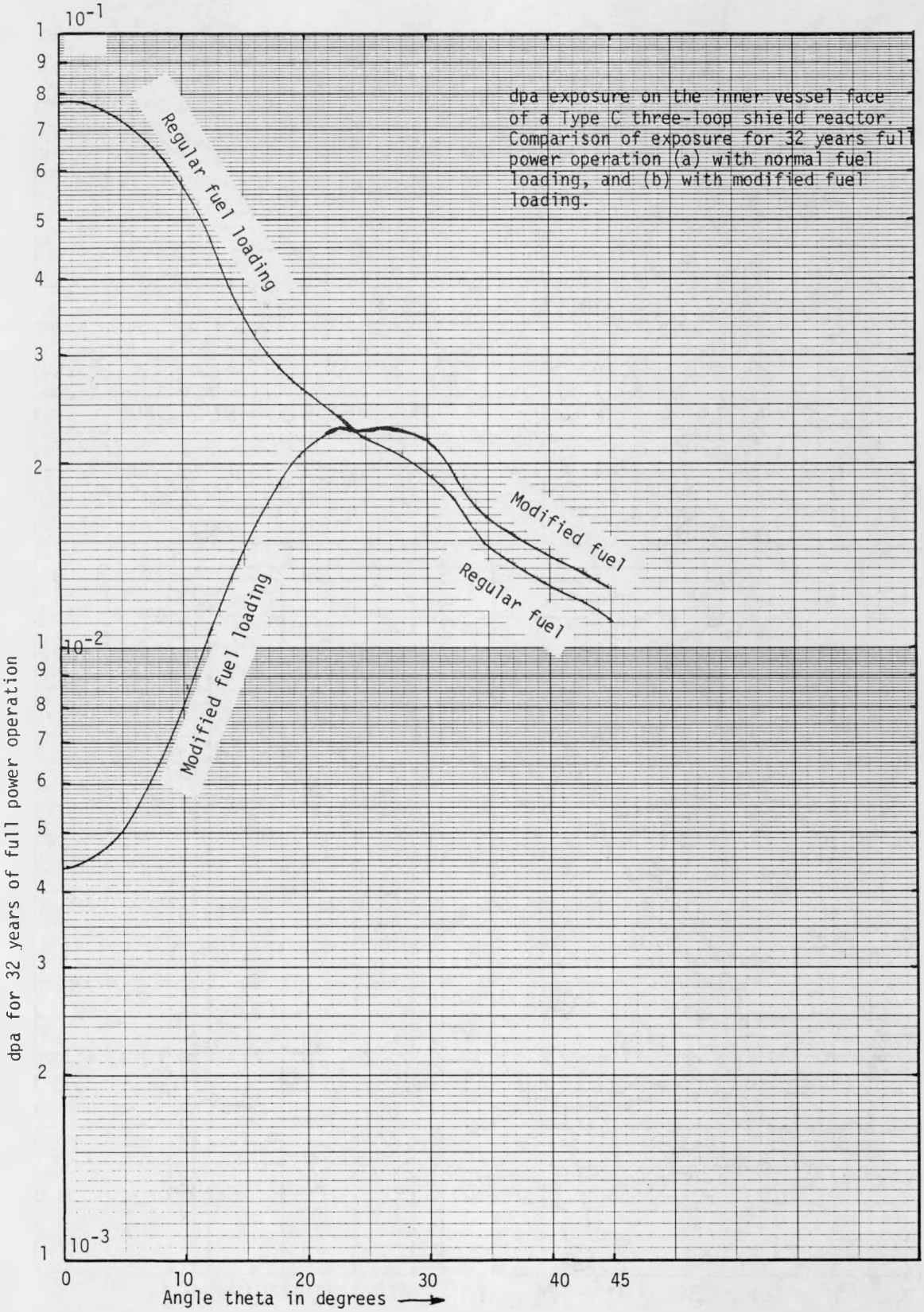

Fig. HEDL-A15. Dpa Exposure on the Vessel Inner Face of a Type C, 3-Loop Shield Reactor.

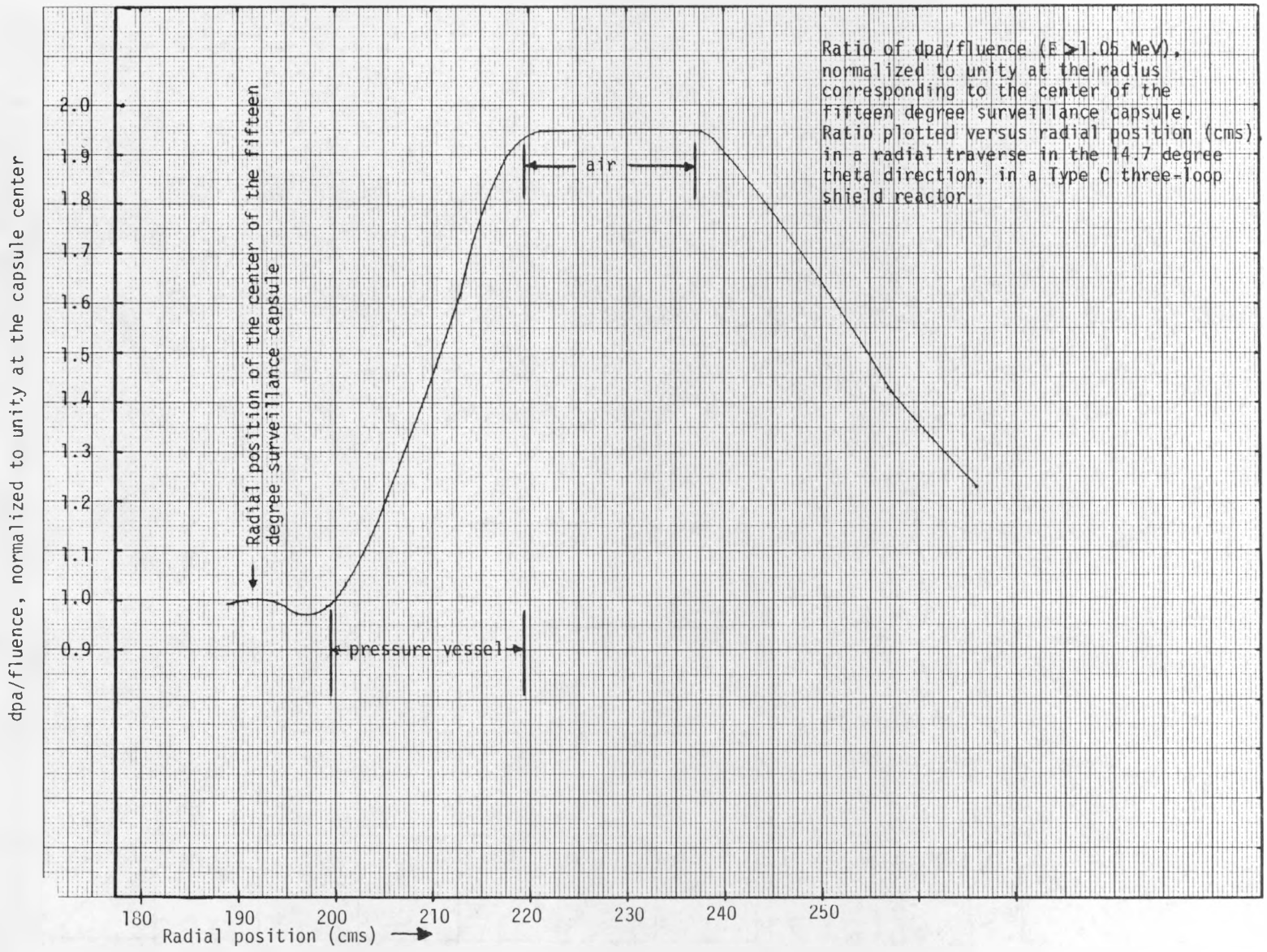

Fig. HEDL-A16. Dpa/Fluence for a Type C, 3-Loop Shield Reactor.

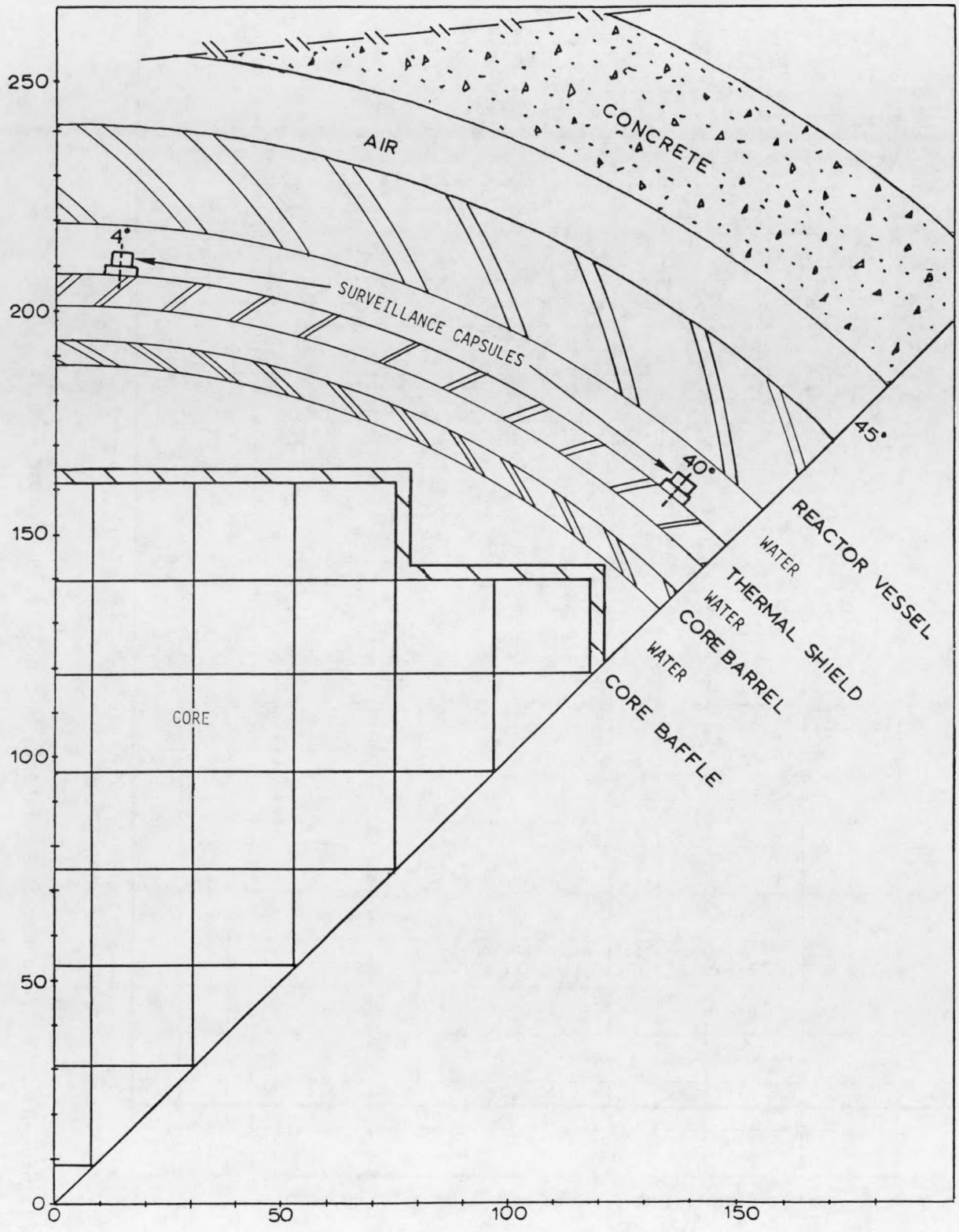

Fig. HEDL-A17. (x,y) Map for the Midplane of a Type D, 4-Loop Shield Reactor.

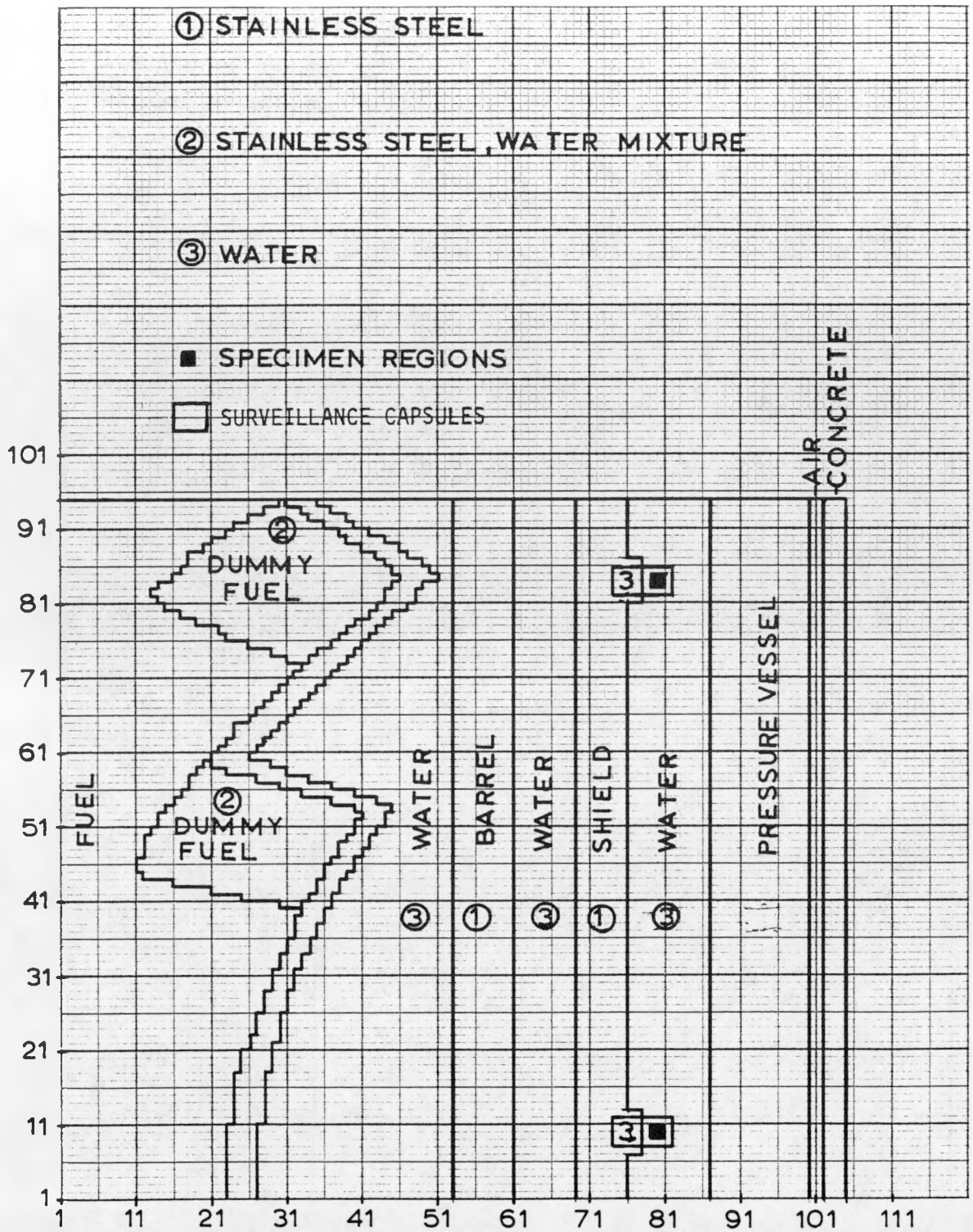

Fig. HEDL-A18. (R,θ) DOT Map for the Midplane of a Modified Fuel, Type D, 4-Loop Shield Reactor.

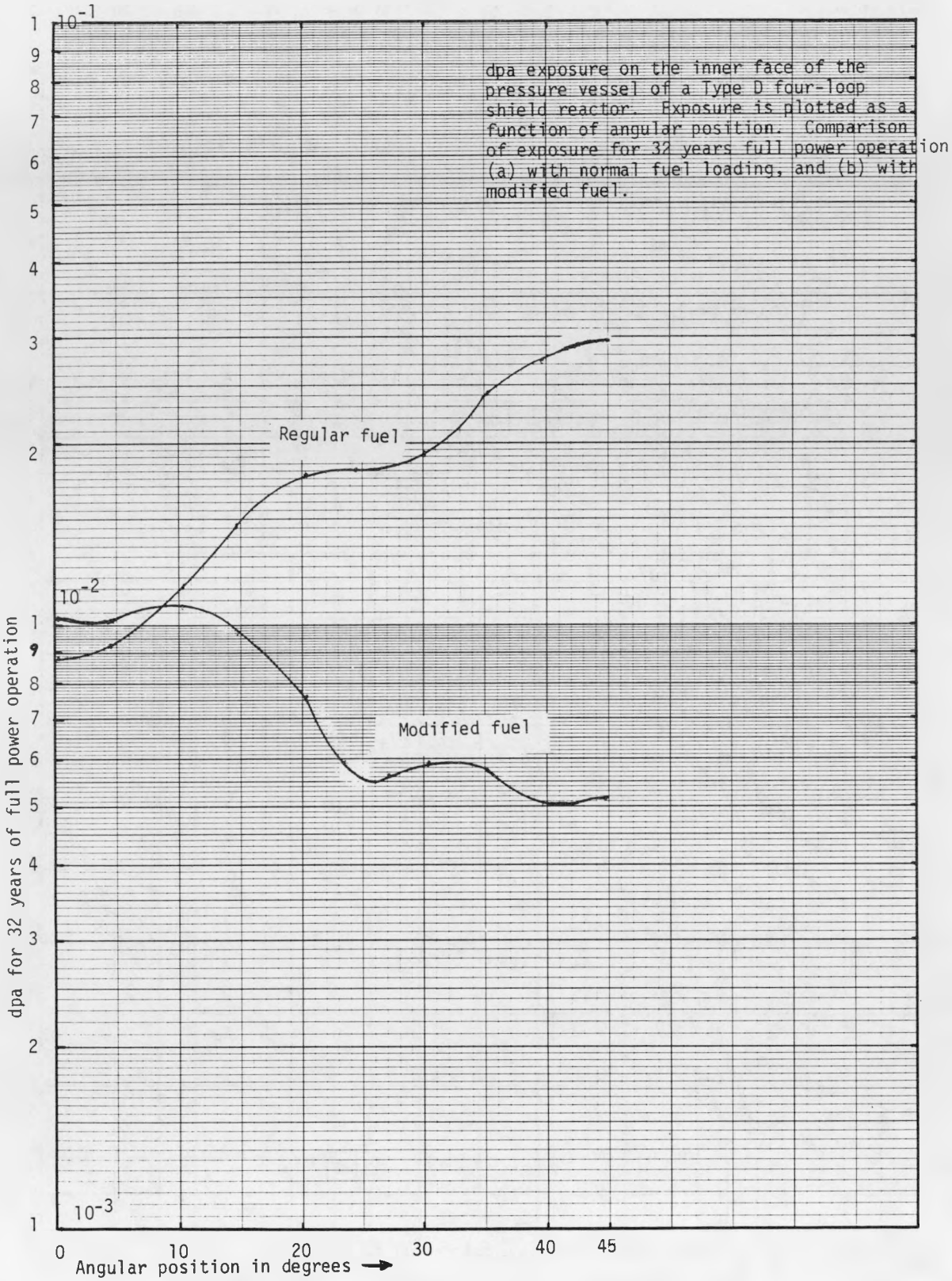

Fig. HEDL-A19. Dpa Exposure on the Vessel Inner Face of a Type D, 4-Loop Shield Reactor.

Fig. HEDL-A20. Dpa/Fluence vs Radial Position for a Type D, 4-Loop Shield Reactor.

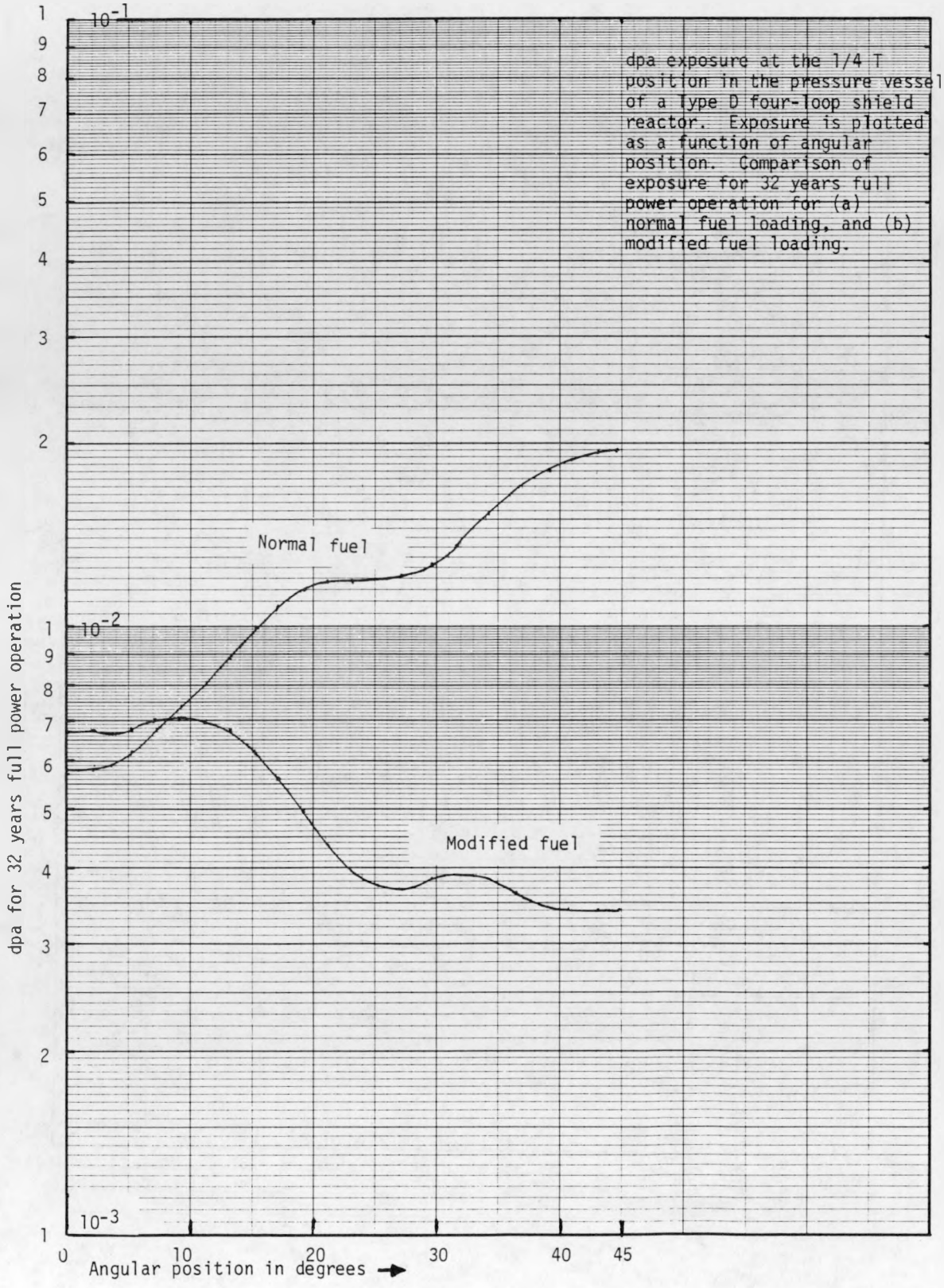

Fig. HEDL-A21. Dpa at 1/4 T Position of a Type D, 4-Loop Shield Reactor.

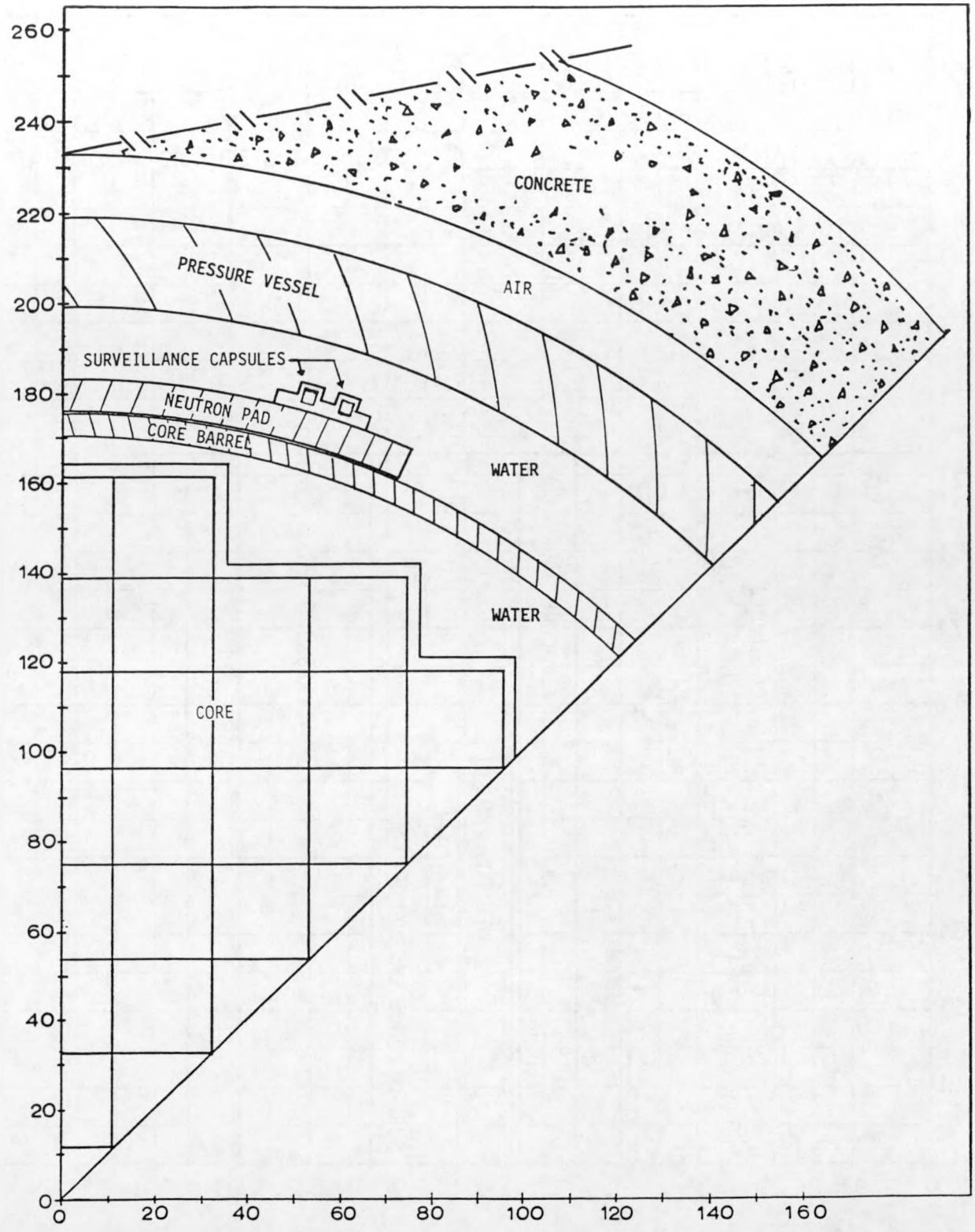

Fig. HEDL-A22. (x,y) Map for the Midplane of a Type E, 3-Loop Pad Reactor.

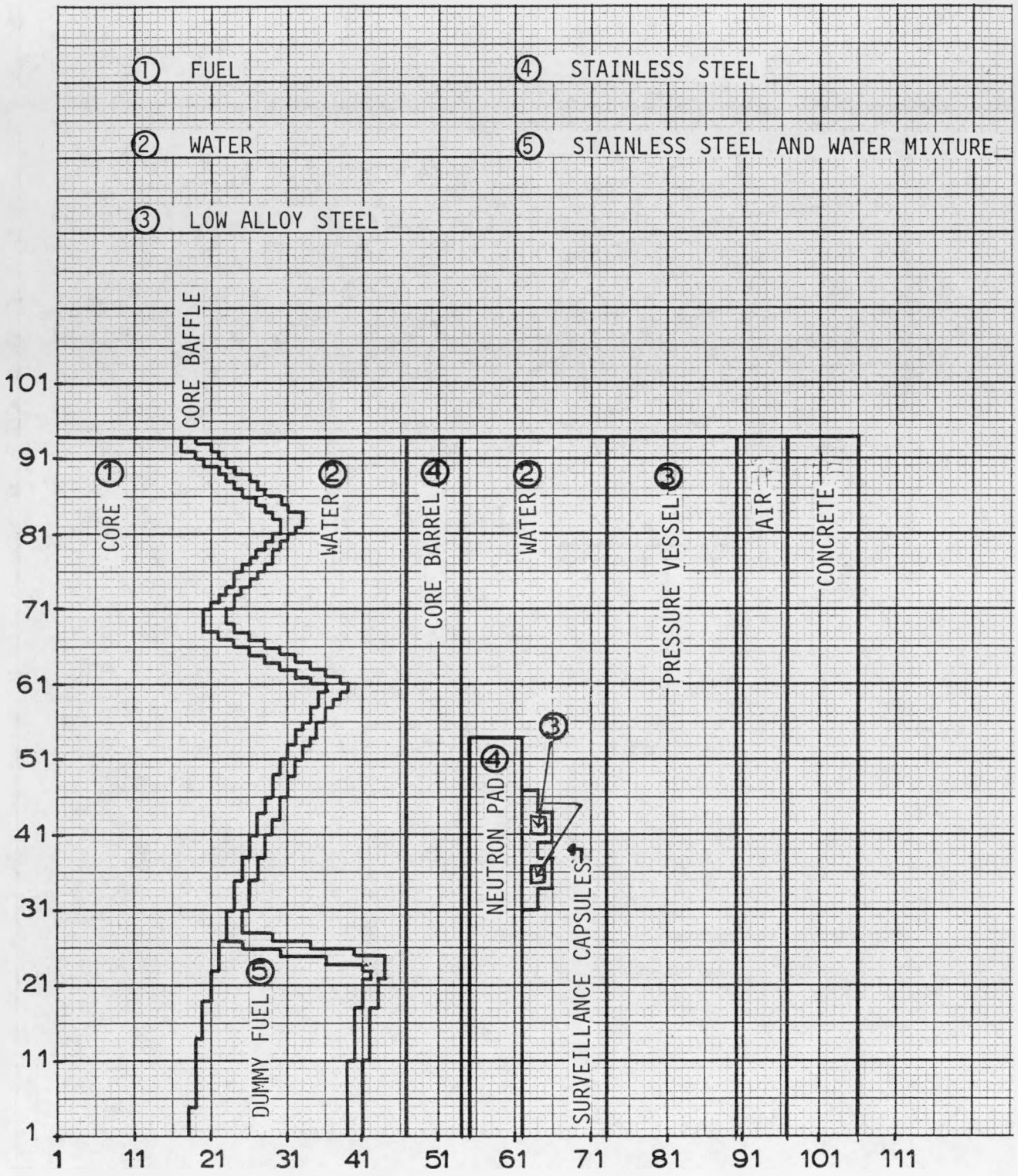

Fig. HEDL-A23. (R,θ) DOT Map for a Type E, 3-Loop Pad Reactor.

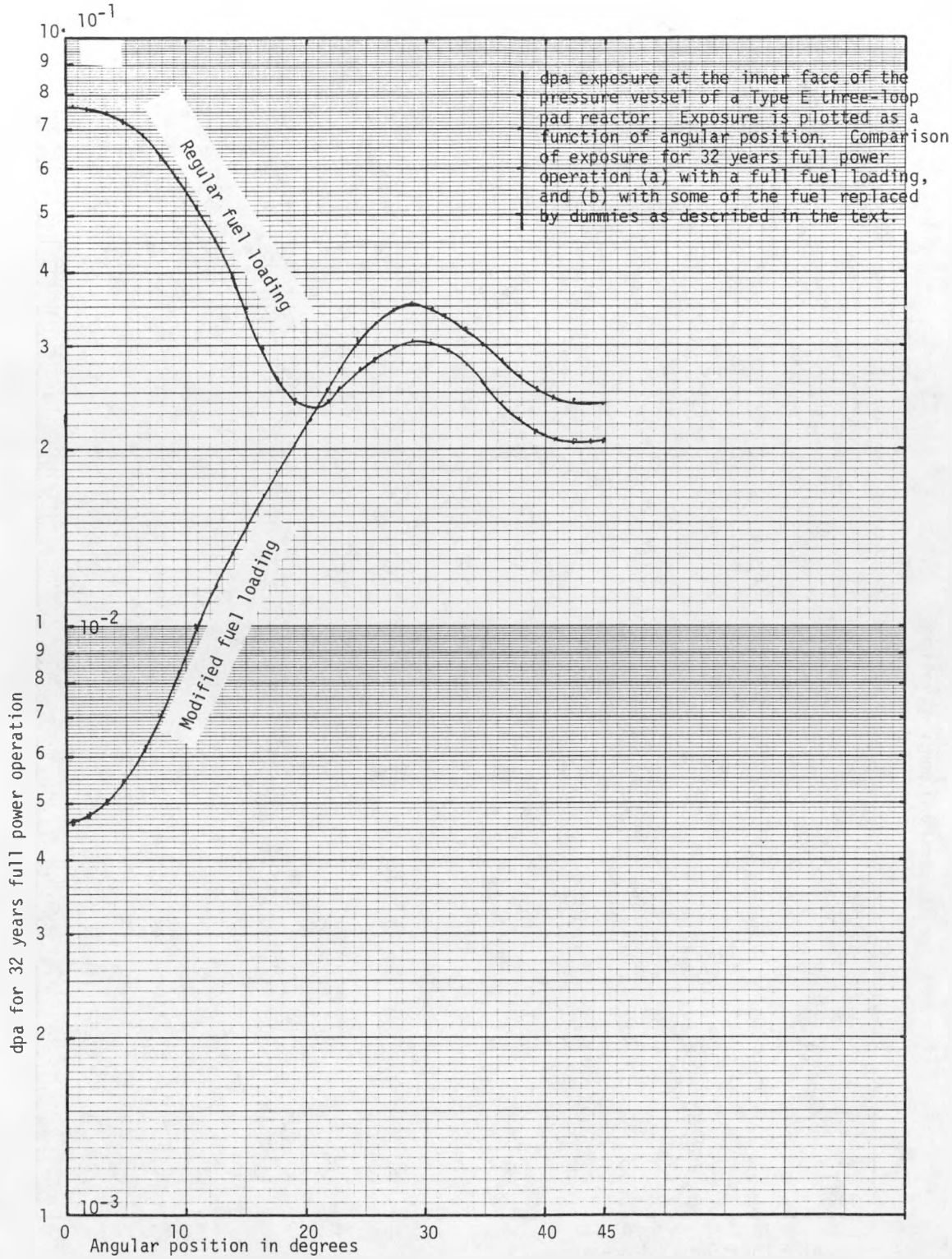

Fig. HEDL-A24. Dpa Exposure on the Vessel Inner Face of a Type E, 3-Loop Pad Reactor.

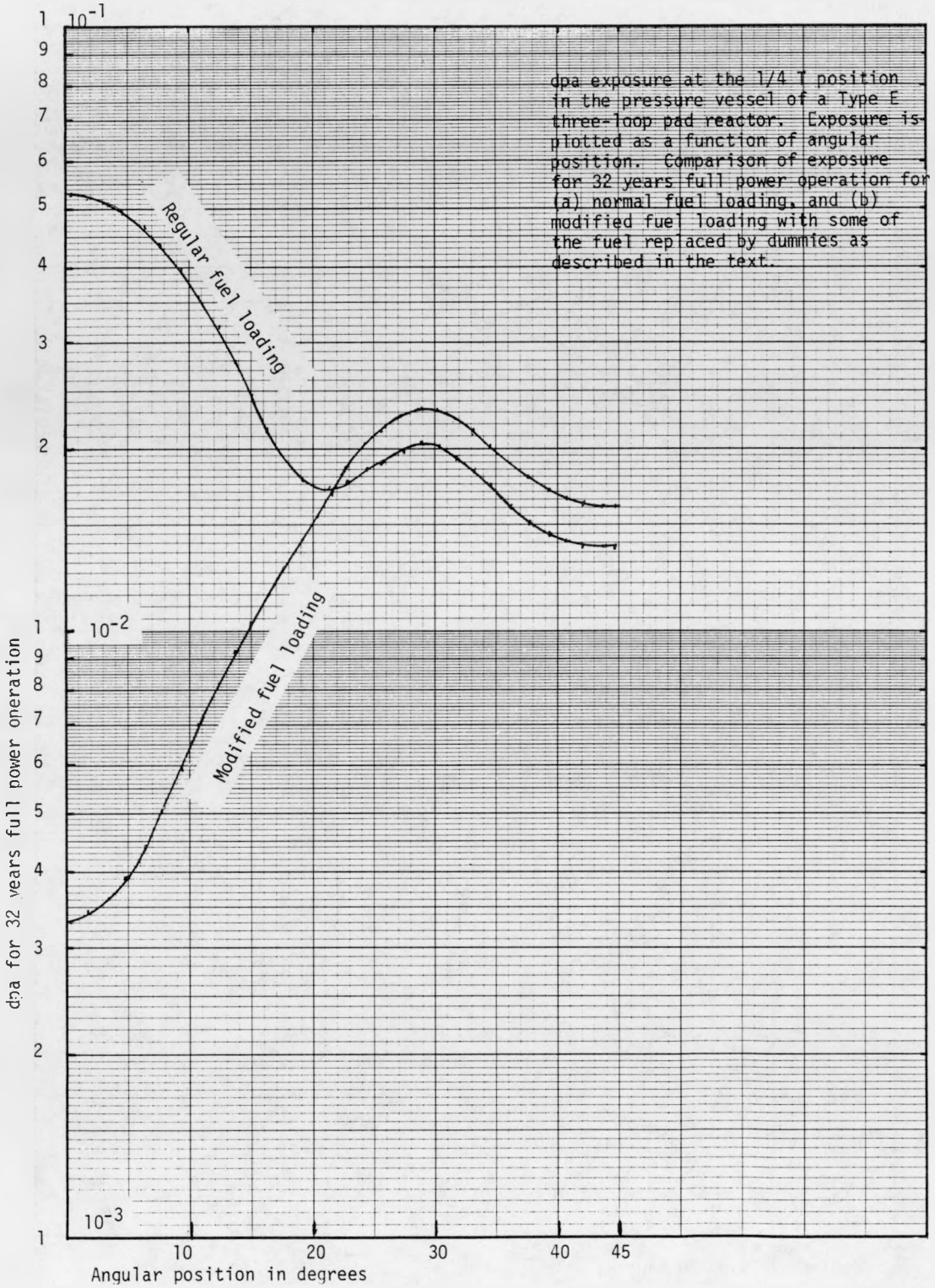

Fig. HEDL-A25. Dpa Exposure at the 1/4 T Position in the Pressure Vessel of a Type E, 3-Loop Pad Reactor.

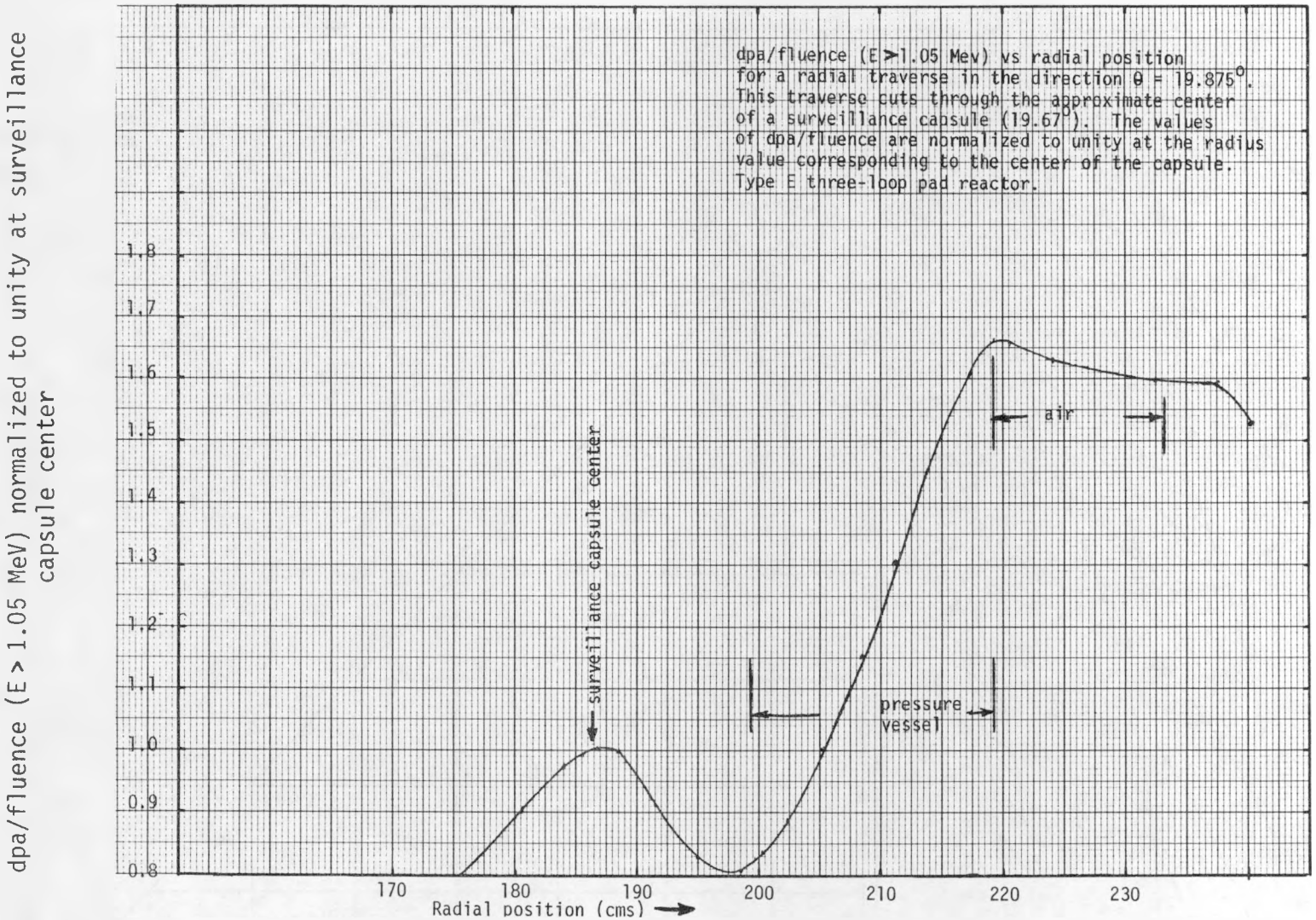

Fig. HEDL-A26. Dpa/Fluence vs Radial for a Type E, 3-Loop Pad Reactor.

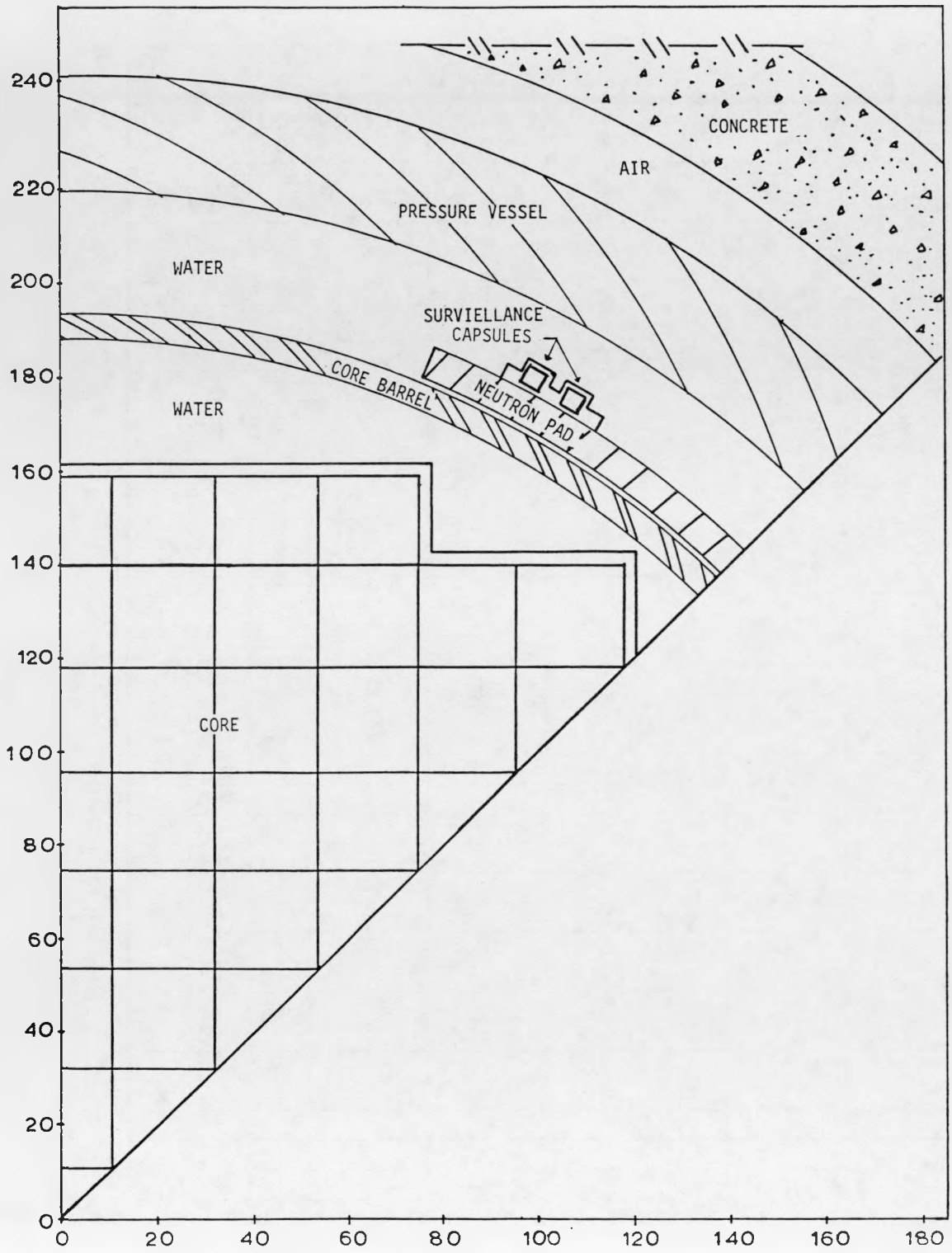

Fig. HEDL-A27. Midplane Geometry for a Type F, 4-Loop Pad Reactor.

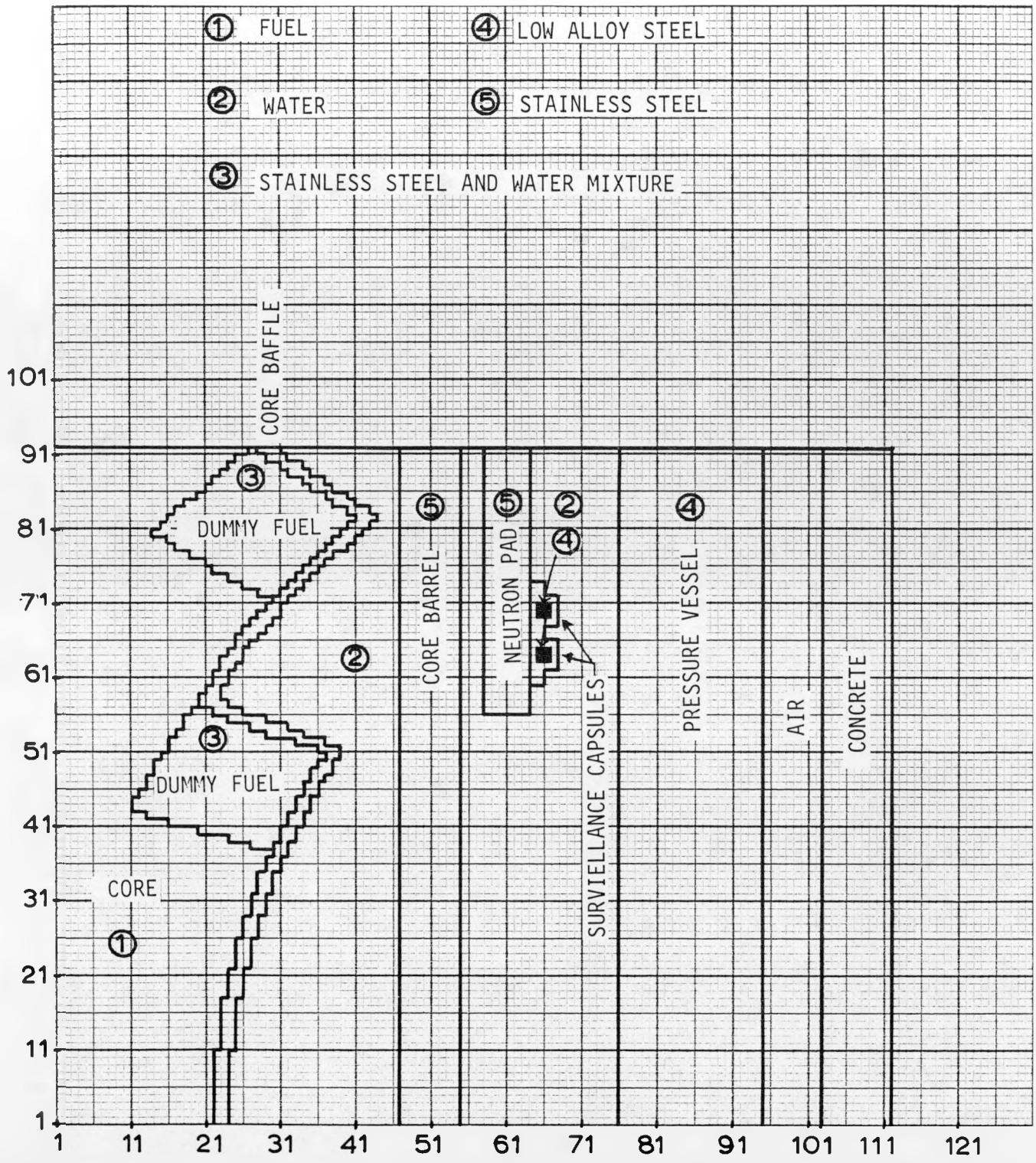

Fig. HEDL-A28. (R,θ) DOT Map for a Type F, 4-Loop Pad Reactor.

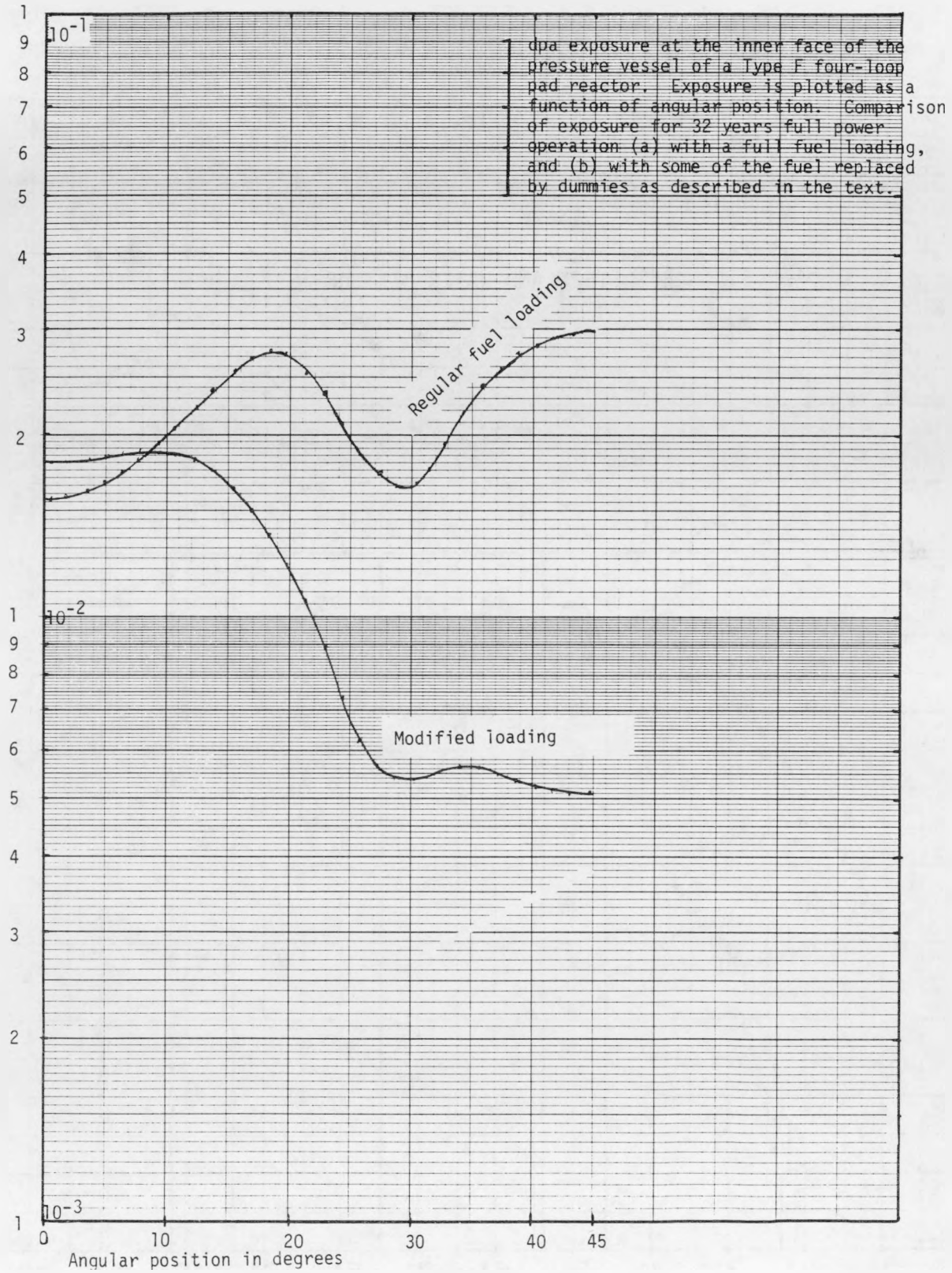

Fig. HEDL-A29. Dpa Exposure on the Vessel Inner Face of a Type F, 4-Loop Pad Reactor.

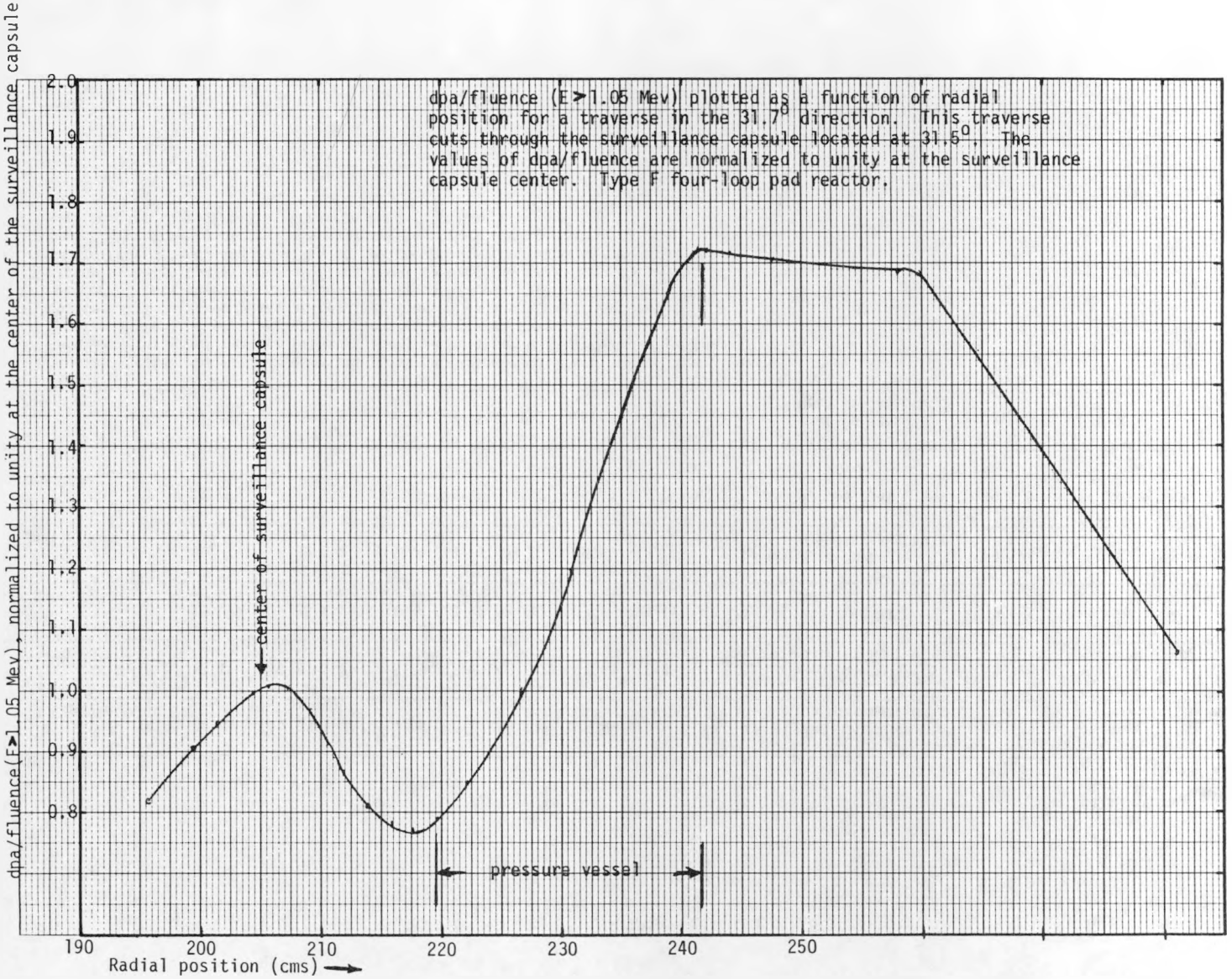

Fig. HEDL-A30. Dpa/Fluence vs Radial Position for a Type F, 4-Loop Pad Reactor.

HEDL-A2

SUMMARY OF FUEL MANAGEMENT RESULTS

Reactor Type	I	II	III	IV	V	III IV	III V	VI	VII	VIII	IX Calculated Capsule Perturbation?	X Radial Traverse Angle
Type A Accel + Wall Capsule	0°	28.5°	2.55 E-2	1.86 E-3	1.58 E-2	13.6	1.58	2.23	Two Assemblies on Flat near 0°	27.125	Yes	35°
Type B Two Loop Shield	0°	32.1°	7.91 E-2	6.79 E-3	3.40 E-2	11.64	2.33	1.62	1.5 Assemblies on Flat near 0°	15.125	Yes	13°
Type C Three Loop Shield	0°	23°	7.85 E-2	4.38 E-3	2.28 E-2	17.9	3.44	1.95	1.5 on Flat Near 0°	19.625	No	14.72°
Type D Four Loop Shield	45°	8°	2.98 E-2	5.14 E-3	1.089 E-2	5.81	2.74	2.12	2 at Corners Near 25° and 40°	24.125	No	39.7°
Type E Three Loop Pad	0°	28.75°	7.69 E-2	4.68 E-3	3.51 E-2	16.43	2.19	2.0	1.5 on Flat Near 0°	19.625	No	19.875°
Type F Four Loop Pad	45°	9.25°	2.99 E-2	5.14 E-3	1.87 E-2	5.82	1.6	2.18	2 at Corners Near 25° and 40°	24.125	No	31.7°

COLUMN NOTES:
- I Angular location of maximum exposure point on PV inner wall with normal fuel.
- II Angular location of maximum exposure point on PV inner wall with modified fuel.
- III dpa for 32 full power years at position I with normal fuel.
- IV dpa for 32 full power years at position I on PV wall with modified fuel.
- V dpa for 32 full power years at position II on PV wall with modified fuel.
- VI Factor by which dpa/ϕt changes (from front to back) in traversing PV wall.
- VII Number (Per Octant) and location of fuel assemblies replaced in modification.
- VIII Number (Per Octant) of fuel assemblies with normal fuel geometry.
- X Angular direction of radial traverse used in column VI.

OAK RIDGE NATIONAL LABORATORY
(ORNL)

A. LIGHT WATER REACTOR PRESSURE VESSEL (LWR-PV) BENCHMARK FACILITIES (PCA, ORR-PSF, ORR-SDMF) AT ORNL

F. B. K. Kam
F. W. Stallman
L. F. Miller

Objectives

In order to serve as benchmarks, the neutron fields at PCA, ORR-PSF, and ORR-SDMF need to be known and controlled within sufficiently narrow uncertainty bounds. To achieve this objective, extensive measurements are combined with neutron physics calculations. Statistical uncertainty analysis and spectral adjustment techniques are used to determine uncertainty bounds. The results of this task will have a direct impact in the preparation of ASTM Standards for Surveillance of Nuclear Reactor Pressure Vessels. The objectives of these benchmark fields are:

1) PCA (in operation)-- to validate and improve neutron transport calculations and dosimetry techniques in LWR-PV environments;
2) ORR-PSF (in operation)--to obtain reliable information from dosimetry measurements and neutron transport calculations and to correlate the spectral parameters with structural changes in the pressure vessel;
3) ORR-SDMF--to investigate results of current surveillance capsules so that dosimetry methods applied by vendors and service laboratories can be:
    a) validated and certified;
    b) improved by development of supplementary experimental data; and
    c) evaluated in terms of actual uncertainties.

A.1 Pressure Vessel Benchmark Facility for Improvement and Validation of LWR Physics Calculations and Dosimetry (PCA)

Accomplishments and Status

Calculations of the gamma group fluxes and the effect of photofission reactions in the PCA experiments have been initiated. A coupled neutron-gamma cross section set (51 neutron groups and 35 gamma groups) will be generated. Because of the importance of the thermal neutrons, a one dimensional run with 30 up-scatter groups has been used to generate a collapsed one thermal group for use in the coupled 51/35 group set.

Expected Accomplishments During the Next Reporting Period

It is expected that the coupled cross-section set will be completed by the next reporting period and the transport calculations initiated.

A.2 Pressure Vessel Benchmark Facility for LWR Metallurgical Testing of Reactor Pressure Vessel Steels (ORR-PSF)

Accomplishments and Status

Cumulative irradiation and temperature data for the Pressure Vessel Capsule through December 31, 1981 are given in Table ORNL-1.

Cumulative irradiation and temperature data for the SSC-2 capsule which was irradiated during the period June 1, 1981 (at 1148) to September 25, 1981 (at 0200) are shown in Table ORNL-2.

Transport calculations and measurements of the ORR-PSF startup experiments are scheduled for presentation at the 4th ASTM-EURATOM Symposium. Comparison between calculations and measurements and an analysis of the results will be presented in Tables.

Expected Accomplishments During the Next Reporting Period

Shipment of metallurgical specimens and dosimetry capsules will be completed.

Data for the ORR-PSF startup experiments will be documented for the next report period.

Table ORNL-1

Cumulative Irradiation and Temperature Distribution Data Through December 31, 1981

Data for PSF Specimen Set 0T
Hours of Irradiation Time = 11118.60
Megawatt Hours of Irradiation = 323032.91

Thermocouple	Hours of Irradiation					Average Temperature	Standard Deviation
	T<270	270<T<280	280<T<296	296<T<306	306<T		
TE 101	83.38	37.66	10964.13	33.38	0.00	288.80	1.65
TE 102	78.93	25.06	10922.84	91.68	0.00	291.20	1.24
TE 103	78.45	20.45	11019.64	0.00	0.00	289.19	0.98
TE 104	70.79	19.45	10856.75	171.53	0.00	292.39	1.01
TE 105	75.70	28.36	11014.50	0.00	0.00	286.32	1.01
TE 106	71.19	19.37	11027.97	0.00	0.00	289.42	0.98
TE 107	76.85	392.69	10649.03	0.00	0.00	283.07	1.25
TE 108	86.92	31.66	10990.86	9.06	0.00	288.84	1.48
TE 109	88.61	33.79	10987.35	8.78	0.00	288.53	1.52
TE 110	78.97	27.42	10999.21	12.95	0.00	289.41	1.27
TE 111							
TE 112							
TE 113	69.53	20.07	11026.81	0.12	2.00	290.08	1.48
TE 114	95.70	33.80	10989.03	0.00	0.00	288.27	1.41
TE 115							
TE 116	85.85	19.73	11012.94	0.00	0.00	290.06	0.77
TE 117	77.59	23.12	11012.02	5.29	0.50	290.92	0.83
TE 118	80.44	29.88	11008.29	0.00	0.00	286.73	0.88
TE 119	76.88	26.73	11014.96	0.00	0.00	286.78	0.89
TE 120	82.40	252.96	10783.27	0.00	0.00	284.01	1.28

Data for PSF Specimen Set 1/4T
Hours of Irradiation Time = 11118.60
Megawatt Hours of Irradiation = 323032.91

TE 201	82.78	31.29	11001.84	2.66	0.00	289.72	1.34
TE 202	83.28	28.78	11006.32	0.17	0.00	288.73	0.83
TE 203	80.84	24.10	11013.65	0.00	0.00	288.60	0.93
TE 204	76.96	23.69	11017.59	0.33	0.00	289.79	0.75
TE 205	77.03	31.19	11010.35	0.00	0.00	286.71	0.88
TE 206	75.21	29.05	11014.32	0.00	0.00	287.20	0.77
TE 207	80.27	115.22	10923.10	0.00	0.00	283.32	0.93
TE 208	83.45	25.94	11008.33	0.83	0.00	288.33	1.12
TE 209	85.43	31.06	11000.09	2.00	0.00	288.71	1.07
TE 210	85.50	41.10	10991.98	0.00	0.00	286.28	0.90
TE 211	90.95	53.73	10973.88	0.00	0.00	284.11	0.79
TE 212	72.96	14.66	11028.83	2.08	0.00	290.71	0.89
TE 213	73.60	16.00	11028.94	0.00	0.00	289.37	1.00
TE 214	86.17	25.06	11007.32	0.00	0.00	290.29	0.90
TE 215	86.62	32.45	10999.45	0.00	0.00	287.31	0.65
TE 216	84.71	25.23	11008.61	0.00	0.00	287.83	0.66
TE 217	79.90	19.54	11019.12	0.00	0.00	289.53	0.81
TE 218	78.61	24.81	11013.14	2.00	0.00	287.08	0.81
TE 219	77.19	21.66	11019.74	0.00	0.00	287.20	0.73
TE 220	76.97	112.81	10928.79	0.00	0.00	285.94	1.03

Table ORNL-1 (Cont'd)

Data for PSF Specimen Set 1/2T
Hours of Irradiation Time = 11118.60
Megawatt Hours of Irradiation = 323032.91

Thermocouple	Hours of Irradiation					Average Temperature	Standard Deviation
	T<270	270<T<280	280<T<296	296<T<306	306<T		
TE 301	82.49	17.54	10979.38	39.18	0.00	289.82	0.89
TE 302	85.22	25.90	11007.46	0.00	0.00	286.61	0.72
TE 303	81.60	21.42	11015.51	0.00	0.00	287.29	0.77
TE 304	74.17	20.26	11023.53	0.58	0.00	291.18	0.68
TE 305	74.86	21.34	11022.31	0.03	0.00	287.52	0.80
TE 306	79.12	26.14	11013.29	0.00	0.00	286.59	0.72
TE 307							
TE 308	85.96	17.31	11015.29	0.00	0.00	288.83	1.11
TE 309	86.50	22.66	11009.42	0.00	0.00	287.90	0.80
TE 310	90.89	43.18	10984.51	0.00	0.00	285.38	0.95
TE 311	89.36	44.59	10984.67	0.00	0.00	285.88	0.98
TE 312	78.32	15.62	11024.44	0.17	0.00	288.58	0.79
TE 313	76.72	16.09	11024.09	1.67	0.00	290.13	0.88
TE 314	88.53	21.14	11008.88	0.00	0.00	289.17	0.94
TE 315	93.38	27.31	10997.87	0.00	0.00	285.30	0.87
TE 316	85.99	13.70	11018.88	0.00	0.00	287.66	0.63
TE 317	78.22	16.89	11023.45	0.00	0.00	290.85	0.75
TE 318	77.51	16.65	11024.37	0.00	0.00	289.30	0.82
TE 319	83.33	28.00	11007.22	0.00	0.00	285.22	0.69
TE 320	79.50	18.62	11020.41	0.00	0.00	287.75	1.06

Table ORNL-2

Cumulative Irradiation and Temperature Distribution Data
From 1148, June 1, 1981 Through 0200, September 25, 1981

Data for PSF Specimen Set SSC-2
Hours of Irradiation Time = 2209.87
Megawatt Hours of Irradiation = 64726.56

Thermocouple	Hours of Irradiation					Average Temperature	Standard Deviation
	T<270	270<T<280	280<T<296	296<T<306	306<T		
TE 1	24.99	33.59	2151.26	0.00	0.00	288.40	2.15
TE 2	15.53	8.43	194.00	1960.54	31.34	299.91	2.38
TE 3	20.84	10.01	2168.02	11.00	0.00	291.97	1.82
TE 4	22.46	11.45	2175.95	0.00	0.00	289.37	2.08
TE 5	30.83	705.94	1473.07	0.00	0.00	282.18	2.79
TE 6	33.76	596.93	1579.15	0.00	0.00	282.67	2.62
TE 7	1070.81	1106.04	33.01	0.00	0.00	273.81	1.82
TE 8	24.83	19.48	2096.53	69.01	0.00	289.28	2.63
TE 9	19.02	16.18	1449.54	725.11	0.00	294.88	2.23
TE 10	72.94	2059.88	77.01	0.00	0.00	276.64	2.23
TE 11	40.86	1165.45	1003.52	0.00	0.00	279.29	2.13
TE 12	25.22	10.52	2169.10	5.00	0.00	290.04	2.16
TE 13	22.16	9.46	1623.77	554.46	0.00	293.81	2.34
TE 14	25.10	7.74	2162.01	15.00	0.00	288.92	1.97
TE 15	14.10	12.07	183.13	1979.54	21.00	300.47	1.89
TE 16	24.11	7.65	2178.11	0.00	0.00	290.08	1.37
TE 17	17.16	12.54	1922.44	257.71	0.00	294.39	1.80
TE 18	32.76	1011.70	1165.38	0.00	0.00	280.71	1.88
TE 19	30.72	204.61	1974.48	0.00	0.00	283.38	1.54
TE 20	1475.81	730.05	4.00	0.00	0.00	272.11	1.55

A.3 Surveillance Dosimetry Measurement Benchmark Facility (SDMF) for Validation and Certification of Neutron Exposures from Power Reactor Surveillance

Accomplishments and Status

As-built drawings for the Babcock and Wilcox surveillance capsule mockup are still not available from the vendor. Plans for the irradiation and characterization of the capsule are scheduled to take place in July 1982.

Expected Accomplishments in the Next Reporting Period

Drawings and fabrication of the Babcock and Wilcox capsule should be completed. The vendor must take action in the next reporting period if we are to meet the scheduled irradiation date in July 1982.

B. ASTM STANDARDS FOR SURVEILLANCE OF NUCLEAR REACTOR PRESSURE VESSELS

F. B. K. Kam
F. W. Stallman
L. F. Miller

Objectives

The primary objective of the LWR Pressure Vessel Surveillance Dosimetry program is to prepare an updated and improved set of dosimetry, damage correlation, and associated reactor analysis ASTM Standards to predict the integrated effect of neutron exposure to LWR pressure vessels and support structures.

Accomplishments and Status

"The ASTM Standard Guide for Application of Neutron Transport Methods for Reactor Vessel Surveillance" was balloted and approved by the ASTM E10.05 Subcommittee and the E10 Committee. A few editorial changes were made and the final approved version (Appendix 1) submitted for final Society ballot.

Expected Accomplishments During the Next Reporting Period

Comments or negative votes will be discussed and reviewed on the "ASTM New Standard Recommended Practice for the Application of Neutron Adjustment Methods in Reactor Surveillance" at the 4th ASTM-EURATOM Meeting at NBS, March 22-26, 1982. A revised version will be submitted for simultaneous balloting by the E10 Committee and the E10.05 Subcommittee.

APPENDIX STANDARD GUIDE FOR APPLICATION OF NEUTRON TRANSPORT METHODS FOR REACTOR VESSEL SURVEILLANCE [E706(II-D)]

1.0 SCOPE

1.1 Need for Neutronics Calculations

An accurate calculation of the neutron flux at several locations is essential for the analysis of integral dosimetry measurements and for predicting irradiation damage exposure parameter values in the pressure vessel. Exposure parameter values may be obtained directly from calculations or indirectly from calculations that are adjusted with dosimetry measurements; in particular, references 2.1.1 and 2.1.2, section 2.1, define appropriate computational procedures.

1.2 Methodology

Neutronics calculations for application to reactor vessel surveillance encompass three essential areas: 1) validation of methods by comparison of calculations with dosimetry measurements in a benchmark experiment, 2) determination of the neutron source distribution in the reactor core, and 3) calculation of neutron flux at the surveillance position and in the pressure vessel.

2.0 APPLICABLE DOCUMENTS

2.1 American Society for Testing and Materials (ASTM Standards)

2.1.1 E706(0), E706 Master Matrix for LWR-PV Surveillance Standards

2.1.2 E706(IA) Analysis and Interpretation of Nuclear Reactor Surveillance Results

2.1.3 E706(IC), E560 Surveillance Test Results Extrapolation

2.1.4 E706(ID), E693 Displaced Atom (dpa) Exposure Unit

2.1.5 E706(IE) Damage Correlation for Reactor Vessel Surveillance

2.1.6 E706(IIA) Application of Neutron Spectrum Adjustment Methods

2.1.7 E706(IIB) Application of ENDF/A Cross Section and Uncertainty Files

2.1.8 E706(IIC) Sensor Set Design and Irradiation for Reactor Surveillance

2.1.9 E706(IIE) Benchmark Testing of Reactor Vessel Dosimetry

2.1.10 E170 Definition of Terms Relating to Dosimetry

2.2 Other Documents

2.2.1 C. R. Weisbin, et al, Application of FORSS Sensitivity and Uncertainty Methodology to Fast Reactor Benchmark Analysis, ORNL/TM-5563 (December 1976).

2.2.2 AMPX-II: A Modular Code System for Generating Coupled Multigroup Neutron-Gamma Libraries from ENDF Format, PSR-63, Oak Ridge National Laboratory, Radiation Shielding Information Center (1978).

2.2.3 B. J. Carlson and K. O. Lathrop, "Transport Theory - The Method of Discrete Ordinates," Computing Methods in Reactor Physics, H. Greenspan, C. N. Kelber, and B. Okrent, p. 165, Gordon and Breach, New York (1968).

2.2.4 W. N. McElroy, et al, LWR Pressure Vessel Surveillance Dosimetry Improvement Program: PCA Experiments and Blind Test, NUREG/CR-1861, HEDL-TME 80-87, Hanford Engineering Development Laboratory, Richland, Washington (July 1981).

3.0 SIGNIFICANCE AND USE

3.1 General

The methodology recommended in this guide specifies criteria for validating computational methods and outlines procedures applicable to pressure vessel related neutronics calculations for test and power reactors. The material presented herein is useful for validating computational methodology and for performing neutronics calculations that accompany reactor vessel surveillance dosimetry measurements (see references 2.1.1 and 2.1.2). Briefly, the overall methodology involves: 1) methods-validation calculations based on at least one well documented benchmark problem, and 2) neutronics calculations for the facility of interest. The neutronics calculations on the facility of interest and on the benchmark problem should be as nearly the same as is feasible; in particular, the group structure and common broad-group microscopic cross sections should be preserved for both problems. The neutronics calculations involve two tasks: 1) determination of the neutron source distribution in the reactor core by utilizing diffusion theory (or transport theory) calculations in conjunction with reactor power distribution measurements, and 2) performance of a fixed fission rate neutron source (fixed-source) transport theory calculation to determine the neutron flux distribution in the reactor core, through the internals and in the pressure vessel. Some neutronics modeling details for the benchmark, test reactor or the power reactor calculation will differ; hence, the procedures described herein are general and apply to each case.

It is expected that transport calculations will be performed whenever pressure vessel surveillance dosimetry data become available and that quantitative comparisons will be performed as prescribed by Section 3.2.2. All dosimetry data accumulated that are applicable to a particular facility should be included in the comparisons.

3.2 Validation

Prior to performing transport calculations for a particular facility, the computational methods must be validated by comparing results with measurements made on a benchmark experiment. Criteria for establishing a benchmark experiment for the purpose of validating neutronics methodology should include those set forth in reference 2.1.9 as well as those prescribed in section 3.2.1. A discussion of the limiting accuracy of benchmark validation procedures for the LWR surveillance program is given in reference 2.2.4.

3.2.1 Requirements for Benchmarks

In order for a particular experiment to qualify as a calculational benchmark, the following criteria are recommended:

1) sufficient information must be available to accurately determine the neutron source distribution in the reactor core,

2) measurements must be reported in at least two ex-core locations, well separated by steel or coolant,

3) differences between measurements and calculations should lie within one standard deviation as determined from the square root of the sum of the variances,

4) quantitative criteria, consistent with those specified in the methods validation section (3.2.2), must be published and demonstrated to be achievable,

5) uncertainty estimates should be reported for directly measured parameters and for exposure parameters derived from measurements,

6) results for exposure parameter values of neutron flux greater than one MeV [$\phi(E>1\ MeV)$] and of displacements per atom (dpa) should be reported consistent with references 2.1.2 and 2.1.4, and

7) reaction rates (preferably established relative to neutron fluence standards) must be reported for $^{237}Np(n,f)$ or $^{238}U(n,f)$, and $^{58}Ni(n,p)$ or $^{54}Fe(n,p)$; additional reactions which aid in spectral characterization such as provided by Cu, Ti, and Co-Al, should also be included in the benchmark measurements. The $^{237}Np(n,f)$ reaction is an important reaction since it gives information similar to dpa. References 2.1.2, 2.1.6, 2.1.8 and 2.1.9 discuss this criterion.

3.2.2 Methodology Validation

It is essential that the neutronics methodology employed for predicting neutron fluence in a power reactor pressure vessel be validated by accurately predicting appropriate benchmark dosimetry results. In addition, the following documentation must be submitted:

1) convergence study results, and

2) uncertainty results based on geometry and source estimates.

For example model specifications for S_n methods on which convergence studies should be performed include: 1) group structure, 2) spatial mesh, and 3) angular quadrature. One-dimensional calculations may be performed to check the adequacy of group structure and spatial mesh. Two-dimensional calculations should be employed to check the adequacy of the angular quadrature. Note that cross section expansion and angular quadrature should be numerically consistent (e.g., S_8 should be the minimum quadrature for a P_3 expansion) and that a P_3 cross section expansion is recommended.

Uncertainties that are propagated from known uncertainties in nuclear data should be obtained, but they are not required [2.2.1]. Appropriate computer programs and covariance data are available, however, and sensitivity data may be obtained as an intermediate step in determining uncertainty estimates.

Effects of known uncertainties in geometry and source distribution should be evaluated based on the following test cases:

1) reference calculation with a time-averaged source distribution and with best estimates of the core, thermal shield and pressure vessel locations,

2) reference case geometry with maximum and minimum expected deviations in the source distribution, and

3) reference case source distribution with maximum expected spatial perturbations of the core, thermal shield and pressure vessel.

Measured and calculated integral parameters should be compared for all test cases. It is expected that larger uncertainties are associated with geometry and neutron source specifications than with parameters included in the convergence study. Problems associated with space, energy and angle discretizations can be identified and corrected. Uncertainties associated with geometry specifications are inherent in the structure tolerances. Calculations based on the expected extremes provide a measure of the sensitivity of integral parameters to the selected variables. Variations in the proposed convergence and uncertainty evaluations are appropriate when the above procedures are inconsistent with the methodology to be validated. As-built data could be used to reduce the uncertainty in geometrical dimensions.

In order to illustrate quantitative criteria based on measurements and calculations which should be satisfied, let ψ denote a set of logarithms of calculation (C_i) to measurement (E_i) ratios. Specifically,

$$\psi = \{q_i : q_i = w_i \ln (C_i/E_i),\ i = 1...N\}, \qquad (1)$$

where q_i and N are defined implicitly and the w_i are weighting factors. Because some reactions provide a greater response over a spectral region of concern than other reactions, weighting factors may be utilized when their

selection method is well documented and adequately defended. The mean of the set q is given by

$$\bar{q} = \frac{1}{N} \sum_{i=1}^{N} q_i \qquad (2)$$

and the best estimate of the variance, S^2, is

$$S^2 = \frac{1}{N-1} \sum_{i=1}^{N} (\bar{q} - q_i)^2. \qquad (3)$$

The neutronics methodology is validated, if (in addition to qualitative model evaluation) the following criteria are satisfied:

1) The bias, $|\bar{q}|$, is less than ε_1,

2) The standard deviation, S, is less than ε_2,

3) All absolute values of log C/E ratios ($|q_i|$, i = 1...N) are less than ε_3,

4) ε_1, ε_2 and ε_3 are defined by benchmark measurement documentation and demonstrated to be attainable for all items with which calculations are compared.

Note that a nonzero log-mean of the C_i/E_i ratios indicates that a bias exists. Possible sources of a bias are: 1) source normalization, 2) neutronics data, 3) transverse leakage corrections, 4) geometric modeling, and 5) mathematical approximations.

Reaction rates, equivalent fission fluxes or exposure parameter values [e.g., ϕ(E>1 MeV) and dpa] may be used for validating the computational methodology if appropriate criteria (i.e., as established by section 3.2.1) are documented for the benchmark of interest. Accuracy requirements for benchmark validation procedures are discussed in reference 2.2.4.

One acceptable procedure for performing these comparisons is:

1) obtain group fluxes at dosimeter locations from neutronics calculations,

2) collapse the ENDF dosimetry cross section data to a multigroup set consistent with the neutron energy group fluxes (note that the dosimetry cross sections should be collapsed with the same energy spectrum as used to obtain the broad-group cross sections) or obtain a fine group spectrum (consistent with the dosimetry cross section data) from the calculated group fluxes,

3) fold the energy group fluxes with the appropriate cross sections, and

4) compare the calculated and experimental data according to the above specified quantitative criteria.

3.3 Determination of the Fixed Fission Source

The power distribution in a typical power reactor undergoes significant change during the life of the reactor. A time-averaged power distribution is recommended for use in determination of the neutron source distribution utilized for damage predictions. For multigroup methods, the fixed source may be determined from the equation

$$S_{r,g} = \chi_g \bar{\nu} P_r \qquad (4)$$

where r denotes a spatial node, g denotes an energy group, $\bar{\nu}$ is the average number of neutrons per fission, χ_g is the fission yield in group g and P_r is the fission rate.

3.4 Calculation of the Neutron Flux Based on a Fixed Source in the Reactor Core

The discussion in this section relates to methods validation calculations and to routine surveillance calculations. In either case, neutron transport calculations must estimate the neutron flux in the core, through the internals, and in the reactor pressure vessel. Procedures for methods validation differ very little from procedures for predicting neutron flux in the pressure vessel or test facility; consequently, the following procedure is recommended:

1) Obtain detailed geometric and composition descriptions of the material configurations involved in the transport calculation. Uncertainty in the data should also be estimated.

2) Obtain applicable cross-section sets from appropriate data bases such as:

   - the evaluated nuclear data file (ENDF/B or its equivalent), or
   - a fine group library obtained by processing the above file (e.g., by using reference 2.2.2)

3) Perform a one-dimensional, fixed-source, fine-group calculation in order to collapse the fine-group cross sections to a broad-group set for multidimensional | calculations. At least two sets of broad-group sets are recommended for performing the one-dimensional group structure convergence evaluation. The broad-group structure should emphasize the high-energy range and should take cross section minima of important materials (e.g., iron) into consideration.

4) Perform the convergence studies outlined in Section 3.2.2.

5) Perform two- or three-dimensional fixed-source transport calculations based on the model established in steps 1-4.

6) Compare appropriate dosimetry results with neutronics results from step 5 according to the procedure given in Section 3.2.2. It is recommended that all valid lifetime-accumulated power reactor dosimetry data be included in this comparison each time new data become

available except when dosimeter specific comparisons are made and that a power reactor benchmark be utilized for power reactor calculations.

7) Repeat appropriate steps if validation criteria are not satisfied. Note that a power reactor dosimetry datum may be discarded if the associated C/E ratios differ substantially from the average of the applicable C/E ratios and a measurement error can be suspected. A measurement error can be suspected if the deviation from the average exceeds the equivalent of three standard deviations. In addition, the source for power reactor calculations may be scaled to minimize the bias and variance defined by equations (2) and (3) providing that data are not discarded as a consequence of scaling the source.

Results from neutronics calculations may be used in a variety of ways:

1) Determine a single normalization constant that minimizes bias in the calculated values relative to the measurements in order to scale the group fluxes.

2) Use a spectrum adjustment computer program as recommended in ASTM E706(IIA) with calculated group fluxes and dosimetry data to obtain an adjustment to the calculated group fluxes. Predicted pressure vessel group fluxes could then incorporate spectral and normalization data from the surveillance dosimetry data.

3) Refer to the Standard Recommended Practice for Extrapolating Reactor Vessel Surveillance Dosimetry Results, ASTM E706(IC).

4) Use the calculated fluxes with ASTM E706(ID) for damage exposure predictions without scaling based on dosimetry data.

It is expected that the procedure recommended above will be inconsistent with some methodologies to be validated. In these cases procedural variations are appropriate but should be well documented.

4.0 PRECISION AND ACCURACY

Uncertainties associated with specifications for neutronics calculations fall into several broad categories: 1) source distribution, 2) nuclear data, 3) geometry, 4) composition, 5) physical property data, and 6) system states (e.g., temperature and pressure). Significant sources of uncertainty should be recognizable from the convergence and model specification studies outlined in Section 3.2.2. Additional direct or adjoint methods may be employed to generate supporting sensitivity data as required. Comments on accuracy requirements for benchmarks are given in reference 2.2.4.

A variance or standard deviation must be assigned to exposure and damage parameters determined from neutronics calculations based on the apparent contributors to the exposure and damage parameter standard deviations. Refined methodology should be developed and incorporated into this guide when it becomes available.

5.0 DOCUMENTATION

The documentation of the neutronics calculations for the neutron flux in the pressure vessel must be sufficient to perform a quality assurance audit. This includes: 1) an accurate description of the geometry and composition of the system, 2) a complete list, with description, of all input parameters for the computer programs utilized, 3) references for sources of the nuclear data, 4) comparisons of experimental data with calculated results, 5) the core power distribution, 6) a normalization factor to obtain the neutron source distribution for any specified power, and 7) neutron spectra at the surveillance position, the inside surface of the pressure vessel, and through the pressure vessel wall. Any of the above items may be documented by referencing other documents.